i

HEAT TRANSFER IN FLUIDIZED BEDS

by

Lorenza C.L. Feng

A thesis submitted in partial fulfillment of the

requirements for the degree of

DOCTOR OF PHILOSOPHY

in the

DEPARTMENT OF CHEMICAL ENGINEERING

UNIVERSITY OF OTTAWA

Ottawa, Canada

August, 1966

Research Director

Ph. D. Candidate

To

Father and Mother

ACKNOWLEDGEMENTS

The author wishes to express her sincere appreciation and thanks to:

Professor B. C.-Y. Lu, Chairman of the Department, for the provision of research facilities;

Professor R. S. Mann, whose guidance and supervision made possible the achievement of this piece of work;

Messrs. G. Gasperetti and F. Giacobbi for services rendered in the building of the apparatus;

Mrs. L. Carriere for typing, and Mr. C. Tiu for proof reading the thesis;

Ontario Research Foundation Fund for the research fellowships;

Jim, whose patience and contributions in various ways without which this work would be impossible.

TABLE OF CONTENTS

LIST OF TABLES

LIST OF FIGURES

I ABSTRACT

The unsteady state heat transfer between gas and solid particles was studied in fluidized beds, 2 and 4 inches in diameter. Air velocities of 0.543 to 4.347 ft./sec. and bed-settled heights to diameter ratios from 0.2 to 8 were employed in transient heating and cooling of 0.004 to 0.2324 inch particles of glass beads, silica gel and alumina between 130 and 288 °F.

The effect of several variables, particle size (0.004 - 0.2324 inch), bed-settled heights (0.8 - 16 inch) particle densities (8.5 - 206 lbs./cu. ft.), thermal conductivities (0.013 - 1.8 Btu/(hr.)(ft.^{2})(°F/ft.) and air velocities (0.543 - 4.347 ft./sec.) on the space-averaged heat transfer coefficient has been investigated.

Using a new approach in interpreting the heat transfer driving force, a correlation between the heat transfer coefficient and several parameters for two ranges of modified Reynolds numbers 10 to 60, and 60 to 2200 has been developed

(a) for Reynolds number 10 to 60

$$\frac{UD_p}{k_f} = (0.08)\left(\frac{C_{p_f}\mu_f}{k_f}\right)^{0.4}\left(\frac{L_s}{D_t}\right)^{-1.3}\left(\frac{D_p}{D_t}\right)^{4.3}\left(\frac{k_s}{k_f}\right)^{-4}\left(\frac{\rho_s}{\rho_f}\right)^{7.8}\left(\frac{D_p V_f \rho_f}{\mu_f}\right)^{-6.1}$$

(b) for Reynolds number 60 to 2200

$$\left(\frac{UD_p}{k_f}\right) = (0.0011)\left(\frac{C_{p_f}\mu_f}{k_f}\right)^{0.4}\left(\frac{L_s}{D_t}\right)^{-1.3}\left(\frac{D_p}{D_t}\right)^{4.3}\left(\frac{k_s}{k_f}\right)^{-4}\left(\frac{\rho_s}{\rho_f}\right)^{7.8}\left(\frac{D_p V_f \rho_f}{\mu_f}\right)^{-3.1}$$

II - INTRODUCTION

From time immemorial, the most original phenomenon depicting a dynamic system of fluid-solid particles has been "Fluidization". The techniques of fluidization have proved very useful in the past, and as such have been used in various phases of human activity. Though the subject of fluidization is very old, and voluminous literature on it exists today, yet it is surprising that the inter-relationships between fluid mechanics and particle dynamics, and transport phenomena involving mass and heat transfer between the phases have never been completely explained.

The most ancient applications that resembled the methods of fluidization were the processes of purifying ores and municipal water supplies. The water, together with its suspended coagulated dirt, was allowed to run through a graded sand by gravity. The graded sand, therefore, served as filter. As the dirt and solids accumulated among the sand filters, the permeability of the sand deteriorated and eventually completely blocked the passage of flow. In order to restore the permeability, the sand was backwashed. The phenomenon of backwashing and expanded sand bed while being backwashed are examples of fluidization with a liquid medium.

However, it appears that the first patent taken on fluidization was by Phillips and Bulteel (1) in 1910. The invention was a process of contacting a gas with a fine catalyst. The catalyst was suspended in the gas and was carried into a reaction chamber. The reaction occurred and

simultaneously the spent catalyst was carried by the products into a recovery vessel and recycled back to mix with the fresh catalyst feed lines. This was finally developed into a fluid catalytic process.

The phenomena described above are the processes in which powdered solids are placed in motion by streams of gas or liquid. Although the processes resembling the backwashing technique have been known for a long time, it was mainly used to transport the solids.

Pioneering operations on commercial scales were those of Winkler gas generators in Germany in 1921 and those in the United States that pertained to catalytic cracking of oil vapors at about the same period. The initial basic flow studies pertaining to the fluidization process were started at Massachusetts Institute of Technology.

Conventionally, two terms are used to describe the two forms of fluidization. "Particulate fluidization" refers to liquid-solid systems where the solid particles are uniformly distributed throughout the mixture. "Aggregative fluidization", typical of gas-solid systems refers to those where solid distribution is extremely non-uniform, heterogeneous mixture of bubbles and particle clusters become very obvious.

A few recent applications of fluidization are:

Fluid catalytic reforming, one of the most frequently used means of upgrading napthas; fluid coking, used in producing higher yields of distillate oils and by-product gas; fluid catalytic oxidation of ethylene; iron ore reductions and more recently, it has been used in paper industries for drying.

The reasons for the rapid and tremendous increase in the utilization of fluidized techniques are attributed to the following:

The first and perhaps the most important factor is the presence of a greater surface area available to the gas which effect better transfer of heat and mass.

A second importance of the fluidized bed is attributable to the rapid agitation of the particles by the incoming fluid. Turbulence in the fluidized bed helps to bring the mass to an isothermal condition. This is so because all the hot spots and cold spots are broken up and thoroughly mixed. Often, it is assumed that there is no temperature gradient in a single particle and that the temperature of one particle does not differ from the other. This is not really true; the activity of a catalyst differs from particle to particle, and thus the temperature differs proportionally with the reaction which in turn depends on the magnitude of the activity of the particle. However, because of the large extent of mixing, the temperature of a single particle is comparatively

close to that of the mean value of the bed.

A third advantage is the ease with which the particles can be transported.

Voluminous work has been reported in the literature (49-59) dealing with the various aspects of fluidization. One of the aspects of fluidization, which has been investigated considerably is the transport of heat in or out of the system. The transfer of heat between particles, or fluid-solid surfaces is as complex in its facets and even more so in its mechanisms, as the problems associated with the many phases of fluid flow in such a two phase system.

The transfer of heat between fluid and particles has been treated theoretically and experimentally by a number of investigators (2). The heat exchange or heat flow is related to the driving force, which is the temperature difference between the phases, by a certain proportionality constant; generally known as heat transfer coefficient and designated as "h". This heat transfer coefficient h has been defined in various ways by different investigators. As far as fluid and solid is concerned, it is defined by the temperature driving force and the area for heat exchange. Up to now, the definition of the temperature difference has been a controversial point. The area of heat exchange is not confronted with as complex a problem as the difficulty

involved in selecting the right temperature difference. To a certain extent, the order of magnitude of the heat transfer coefficient is dependent upon the definition of the area of heat transfer, nevertheless, the uncertainty involved is comparatively insignificant, hence an arbitrary area can be used. Accuracy in the determination of the heat transfer coefficient is primarily dependent upon the use of the temperature difference between the solid and the fluid surrounding it. But because there is a large turbulence in a fluidized threshold, it is extremely difficult to differentiate between the temperature of the solid from that of the fluid. So far no single technique is known which could be used to measure accurately the true temperatures of the two phases. Therefore, as an alternative, scientists have resorted to different techniques and made various assumptions, which may give values that are close to the true values.

The fluidized system is found to have a characteristic flow. Although the mixture is believed to be perfectly mixed and uniform, in reality the picture does not appear to be so. Within the threshold of fluidization, there appears to be two streams of fluid flow. One stream is in the form of bubbles that bypass most of the particles while a partial stream actually supports the mass of the particles. The bubble-like stream is the dilute phase while the supported particles form the dense phase. If this were so, the heat exchange between solid

particles and the entire gas stream must involve more than one step. Within the core of the dense phase, heat exchange must take place between the particles and the fluid. Furthermore, the dense phase must mix with the dilute phase so as to impart its heat to the dense phase where solid concentration is high. The heat exchange between dilute and dense phases would perhaps involve more than one step. This phenomenon is therefore complex, ever changing and confusing. It is not feasible to measure local particle and dense phase gas temperatures separately. Neither is it possible to measure the dilute phase temperature alone. Since it is not possible to locate local temperature differences correctly, the evaluation of local heat transfer coefficients is not much of a significance. It is therefore most appropriate and most convenient to use an overall heat transfer coefficient U.

Various methods have been used to measure the temperature of the solids. While in some cases bare thermocouples were used near the distributor plate, and an assumption was made that the temperature was constant over the remaining heights of the bed, suction type of probes were used in other cases for the measurement of temperature. Some investigators have also used the terminal (exit) temperature of the gas as the temperature of the solid. These assumptions, reasonable as they may appear, in the measurement of the solid temperature, do constitute compromise in different aspects. The use of a bare thermo-

couple to indicate the temperature of the fluidized solid would constitute an error, since there is no guarantee as to what the sensing element is measuring. Whether it measures the temperature of the solid or that of the fluid, it is constantly bathed in a vigorously mixing fluid and particle. Should the dilute phase happen to traverse its path across a thermocouple station, the sensing element would then be indicating the temperature of the fluid; should the dense phase be in touch with the sensing element, then the temperature indicated would be that of the solid. As such, in this case, an error would be constituted.

The temperature probes of suction type thermocouples were inserted by some investigators at the critical regions in a fluidised threshold, oftentimes at a point very close to the distributor which is a porous plate. In this case, it was assumed that the solid temperature was equal to the exit gas temperature and that the fluid temperature was indicated by the sensing element in the stream of the suction. These have been found to be inadequate assumptions and measurements.

Another group of research workers have characterised the heat transfer measurements by using the exit gas temperature as the solid temperature. This seems to be comparatively logical since the solid bed as a whole reaches an isothermal condition with that of the fluid. As such, it would be very easy to evaluate the heat transfer coefficient. However, the main difficulty involved with this would be the

measurement of the exit temperature.

Since the expanded bed height depends on the type of the solids used and the velocity of the fluidizing gas, the measurement of the exit temperature at the boundary of the expanded bed would be unreliable. Some scientists have measured the exit temperature at certain locations near the outlet and used this as exit gas temperature. Such measurement could not be expected to give accurate results, since these measurements are already approximate in nature due to the reasons discussed.

In the present investigations, using more precise and accurate measurements, a correlation between overall heat transfer coefficient as a function of various characteristic properties of the fluid-solid system has been obtained, and efforts made to reconcile the conflicting views that have appeared in the past.

A preheated stream of gas was introduced into a bed of solid at an initially low temperature, normally at room temperature. During heating and cooling of the particles, the temperature-time relationship was recorded automatically and simultaneously. These measurements are then used in evaluating the heat transfer coefficients.

The process of heat transfer in a fluidized bed involves most often the heat flow in two channels, namely, heat flow between

the fluid and particles and heat exchange between system and container wall or immersed surfaces. The present investigations are related to the internal process of the system where large amounts of heat exchanges take place between fluid and solid particles. In such systems, a steady state heating or cooling process is only possible if the rate of heat removal or supply could be of the same order of magnitude as the fluid-solid heat transfer rate. Such systems could possibly be developed by generating heat on the solid by chemical reaction or physical adsorption or radio-active disintegration. Since it is very difficult to install such a system, most of the research workers have used different types of jackets to remove or supply heat.

In order to circumvent the foregoing difficulties, a transient system was used to determine heat transfer coefficients as a function of superficial gas velocities, bed settled heights and physical characteristics, such as diameter, density and thermal conductivity of particles. Results thus obtained have been compared with others and used in bringing about a better and deeper understanding about the heat transfer mechanism and its use as a design parameter.

III LITERATURE REVIEW

Scattered reference to early observations of what is known as fluidisation can be found in published literature as far back as 1878. However, the fluidised technique, as it is now known, was initiated by the pioneering work of the Standard Oil of Indiana, The M.W. Kellogg Company and the Standard Oil Company, in their efforts to find a better catalytic cracking process than the fixed bed method introduced commercially in 1937. The fluidised technique has now many applications, such as the catalytic cracking of petroleum; fluid catalytic reforming; fluid coking; fluid catalytic oxidation of ethylene; fluid bed hydrocarbon synthesis and fluid bed nuclear reactor, etc. The early studies closely related and pertaining to fluidization were those of sedimentation and fixed beds. The flow of fluid in porous media can be best visualised by considering it to be something in between two types of flows: one as flow past separate particles in a continuous medium and the other as flow through a solid body containing channels or pores. Some notable examples of fluid flow through porous systems are: flow of ground water, seepage through earth dams, pool flow in oil sands, removal of suspended impurities by filtration and the use of packed columns in chemical operations. The classical expression for flow through porous media was contributed by the works of D'Arcy (3). The expression is:

$$u = K(\Delta p/L) \qquad (1)$$

where u is the average rate of flow through the porous structure and K is the coefficient of permeability. The pressure drop due to friction in a stream of fluid flowing through a packed bed of height L_s is given by the equation:

$$\frac{\Delta p}{L_s} = \left(\frac{2 f \rho_f V^2}{g_c D_p}\right) \qquad (2)$$

where f is the friction factor, V is the superficial velocity.

Many investigators have sought to derive empirical correlation of the friction factor (f), and variables of particle shape, roughness, distribution, manner of packing and similar difficultly definable parameters for flow of fluids through fixed beds. Significant work in this direction was carried out by Coulson (4), Schwartz (5), Cooling (6), Martin (7) and Van Heerden (8).

A correlation for the pressure drop in the fixed bed column in terms of the characteristic properties of the solid and fluid from dimensional analysis was first presented by Blake (9) in 1924. His work was further extended by Carman and Kozeny (10); Bakhmeteff and Feodoroff (11); Oman and Watson (12) and Chilton and Colburn (13). Chilton and Colburn drew an average curve of f versus Reynolds number through the data of many investigators. The error resulting from the Chilton-Colburn correlation can be sometimes quite large as it does not allow for the variation of voidage of the packed bed. However, they

did present a well organized correlation.

The mechanics of fluid flow in fluidization was first discussed by Daniels (14) who dealt with the mechanics of flow in a fluid catalytic cracking unit. This was followed by the investigation of Parent, et al.(15). Thirty different materials were tested and several gases were used as the fluidizing medium. The effect of particle size distribution, vessel diameter, particle shape and gas velocity were investigated. Wilhelm and Kwauk (16), Parent and Leva (17) presented an equation for the pressure drop in a fluidized bed as follows:

$$\Delta p_e = L_e (1 - \epsilon_e) (\rho_s - \rho_f) \qquad (3)$$

where L_e is the bed height, ϵ_e voidage, ρ_s and ρ_f solid and fluid densities.

To explain the above equation, a column was first subjected to a gas that traversed counter gravity wise at a superficial velocity V_f. As a result, a pressure drop equal to Δp occurred. The order of magnitude of the pressure drop was determined by the gas rate and the characteristics of the bed. As the gas velocity was increased, the pressure drop increased. Eventually, a condition was reached wherein the pressure drop was equal to the one represented by the above equation. This basic equation is generally used in predicting the point of initial bed expansion or the point of incipient fluidization.

In order to predict the onset of fluidization where ϵ_e is ϵ_{mf} and V_f is V_{mf}, a condition in which the bed starts to be in a pseudofluid state, with all the particles in motion, a characteristic voidage of the bed must be reached. This voidage, also conventionally termed as "minimum fluid voidage" is determined by subjecting the bed to a rising gas stream and recording the bed height L_{mf} that coincides with incipient particle motion. The minimum fluid voidage in terms of the buoyant weight of the bed W_s, the column cross section S, and solids and fluid densities, is given by the equation:

$$\epsilon_{mf} = 1 - \frac{W_s}{L_{mf} S (\rho_s - \rho_f)} \tag{4}$$

Leva (18) derived V_{mf} in terms of G_{mf} as follows:

At the point of initial bed expansion the pressure drop is given by:

$$\Delta p = L_{mf} (1 - \epsilon_{mf}) (\rho_s - \rho_f) \tag{3a}$$

Since this is a fixed bed, pressure drop is also defined by

$$\Delta p = \frac{2 f_m G^2 L (1 - \epsilon)^{3 - n_l}}{D_p \psi^{3 - n_l} g_c \epsilon^3 \rho_f} \tag{5}$$

Upon equating and recalling that, in order to permit fluidization, the bed must be at the minimum fluid voidage ϵ_{mf}, there results

$$G^2_{mf} = \frac{D_p g_c (\rho_s - \rho_f) \epsilon^3_{mf} \psi^{3 - n_l}}{2 f_m (1 - \epsilon_{mf})^{2 - n_l}} \tag{6}$$

Since most gas-solid systems begin to fluidise at rates for which Re <10, substitution of

$$fm = \frac{100}{Re} \quad \text{and} \tag{6a}$$

$$n = 1.00 \tag{6b}$$

into equation (6) yields

$$G_{mf} = \frac{0.005\, D_p^{\,2}\, g_c\, \rho_f\, (\rho_s - \rho_f)\psi^2\, \epsilon_{mf}}{\mu\ (1 - \epsilon_{mf})} \tag{7}$$

Equation (7) is the most commonly used correlation in fluidization.

One of the main advantages of fluidised technique is in the field of heat transfer. Apart from the work done on pressure drops, a great deal of work directly or indirectly related to heat transfer in fluidized beds has been carried out since the technique became known. There are three main types of heat transfer in fluidised beds, namely, the heat transfer between fluidised beds and a heat transfer surface; heat transfer between pneumatic systems and the exterior, and heat exchange between the particles and the ambient fluid.

The pattern of correlating heat transfer data in fluidization seems to have taken shape from convective heat transfer in pipe flow. It is for this reason that most of the correlations for heat transfer coefficient in a fluid-particle system are obtained from dimensionless analysis. This type of approach gave a correlation relating the different dimensionless numbers in the form of

$$\frac{h D_t}{k_f} = f\left(\frac{DG}{\mu_f}, \frac{C_{p_f} \mu_f}{k_f} \text{ ------}\right) \qquad (8)$$

The numerous data pertaining to heat transfer in packed beds, fixed beds and fluidized beds have been correlated based on such kind of relations.

Mechanism of Heat Transfer

I Heat Transfer Between Fluidized Beds and Boundaries

a. Heat Transfer Between Bed and Confining Wall

The mechanism of heat transfer between fluidized beds and boundaries was first explained by Leva, Weintraub and Grummer (19) based on the "film theory". The experimental data by Van Heerden, Nobel and Van Krevelen (20) (21), further substantiated the film theory. According to this theory, the heat transfer properties of a fluidized bed could be compared to a well stirred liquid with interstitial gas flow serving mainly as a stirring agent. Since the heat capacities of the particles are greater than the ambient fluid, they are mostly responsible for heat dispersion throughout the bed. While the gas acts as a stirring agent, it is also believed to be acting as a medium of heat transfer between particles as well as between the particles and the confining walls. This therefore, not only indicated the role played by the particles in its capacity of carrying heat but also recognized the existence of a film between the main core of the bed and the wall.

Wicke and Fetting (22) further correlated heat transfer coefficients to the fundamental quantities such as fluid film thickness and fluidized solids boundary layers. The model of Wicke and Fetting is indicated in Figure 1, where x is the fluid film thickness in contact with the wall. The film is followed by a solids boundary layer of thickness δ_p and a layer of the fluidized core. Within the boundary layer, the movement of the solids is mainly parallel to the wall and simultaneous to this, there is the lateral solids exchange between the boundary layer and the core. Regarding the temperature profile, temperature drop is abrupt from 1 to 2 within the film, in the boundary layer, the temperature is comparatively constant whereas beyond 3 it remains constant due to the vigorous mixing of solids.

According to Wicke and Fetting the total heat flux q into the unit could be divided into two separate components, longitudinal component q_z and a radial component q_r. The relative values of these components are height dependent. Leva, Weintraub, and Grummer (23) studied the longitudinal temperature profile pertaining to a silica sand fluidized with air. Heat transfer coefficients in fluidized beds were also measured by Agarwal and Storrow (24).

Baerg, Klassen and Gishler (25) obtained the radial temperature profile for a bed in an annular space. They obtained a very

steep temperature drop adjacent to the heat transfer surface followed by a very flat course leading to the other boundary of the bed.

b. Internal Heat Transfer Elements

Units with internal heat transfer elements are extensively used in industry. All large scale fluid catalytic equipment is of this type. Such an equipment is comparatively more costly than the ones that are externally heated, but they are more efficient and more suitable for large capacity heating and cooling. Toomey and Johnstone (26) have made a direct comparison between the two modes of heat exchange based on their data obtained from experiments performed simultaneously with the same solids in the same equipment.

Vreedenberg(27) obtained his data by immersing cooling tubes, through which water was circulated, in various horisontal and vertical positions in a 22 inch diameter fluidized bed.

II Pneumatic Systems Heat Transfer

a. Pneumatic System and the Exterior Wall

The only published data on heat transfer film coefficients pertaining to pneumatic systems are those of Koble, Ademino, Bartkus and Corigan (28) and of Farbar and Morley (29). Koble used a column of 20 feet in length of standard 10 inch steel pipe for fluidization. The fluidized solids were carried from the column through a 1/4 inch O.D.

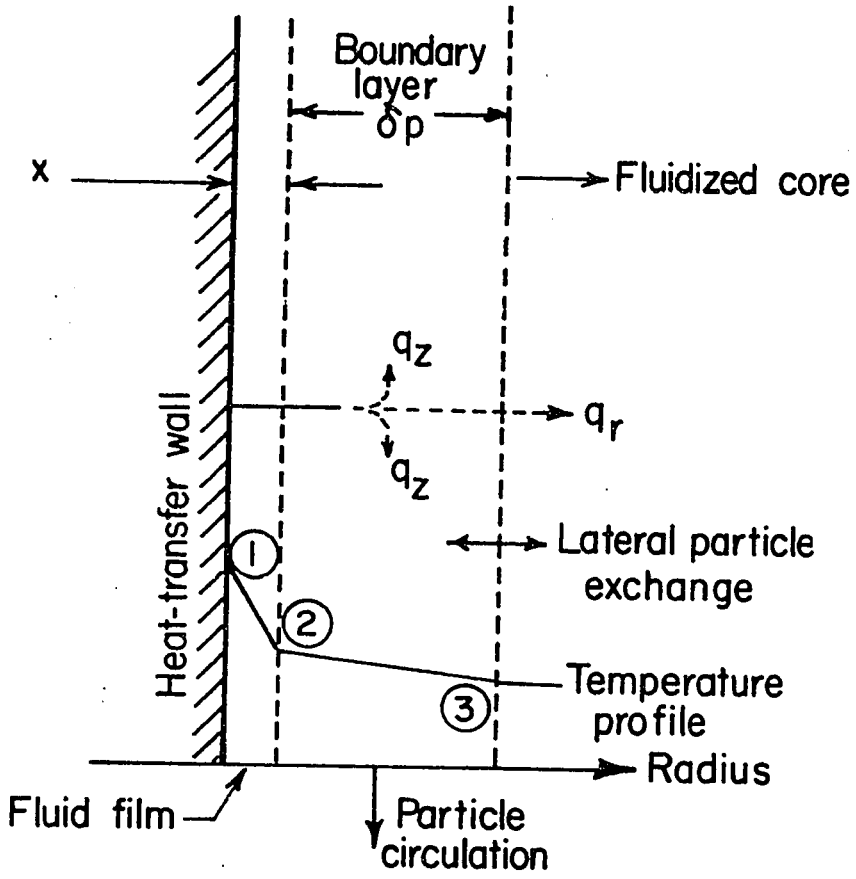

Fig. 1 Heat transfer model of Wicke and Fetting

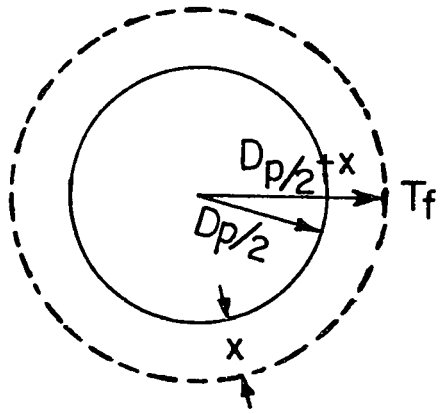

Fig. 2 Schematic diagram of a fluid film around a single particle

copper tube. A six foot length of this tube was enclosed by a jacket of 2-inch iron pipe with provisions for introducing steam. Inlet and outlet temperature of solids-air mixture were measured by thermocouples of 30 gage iron-constantan. The actual thermal driving force along the length of the heater was equal to the log mean temperature difference. The result was correlated by the relation:

$$U_n = 0.32\, G_s^{0.39} \tag{9}$$

Farbar and Morley used a vertical tube of 7 inches I. D. 33 inches long for fluidization of alumina catalyst. The unit was surrounded by a vapor jacket to permit addition of heat. Heat transfer coefficients were based on inside area of the tube and a logarithmic mean temperature difference, as observed from terminal data. Their data correlated very well with the following equations

(i) for $\frac{G_s}{G_f} > 2.0$

$$\frac{hD_t}{k_f} = 0.14 \left(\frac{D_t G_H}{\mu_f}\right)^{0.6} \left(\frac{G_s}{G_f}\right)^{0.45} \tag{10}$$

(ii) for $\frac{G_s}{G_f} < 2.0$

$$\frac{hD_t}{k_f} = 0.025 \left(\frac{D_t G_f}{\mu_f}\right)^{0.8} \left(\frac{C_p \mu_f}{k_f}\right)^{0.4} \tag{11}$$

where D_t = diameter of tube

G_s and G_f = solid and gas mass velocities

b. Heat Transfer from Fluid to Solids Conveyed by the Stream

Recently, Richardson and Ayers (30) have done some work on pneumatic transport heat transfer. As the system they studied is somewhat different from ordinary pneumatic heat exchange, it is discussed later.

III. Particle to Fluid Heat Transfer in Fluidized Beds

Mechanism and Theory

Though the heat transfer coefficient between fluid and solid in a fluidized bed is usually small, the rate of heat transfer per unit height or per unit volume is extremely high due to the large particle area for fluid-solid contact. Usually the contact area vary from 1000 to 1500 sq. ft/cu. ft. of bed. The main resistance to heat flow between gas and solid in fluidized beds is due to conduction through a thin gas film around the particle. The local coefficient h_i is a function of the local film thickness, x_i and is given by a heat balance equation:

$$q_i = h_i A_i \Delta T_i = \frac{k_i}{x_i} A_i \Delta T_i \qquad (12)$$

$$h_i = \frac{k_i}{x_i}$$

Defining x_i to be the mean effective film thickness, the mean coefficient is given by the equation:

$$h_p = \frac{k_f}{\bar{x}_f} \tag{14}$$

The mean film thickness is obtained by integrating the point thickness over the entire area, A_p of the particle,

$$\bar{x}_f = \frac{\int x_f \, dA_f}{A_p} \tag{15}$$

where $A_p = \psi \pi D_p^2$ and (16)

substituting therefore

$$\bar{x}_f = \frac{1}{\psi \pi D_p^2} \int x_f \, dA_f \tag{17}$$

The mean effective thickness of the film is a function of the properties of the fluid-solid system, especially the Reynolds number, particle shape ? and particle roughness ?. Since heat transferred to the surface of particles is also transferred into the particles, it is but logical to assume that the physical properties of the solid partly would affect the thickness of the film. The presence of other particles in the neighborhood of a given particle or conversely the void fraction, ? would also affect the film thickness. Therefore

$$x_f = f\left(\text{Re}, \psi, \delta, \epsilon \text{ and physical properties of solid}\right) \tag{18}$$

and $$\bar{x}_f = \frac{1}{D_p^2} \int \left[\varphi\left(\frac{D v \rho}{\mu}, \psi, \delta, \epsilon \text{ ------}\right)\right] dA_f \tag{19}$$

Since complete information is not available showing how one variable is related to the other in the fluid-solid system, the integration of such an expression is as yet impossible. More information is therefore required regarding the flow characteristics of gases around single particles, in fluidized beds as well as the particle interaction effects.

Theoretical Consideration for a Single Particle

The conduction of heat from the surrounding medium to a single solid particle (Figure 2) can be represented by the equation

$$dq = -k_f A_p \, dT/dr \tag{20}$$

Equation (20) can be integrated, for a steady state conduction of heat to or from an infinite fluid as follows:

$$A_p = \pi D_p^2 = 4\pi r^2$$

$$q = -4\pi k_f r^2 \, dT/dr \tag{21}$$

$$q \frac{dr}{r^2} = -4\pi k_f \, dT \tag{22}$$

and integrating both sides of the equation:

$$q \int_{\frac{D_p}{2}}^{(\frac{D_p}{2} + x)} \frac{dr}{r^2} = -4\pi k_f \int_{T_s}^{T_f} dT \tag{23}$$

$$\dot{q} \left(\frac{1}{\frac{D_p}{2}} + \frac{1}{\frac{D_p}{2} + x} \right) = 4 k_f (T_s - T_f) \qquad (24)$$

$$\dot{q} = \frac{k_f (T_f - T_s) D_p (D_p + 2x)}{x} \qquad (25)$$

If the same amount of heat were transferred by convection and through the gas film, the equation may then be written:

$$\dot{q} = h A \Delta T = \pi h D_p^2 (T_f - T_s) \qquad (26)$$

Equating (25) and (26), we have

$$h D_p = \frac{k_f (D_p + 2x)}{x} \qquad (27)$$

$$\frac{h D_p}{k_f} = \frac{D_p}{x} + 2 \qquad (28)$$

at $$x \longrightarrow \infty \quad \frac{D_p}{x} \longrightarrow 0 \qquad (29)$$

So that $$\frac{h D_p}{k_f} \longrightarrow 2 \qquad (30)$$

Single particle technique was investigated by Johnstone, Pigford and Chapin (31). Solids were dispersed and allowed to fall by gravity inside a furnace whose walls were at temperature of 550 °F to 1100 °F. Radiative and convective coefficients were acquired for

various particle size ranges. Since the investigations were made with clouds of particles, data obtained for solid concentrations were several orders of magnitude less than those normally found in fluidized processes. Hence, in effect, their data could not be compared with a theoretically derived equation for heat transfer from a single particle to a surrounding fluid. Johnstone derived the mathematical solution from the Fourier-Poisson conduction equation by assuming that the velocity of the fluid around a sphere is tangential to its surface at all points. At Reynolds numbers greater than 500, the solution could be expressed in the form of

$$Nu = \frac{h D_p}{k_f} = 0.714 \left(\frac{D_p V_f \rho_f}{\mu_f} \right)^{0.5} \left(\frac{C_{p_f} \mu_f}{k_f} \right)^{0.5} \qquad (31)$$

Several other equations resulting from theoretical consideration are given by Zenz and Othmer (32).

The earliest work on fluid-solid heat transfer in fluidized bed reported in the literature was that of Kettenring, Manderfield and Smith (33). Their work involved simultaneous heat and mass transfer

during the drying of some adsorbents. Materials used were silica gel and alumina. The size range used were rather narrow, particle diameters ranged from 360 to 1000 microns. The particles were wetted to start with and were fluidised by preheated air at 88-108° F. The diameter of the column was 2.3 inches and the gas mass velocities ranged from 250 to 720 lbs/hr. sq. ft. The temperature of the gas at various positions of the bed was indicated by a bare thermocouple, and the bed temperature assumed equal to the exit gas temperature. The equation used to calculate the heat transfer coefficient was:

$$dq = h\,(t_f - t_s)\,a\,d\,L \tag{32}$$

$$h = \frac{q}{a\int_0^L (T_f - T_s)\,d\,L} \tag{33}$$

The value of h was obtained by graphical integration using equation (33) together with a plot of t_f versus L shown in Figure 3. The particle surface area was calculated on the basis of spherical particles and observed bed heights. Heat transfer coefficients reported by Kettenring, et al were significantly lower than in fixed beds operating under similar rates of mass flow. The possible explanations for this are: the particles tend to move with the gas in a fluidised condition; or the measured temperature of solids were too low. Kettenring,

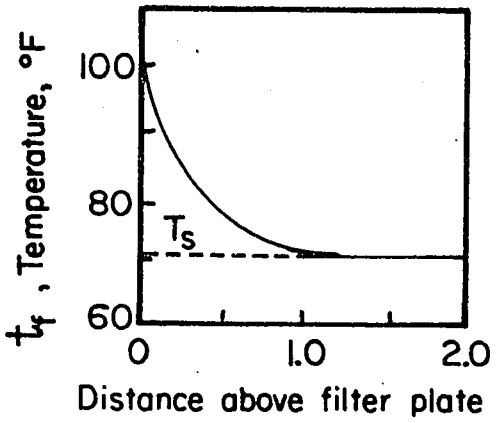

Fig. 3 Fluidized bed temperature profile, data of Kettenring

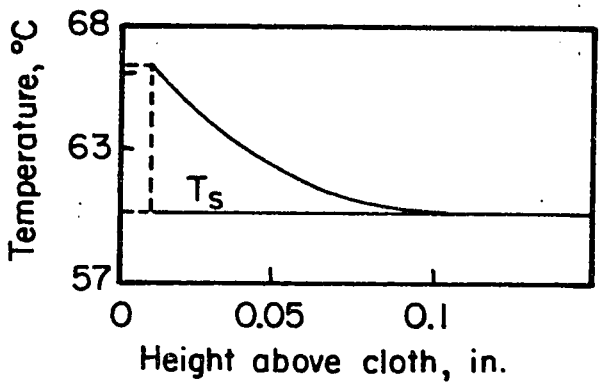

Fig. 4 Vertical temperature gradient in fluidized bed, data of Richardson and Ayers

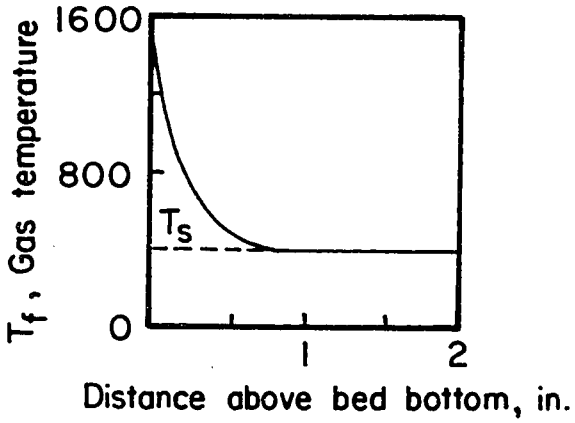

Fig. 5 Fluidized bed temperature profile, data of Frantz

Mandersfield, etc. evaluated the temperature driving force by assuming that the temperature of the solids throughout the entire bed was that of the bed at its upper interface. An error of only a few degrees in the lower part of the bed would have thus affected the temperature difference severely and consequently the overall coefficient. Data were correlated in terms of Nusselt and Reynolds numbers by the equation:

$$h D_p / k_f = 0.0135 \left(\frac{D_p V_f \rho_f}{\mu_f} \right)^{1.3} \qquad (34)$$

Walton and co-workers (34) measured the heat transfer coefficient between fluidising air and 360 micron size crushed coal particles in a 4 inch diameter column. They incorporated a shape factor of 0.88 for the particles and neglected 5% of heat losses. They were very much aware of the difficulties encountered in the measurement of the temperature of solid particles. Since the true temperature of the solids could not be measured, the average of the two limiting values was used. The two limiting values were obtained by: (a) immersing an unprotected thermocouple in the bottom of the column; (b) assumed equal to the temperature of gas and solids mixture at the top of the bed. The gas mass velocity was varied between 325 and 930 lbs/hr. - sq. ft. The gas temperatures were measured by a high speed movable thermocouple. The heat transfer rate is given by the equation:

$$C_{p_f} G_f S \, dt_f + h \, a \, dL \, (t_f - t_s) = 0 \qquad (35)$$

Equation (35) is integrated with the help of a figure in which gas temperatures are plotted against the distances above the bottom of the bed in inches. Integration of equation (35) between the limits $L = 0$ and $L = L$ yields:

$$\ln \frac{(t_f - t_s)_o}{(t_f - t_s)_L} = \frac{A_p \, h}{C_{p_s} G_f S} L \qquad (36)$$

The average minimum values of heat transfer coefficients were found to increase with increasing air mass velocity and particle size. The data were correlated by the equation:

$$\frac{h D_p}{k_f} = 0.0028 \left(\frac{D_t}{D_p} \right)^{0.2} \left(\frac{D_p V_f \rho_f}{\mu_f} \right)^{1.7} \qquad (37)$$

Heertjes and McKibbins (35) studied heat transfer between silica gel particles and air. Particle size range used was narrow, and mass velocity of the fluidizing gas varied from 320 to 630 lbs/hr. sq. ft. Screen protected thermocouples were used in place of bare thermocouples for measuring the temperature of the gas, thus avoiding the possibility of errors owing to collision of cooler particles from the lower regions of the bed with the sensing element. The bed temperatures were measured by bare thermocouples along the wall. This temperature was compared and checked from time to time by stopping the air flow and inserting a

bare thermocouple into the collapsed bed. The evaluation of the heat transfer coefficients was similar to the method used by Walton, et al. They correlated their results by the relation:

$$h = 1.31 \left(\frac{D_p V_f \rho_f}{\mu_f} \right)^{0.76} \qquad (38)$$

Similar errors to those previously mentioned were introduced here by using a bare thermocouple, bearing an uncertainty in the interpretation of solids temperature. A screen protected thermocouple seemed to be a better way of measuring the gas temperature.

The investigations of Heertjes, de Boer and Van Dorser (36) were mainly connected with the measurement of temperature and humidity variations in a drying fluidised bed of wet silica gel in a 2.3 inch diameter column. Particle sizes ranged from 300 to 500 microns. Gas temperatures were measured by bare thermocouples along the bed wall. Air supply was cut off occasionally and a bare thermocouple inserted into the bed to check the bed temperature. They found that heat was transferred to particles by the support screen as well as by the gas, and that heat and mass transfer occurred mainly in a thin layer at the bottom of the bed. They also observed that air temperature and humidity were independent of position in a horizontal plane.

Steady State

Anton (37) used steady state process in obtaining heat transfer coefficients in a 6-inch column. Cold sand particles were circulated in a fluidized bed. Hot air was used as a fluidizing gas. Gas velocity varied between 130 and 320 lbs/hr. sq. ft. Particle diameters were about 360 microns. Anton, in his calculations for the heat transfer coefficient, has defined the temperature driving force, Δt_1 as

$$\Delta t_1 = \frac{(T_{1f} - T_{2s}) - (T_{2f} - T_{1s})}{\ln \frac{(T_{1f} - T_{2s})}{(T_{2f} - T_{1s})}} \qquad (39)$$

whose correlation is

$$h = 0.0465 \left(\frac{D_p G_f}{\mu_f} \right)^{1.0} \qquad (40)$$

He has assumed that all the heat transfer occurred at about 0.5 inch from the bottom of the bed. Although only one particle size of sand was used, the heat transfer coefficient were correlated with the Reynolds Number.

Another steady state heat transfer between gas and solids was conducted by Richardson and Ayers (38). They used a rectangular fluidising column in which the circulation of solid particles was effected by feeding them to the bed along one of the shorter sides of a 10 x 5 cm. rectangular box. The solids would overflow at the opposite end. A

screw conveyor fed the materials into a preliminary bed from which they flowed into the test section. In doing so, an even distribution of solids was achieved. Air and CO_2 at mass velocities of 40-480 lbs/hr. sq. ft. were used for fluidisation between 116 and 158° F. The solids were fed at a rate of 3 to 25 lbs/hr. The temperature profile was taken from a height of 0.1 inch from the bottom of the bed with 40 gauge copper constantan wire thermocouple. Glass beads, lead shots and petunia seeds of 110 to 670 micron size were fluidized. Emphasis was placed on the measurement of gas temperature gradient confined to a shallow region at the bottom of the bed. A very thin temperature measuring element was arranged in such a way as to be coupled with a micrometer that measured the distances above the bed. The total rate of heat transfer in a bed of depth L was obtained by the expression:

$$q = h\,a \int_0^L \Delta T \,.\, dL \qquad (41)$$

They assumed that h and a were independent of depth and evaluated the integral for each of the systems used by measuring the area under the curves of ΔT plotted against height as shown on Figure 4.

Investigations in Liquid Medium

Frantz (39) studied the evaporation of brine solutions in a fluidized salt bed in a 4 inch diameter glass column. A ten-fold variation in particle diameter was used. However, the average particle

size was 225 microns. Combustion products from a propane air burner at mass velocities between 120 and 250 lbs/hr. sq. ft. were used for fluidization. Bed heights varied from 6 to 11 inches. The gas temperature was measured by a bare thermocouple which was inserted at various positions in the bed. The temperature of the fluidized bed was assumed to be equal to the exit temperature. The inlet temperature varied from 1260 to 1710° F. Figure 5 is a representative temperature profile.

The calculation of the heat transfer coefficients was done by using Walton's equation but because of insufficient data, several assumptions were made. Surface area was calculated on the basis of spherical particles. The void fraction at fluidized conditions was calculated from bed expansion data. His correlation was represented by:

$$\frac{h D_p}{k_f} = 0.00064 \left(\frac{D_p G_f}{\mu_f}\right)^{1.48} \qquad (42)$$

Sunkoori and Kaparthi (40) studied the heat transfer between fluidized particles and a liquid medium. They modified the unsteady state method of Wamsley and Johanson. Mass velocity of water varied from 12000 to 20000 lbs/hr. sq. ft. They fluidized granite and quartz solids in a 3.25 inch diameter column. The particle diameter of each bed was composed of closely sized fractions ranging from 540 to 1100 microns. They used the equation of Wamsley for calculating

the heat transfer coefficient and expressed their correlation by the relation

$$\frac{h D_p}{k_f} = 0.00391 \left(\frac{D_p G_f}{\mu_f}\right)^{2.1} \qquad (43)$$

Unsteady State

Wamsley and Johanson (41) studied the unsteady state heat flow from gas to solid. The exchange of heat took place when the solids were suddenly introduced into the gas stream. Glass beads, "Dowex" resin spheres and crushed alumina of 135 to 910 micron size were fluidized in a 4 inch diameter column by 160 to 600 lbs/hr. sq. ft. of hot air and carbon dioxide. While the bed temperature was assumed equal to the exit gas temperature, the gas temperatures were measured at the inlet and the outlet by thermocouples. The heat transfer coefficients were calculated from the time-temperature history curves for the solids and the gas and from the equation:

$$\ln \frac{(T_{1f} - T_{2f})_{\theta = \theta_1}}{(T_{1f} - T_{2f})_{\theta = 0}} = h A_t \frac{W_g C_{p_f}}{W_s C_{p_s} (h A_t + W_g C_{p_f})} \qquad (44)$$

Where A_t, the surface area represents the area of the entire bed. They found that the heat transfer coefficient was independent of gas velocity and dependent only upon the particle size. Their correlation was

$$h = 1270\ D_p^{1.27} \qquad (45)$$

Fritz (42) studied the unsteady state gas to solid heat transfer at settled bed heights of 4.5 to 47.5 inches with a gas velocity ranging from 0.139 to 1.31 ft./sec. and the inlet gas temperatures of 104 to 186°F in a 16 inch diameter column. Cracking catalyst with an average diameter of 60 microns was used. The solid temperature was indicated by a bare thermocouple inserted into the static bed while the inlet gas temperature was measured with a thermocouple. The exit temperature of the gas was obtained from a heat balance. Fritz derived equations based upon a parallel reactor model that predicted a reciprocal relationship between overall coefficient and bed-height-to-diameter ratio. The results were correlated by the following equation:

$$U = \frac{V}{116 + 52.4\left(\frac{L_s}{D_t}\right)} + \frac{1 - 0.6\left(\frac{L_s}{D_t}\right)}{274 + 447\left(\frac{L_s}{D_t}\right) + 146\left(\frac{L_s}{D_t}\right)^2} \qquad (46)$$

The average deviation was found to be $\pm$ 17% and the maximum 51%. It seems more logical to use a bare thermocouple here since the bed was a collapsed one. But since the system was an unsteady state, a time lag error was introduced.

Ferron (43) investigated gas to particle heat transfer for bed settled heights corresponding to $\frac{L_s}{D_t}$ values of 0.3 to 3 where D_t was the diameter of the column. The range of gas superficial velocities

studied was 0.08 to 1.94 ft/sec. Transient heating and cooling experiments were conducted with silica alumina cracking catalysts of 60 micron size. Inlet temperature ranged from 140 to - 180°F thermocouples used were of iron constantan type. Inlet gas temperature was measured by a single thermocouple whereas temperatures indicated by thermocouples immersed in a fluidized bed gave the space average temperature of the solid. The fluidizing columns used were made of concentric pipes. The annular space served the purpose of a bath. Heated gas at about the same temperature range was simultaneously introduced into the annular space while the fluidizing fluid was introduced into the column. By doing so, heat lost through the wall was reduced to a minimum. Ferron correlated the data with the equation

$$U = 0.0029\ V^{0.5}\ D_t^{-0.7}\ \left(\frac{L_s}{D_t}\right)^{-0.7} \qquad (47)$$

IV EXPERIMENTAL

Equipment

A schematic diagram of the fluidization apparatus is shown in Figure 8. The apparatus consisted of four main units, namely: the compressor and the auxiliary metering devices for flow measurement; the filtering, drying and preheating systems; the fluidizing columns and the automatic temperature recorder linking with the system of thermocouples.

Compressed air at a constant 120 lbs/sq. in gage pressure was obtained from the building compressors. It was first passed through two oil filters manufactured by Keller Air Line Filter Company so as to remove the entrained oil droplets carried along from the compressor. Often, the water vapor in the line condensed and remained in the line while being left overnight. This was also removed by the filters. Furthermore, a column four inches in diameter and three feet in length containing silica gel was installed immediately after the filters to remove the excess moisture content from the air before its delivery to the heaters and fluidizing columns. The height of the packing of the silica gel was about 30 inches and was confined in the middle portion of the column. The remaining spaces at both ends of the column were then packed with glass wool. While the gel column was in the line where air traversed through to the fluidizing unit, an extra outlet or exhaust was provided at one end of

the gel column to serve as an outlet when the gel was being regenerated. A number of inspection holes were provided near the ends of the column. Silica gel could be removed from time to time for inspection and regenerated if necessary. Regeneration of the gel was done by cutting off the stream of air just before the fluidizing unit and by manipulation of a number of valves. The regeneration process normally took five to six hours. Silica gel was usually regenerated after 2 - 3 weeks interval.

The dried air passed through a Nulmatic pressure regulator, model 42H100, and was pressure regulated to that desired. The pressure regulated air stream was then split into two streams, one for fluidizing and the other to be used as a bath in the jacket of the fluidizing column. While the main stream (A) was metered by rotameter I or rotameter II, the air stream (B) to the jacket was metered by an orifice 1/8" in diameter. Rotameter number I having a tube size of RM12M-25-5 and used for metering higher flow rates was calibrated by a Wet Test meter. Rotameter No. II having a tube size of R9M-25-3, used for metering lower flow rates was calibrated against a standardized rotameter.

From the rotameter and orifice air streams A and B were both simultaneously introduced into two forced convection type Canadian General Electric KX4AZB Finned Tubular Heaters respectively. The power input to the heaters was controlled by two separate powerstats.

A finer control of the air temperature was obtained by a Honeywell Brown Pyr-O-Vane temperature controller equipped with a time proportioning band. The preheated air streams were then ready for the fluidizing column or jacket as the case may be. A by-pass to the fluidising column was provided.

Fluidizing columns of two and four inches diameters were used. They were installed in such a way that each had to be operated alternately. The 4 inches column was made up of three sections, the bottom part was a conical end where air was disengaged from the 3/4" pipe line into a section of pipe 4" in diameter and 12" long. This was to insure even distribution of the air stream before entering the fluidized bed. The air was then passed through a porous stainless steel plate manufactured by Pall Corporation. It had a mean pore opening of 20 microns and a thickness of 3/8". The porous plate was installed in between the flanges of the fluidising column and the bottom disengage sections. The flanges were grooved in at the junction so that the filter plate was fitted into the groove and prevented from moving. Fluidisation took place above this and the air exhausted into the atmosphere.

The column has a jacket of 6" in diameter with a jacket space of one inch in cross section. The jacket air stream was introduced at the bottom of the column through a one inch diameter inlet and exhausted at the top and into a hose that led out of the laboratory.

The top of the column was covered with a cap that fitted the column very tightly from above. The cap has two layers of screens with quarter of an inch empty space in between filled with fiber glass. This was to minimise elutriation as much as possible.

Thermocouples were located in the fluidised bed, fluidising column wall, inside the jacket space; in between the inner wall of the insulation and the jacket surface. Figure 6 is a schematic drawing of the distribution of the thermocouples. A melting ice bath in a vacuum thermoflask was used for the cold junction. The melting point of the bath was checked constantly. The thermocouples used were of iron constantan insulated by asbestos fiber glass with silicone, gauge number 30. At the cold junction, thermocouples were soft soldered to size 30 lead wires (from Tensolite Insulated Wire Co. Inc.) which were then connected to a Philips Automatic Compensator Temperature Recorder (model PR3210 A/00) with twelve channels. The recordings were in terms of millivoltages and were taken down every five minutes and converted to temperatures in degrees Farenheit.

Shielded thermocouples were used in the fluidised beds; these thermocouples were placed at different height levels and the average of them all was taken and recorded. The data taken therefore

represented the solid temperatures, which were equivalent to exit gas temperatures at different levels. Some authors have made the same assumption, but the assumed temperature was taken at the very exit of the fluidising column, this was certainly not representative of the overall solid temperature.

Particular attention was given to the thermocouple which measured the inlet air temperature. A radiation shield was provided for the hot junction (Figure 7). It was made by welding a thin piece of silver metal into the shape of a ring and fitted around the hot junction.

The fluidising columns and jackets are made of iron, 1/4 inch thick with specific heat of 0.136 Btu/lb F. The 4 inch column weighs 30 lbs per foot of jacket wall and 19.2 lbs per foot of reactor wall. The 2 inch column weighs 10.8 lbs per foot of jacket wall and 3.66 lbs per foot of reactor wall. Both columns were insulated with glass fibers.

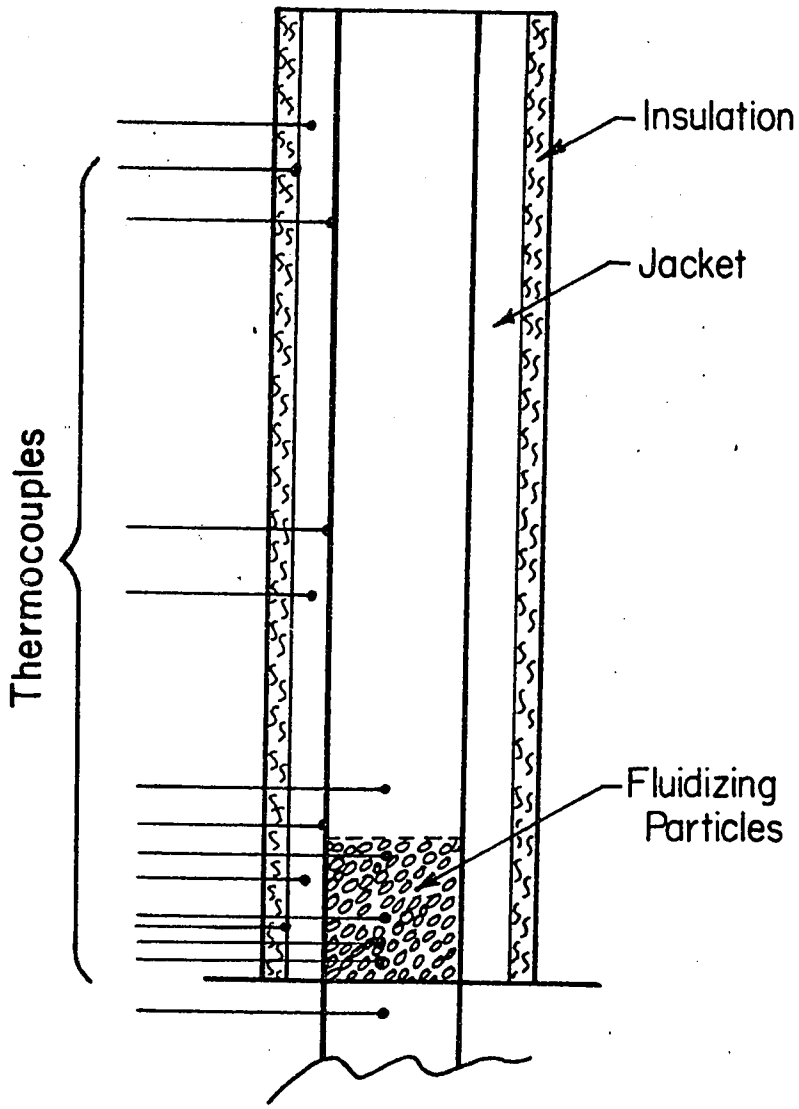

Fig. 6. Positions of thermocouples

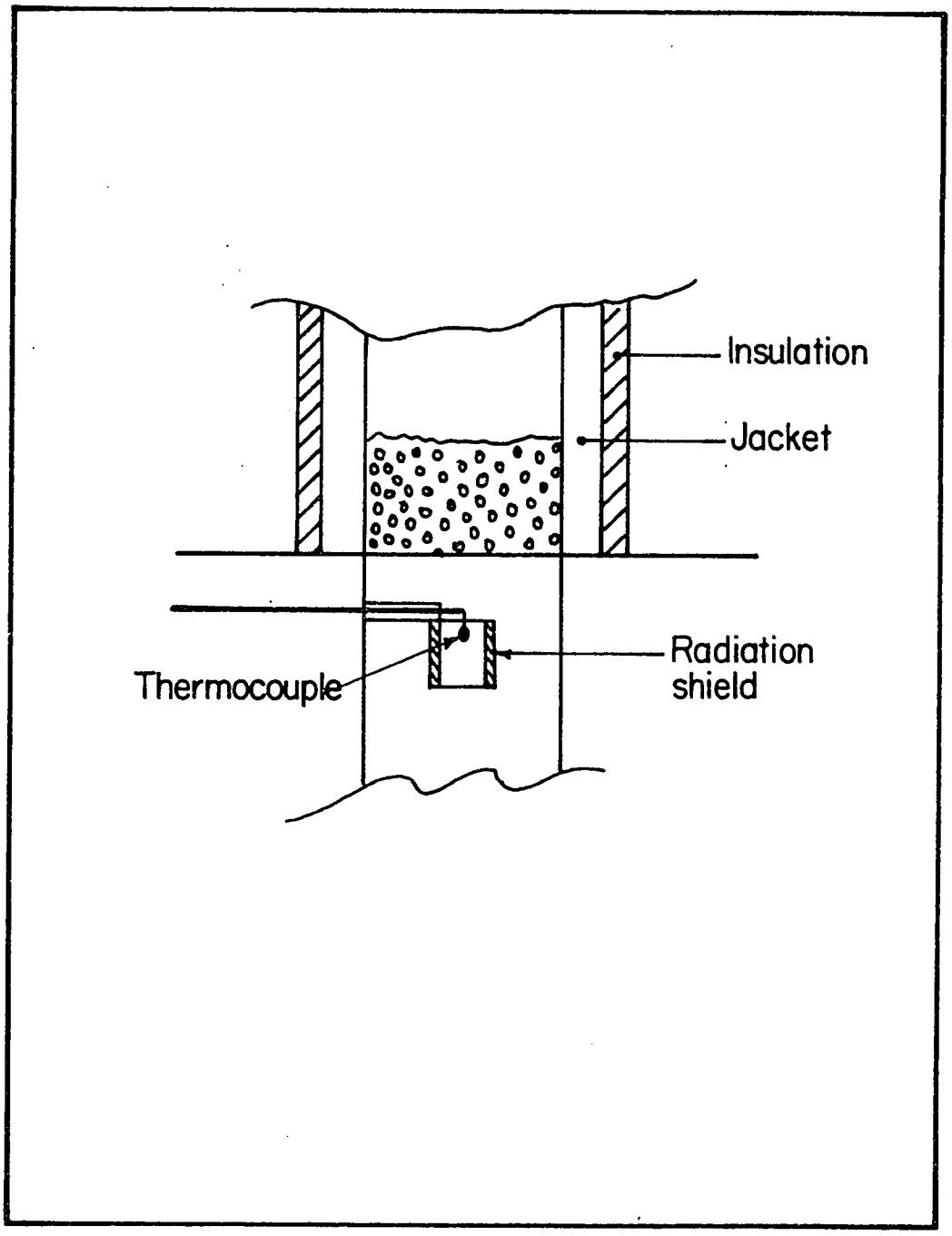

Fig. 7 Radiation shield for thermocouple

The hot junction and ring were altogether placed perpendicular to the direction of fluid flow. The silver metal was properly polished. Radiation was thus minimized.

A separate setup was assembled for the expanded bed height measurements. A line was connected to the main stream and a valve provided to cut off and divert the fluidizing stream into the separate column when expanded bed heights were to be measured. The column was made of glass and identical in design to the fluidizing column and was calibrated in inches. The column was adjoint to the whole setup, and when it was not in operation, the air stream was diverted back to the fluidizing column.

For most of the work, three fluctuated values of the height were taken. However, in some cases of more uncertainty, four readings were taken, which especially pertained to those at higher Reynolds numbers. In any case, the mean of all the readings was then sorted out and taken as the final reading for each height.

Procedure

At the start of a series of runs each morning, the water condensed overnight in the line between the compressor and the fluidising unit (Figure 8), was removed by blowing the compressed air through the exhaust valve 1. The draining procedure usually lasted for 30 to 40 minutes. In spite of this, some water continued to be carried along in the line until it reached the oil filter 2 where it was removed by the filter. Excess moisture, unremovable by the filter, was then absorbed by the gel in the silica gel column 3. While water was being removed from the lines, the system was brought into operation by carrying out the following:

1. All valves, 4,5 and 6,7 (or 8,9) leading the air stream through the rotameters, orifice and preheaters were kept open while those 10,11 or 12,13 introducing air into the fluidising columns and jackets were kept closed.

2. Powerstats 14,15 for the heaters were set to the proper readings for each particular run.

3. Temperature controller 16 was also set at the desired temperature reading.

4. Particles were weighed.

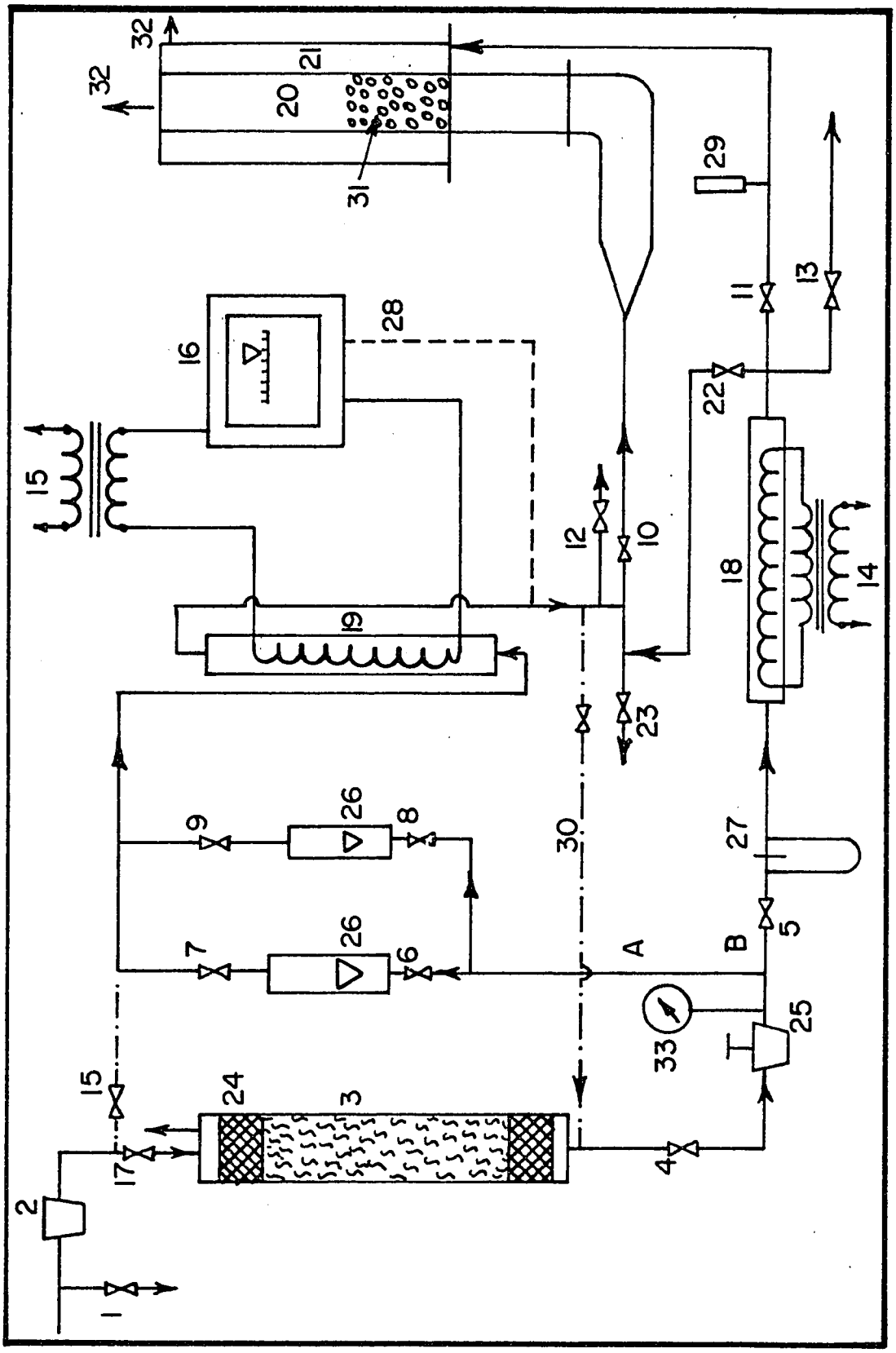

Fig. 8 Schematic diagram of the apparatus

Key to Numbers

1	Drain value
2	Oil filter
3	Silica gel column, air dryer
4	Valve used to cut off the main stream when regeneration of gel column was on
5	Valve leading to orifice
6,7,8,9	Valves for rotameters I and II
10,12	Valves leading to the fluidising columns
11,13	Valves leading to the jackets
14,15	Powerstats
16	Temperature controller
17	Main valve leading to the setup
18,19	Preheaters
20	Fluidizing column
21	Jacket of fluidizing column
22	By-pass
23	Exhaust
24	Glass wool
25	Pressure regulator
26	Rotameter I and II
27	Orifice
28	Thermocouple
29	Thermometer

30	Regeneration line
31	Fluidising particles
32	Exhausts from fluidising column
33	Pressure gauge

5. Cold junctions : thermocouples were prepared by surrounding the junction with freshly crushed ice. The temperature of the ice was measured by a potentiometer. A little water was added to make the ice mixture homogeneous and to bring it to its melting point. Water from the melted ice was siphoned from time to time.

6. The weighed solid particles were poured down into the column with utmost care.

7. Temperature recorder was checked and oiled if necessary.

8. Oil filter was drained.

9. Rotameters were drained and cleaned.

10. Positions of measuring point in the bed were checked and readjusted.

During the time the above mentioned steps were carried out, water in the line was completely drained.

11. The exhaust valve 1 was then shut off and the main valve 17 leading to the setup was opened. However, the valves 10 or 12 leading to the fluidizing column and 11 or 13 leading to the jackets remained closed while valves 22 and 23 were opened. The air streams thus passing through the meters, gauges, heaters, still by-passed the fluidizing column and jacket. The air was by-passed in order to preheat it to

the desired temperature and maintain it at that temperature for a short period of time.

12. The preheaters 18 and 19 were turned on. The preheated air was allowed to by-pass the column until such a time that the air coming out of the preheating column was at the desired fluidizing temperature.

13. Once the air was preheated to the desired fluidizing temperature, the valves 10 and 11 leading air into the fluidizing column 20 and jacket 21 were opened and the exhaust or by-pass valves 22,23 were shut off.

14. The initial time at the start of the run was taken at the time when the preheated air was introduced into the fluidizing column.

15. The run was allowed to proceed for two hours. The temperature of the ice bath housing thermocouple junction was checked from time to time and water was drained and fresh ice was added.

16. After two hours, the heaters were shut off and particles allowed to cool down for a cooling run. The end of a heating run was the initial point for a cooling run. The time at this change over was noted.

Measurement of the Expanded Bed Height and the Bed Settled Height

Bed settled height measurements were carried out in the fluidizing column 20. For each settled height, two readings were taken, one before a run and one after the run. The average of the two was taken as the reading of the settled height. The actual measurement then proceeded as follows: A comparatively large amount of air at a high rate of flow was allowed to pass through the fluidized bed in order to fluidize for a few minutes. The air stream was next shut off gradually in order to obtain an even distribution of all the particles across the cross sectional area of the column. This was also found to be the best method for measuring the height of a packed bed and equally well applicable to settled beds in fluidized beds. In the present work, the bed height was measured by a meter stick where the tip was partially wetted. The wetted portion was then lowered down to the bed where it barely touched the surface of the particle layer. Knowing the original length of the column, the height of the fluidizing bed was then evaluated. It was then compared with measurements made on the transparent glass column.

The expanded bed heights could not be measured directly from the metal fluidizing column but were measured from a transparent glass column. The design of the column, the materials used for fluidizing,

the fluid flow rates and the quantities of materials used were all similar to metal column in which heat transfer rates were measured. For each set of runs, three visual observations were made and the average of these was incorporated into the calculations. The data were taken for different bed heights for different flow rates. Figure 13 is an illustration showing the relationship between the expanded bed height as a function of flow rate.

Materials Used:

Glass beads from 3M Microbeads Company, silica gel from Fisher Scientific and fused aluminum oxide from Carborundum were used for fluidization studies. Most of the pertinent data for these materials were supplied by the manufacturer and some was obtained in the laboratory. Table I shows the characteristic properties of the materials. Particle diameters were screen analysed in the laboratory, the equations used for calculating the mean particle diameter were:

$$A_p = \frac{6\, W_s}{\rho_s\, D_p} \qquad (48)$$

and

$$D_p = \frac{1}{\sum \frac{X_i}{D_{pi}}} \qquad (48a)$$

Table I Pertinent Properties of Solid Particles

Solid	D_p	ρ_s	k_s	C_{p_s}	Shape
glass	0.0039	93.6	0.605	0.27	Spheres
beads	0.0110	93.6	0.605	0.27	Spheres
	0.0185	93.6	0.605	0.27	Spheres
Silica	0.06569	8.5	0.013	0.22	Spherical
gel	0.2324	8.5	0.013	0.22	(approx. factor 0.7 - 0.9)
Alumina	0.0164	206	1.8	0.20	Granular
	0.2411	206	1.8	0.20	Granular

V RESULTS

A time dependent heat balance on the fluidized bed is:

$$W_g C_{p_f} \frac{dT_g}{d\Theta} + W_s C_{p_s} \frac{dT_s}{d\theta} =$$

$$W_g C_{p_f} (T_1 - T_2) - q_l - q_r \qquad (49)$$

where $dT_s/d\theta$ = slope taken from a temperature-time curve (Figure 9) at a time interval θ = 60 minutes

W_g = mass flow rate of gas entering the bed

W_s = mass of solid

T_1, T_2 and T_s = Temperature of the inlet gas, outlet gas and fluidized bed respectively

C_{p_s} and C_{p_f} = heat capacity of solid and fluid respectively

q_l = heat lost to the surroundings

q_r = heat lost due to chemical reaction

The time dependent heat accumulation term is negligible compared to the heat accumulation term of the solid. The first term on the left hand side of equation (49) is therefore dropped out. Since no chemical reaction took place, q_r term has been disregarded. In terms of the driving force ($\triangle T$) and heat transfer area (A_t), the overall heat transfer coefficient U (θ) is:

$$W_s C_{p_s} \frac{dT_s}{d\theta} = U(\theta) A_t \quad T \qquad (50)$$

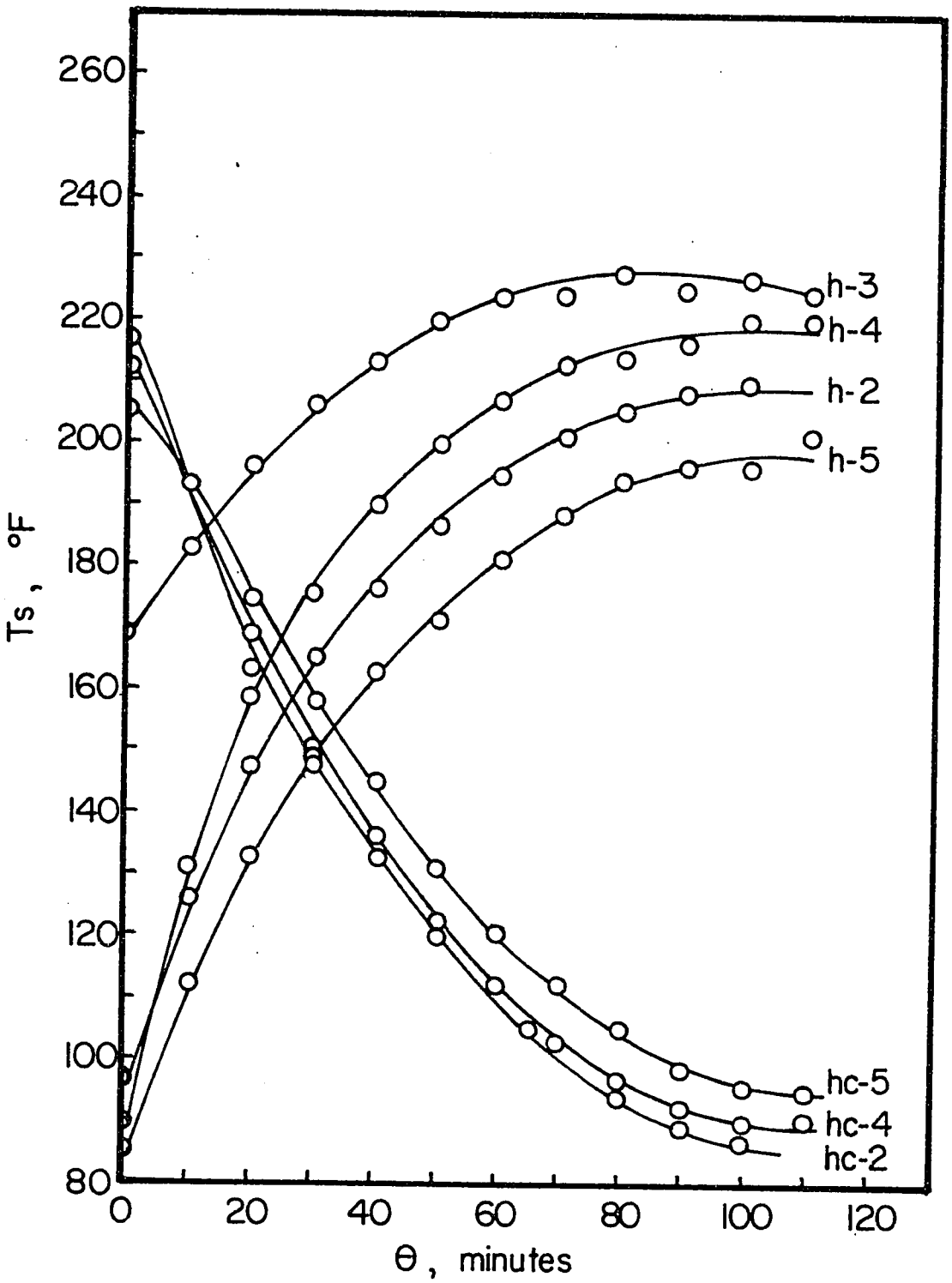

Fig. 9 Temperature-time curves of a few runs

where

$$\Delta T = \frac{(T_1 - T_s) + (T_2 - T_s)}{2} \tag{51}$$

Combining equations (49) and (50), we have

$$U(\theta) A_t \Delta T = W_g C_{p_f} (T_1 - T_2) - q_1 \tag{52}$$

Substituting equation (51) and (52) and evaluating U we have

$$U(\theta) = \frac{2 W_g C_{p_f} (T_1 - T_2) - 2 q_1}{A_t [(T_1 - T_s) + (T_2 - T_s)]} \tag{53}$$

Defining

$$1 - n = \frac{T_1 - T_2}{T_1 - T_s} \tag{54}$$

and dividing the numerator and denominator of (53) by $T_1 - T_s$, and combining with equation (54) we get

$$U(\theta) = \frac{2 W_g C_{p_f} (1 - n)}{A_t (1 + n)} - \frac{2 q_1}{A_t (1 + n) (T_1 - T_s)} \tag{55}$$

Equation (55) requires two kinds of information, namely, values of $(1 - n)$ and q_1. Rewriting equation (49) as:

$$T_1 - T_2 = \frac{W_s C_{p_s} \frac{dT_s}{d\theta}}{W_g C_{p_f}} + \frac{q_1}{W_g C_{p_f}} \tag{56}$$

and dividing both sides of the equation by $(T_1 - T_s)$ we have

$$(1 - n) = \frac{W_s C_{p_s} \frac{dT_s}{d\theta}}{W_g C_{p_f} (T_1 - T_s)} + \frac{q_1}{W_g C_{p_f} (T_1 - T_s)} \tag{57}$$

To evaluate the first term of equation (57) temperatures were measured at intervals of every five minutes by the 12 point temperature recorder. Temperature-time curves were plotted for each run. Some of such curves are presented in Figure 9. Slopes of tangents drawn to the temperature-time curves were taken at time θ = 60 minutes. This was representative of the mean value of the middle portion of a run which lasted for about 2 hours. These slopes were then used in evaluating the values of

$$W_s C_{p_s}\left(dT_s/d\theta\right) \tag{58}$$

The values of q_1 were evaluated as follows:

Making energy balances around Figures 10 and 11, we have:

Figure 10

$$W_g C_{p_f} (T_1 - T_2) - q_1 = W_s C_{p_s} \frac{dT_s}{d\theta} \tag{59}$$

Figure 11

$$W_g C_{p_f} (T_1 - T_2) + W_g C_{p_f} (T_{j1} - T_{j2}) - q_{ins.}$$

$$= W_s C_{p_s} \frac{dT_s}{d\theta} + C_j L_{ex} \frac{dT_{j,\,avg.}}{d\theta} \tag{60}$$

where $T_{j,\,avg.}$ is the average temperature for the bed and jacket hardware. Combining equations (59) and (60):

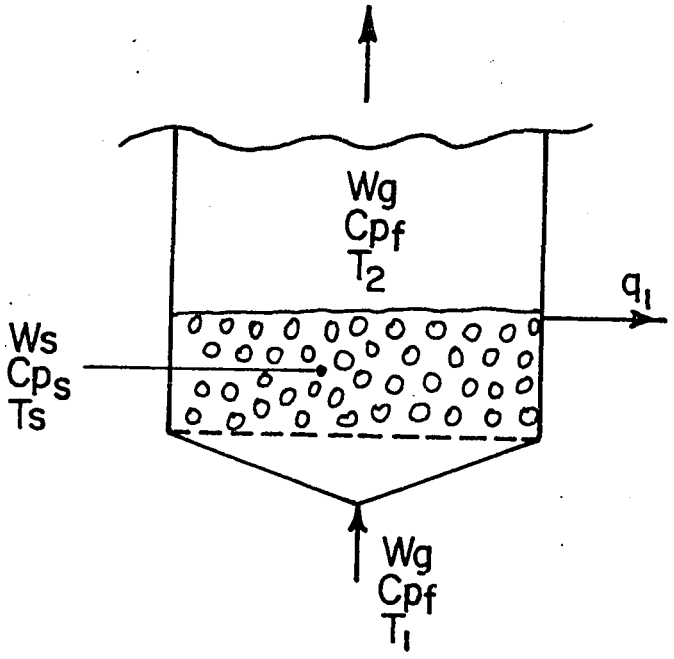

Fig. 10 Schematic section of isolated reactor

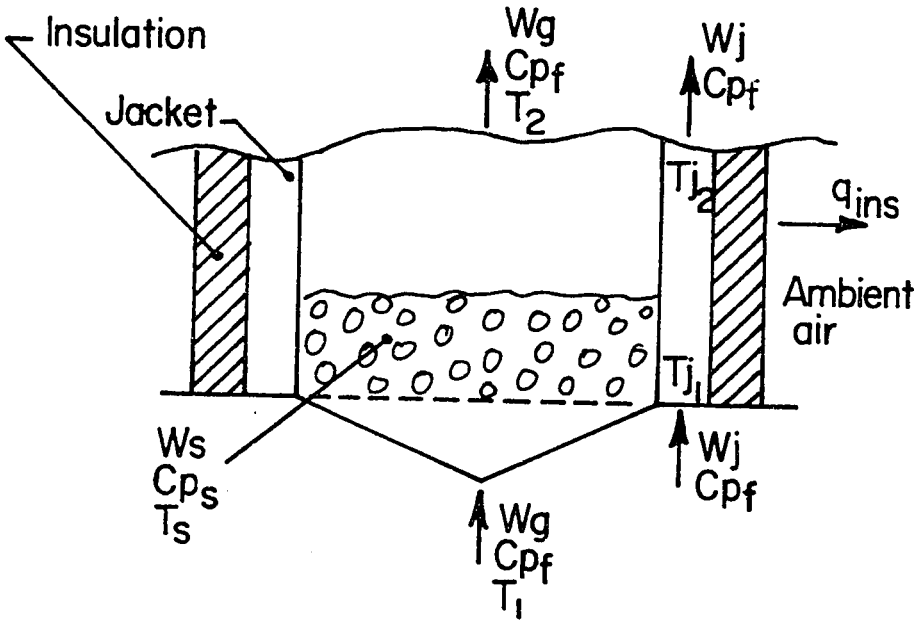

Fig. 11 Schematic diagram of reactor with jacket and insulation

$$q_1 = C_j L_{ex} \frac{dT_{j,\,avg.}}{d\theta} - W_j C_{p_g} (T_{j1} - T_{j2}) + q_{ins.} \tag{61}$$

The average temperatures for bed and jacket hardware, $T_{j,\,avg.}$ were obtained from the empirical equations

$$T_{j,\,avg.} = 2.1\% \left(T_{room} + \frac{\Delta T_{ins.}}{2} \right) + \frac{59.8\%}{2} \left[\frac{5}{3} \left(T_{room} + \Delta T_{ins.} \right) + \frac{1}{3} T_j \right] + 38.2\% T_s \tag{62}$$

$$T_{j,\,avg.} = 4.65\% \left(T_{room} + \frac{\Delta T_{ins.}}{2} \right) + \frac{71.2\%}{2} \left[\frac{5}{3} \left(T_{room} + \Delta T_{ins.} \right) + \frac{1}{3} T_j \right] + 24.14\% \tag{62a}$$

Equation (62) was for the four inch column and (62a) was for the two inch column.

T_{room}: ambient room temperature

$\Delta T_{ins.}$: temperature drop across insulation

T_j : temperature of jacket stream air

Equation (62) and (62a) were obtained by combining various resistances and using the literature values of the thermal conductivities of insulation, jacket wall and reactor wall. The derivation of equations (62) and (62a) is given in Appendix B.

The heat capacity of the jacket was evaluated from a blank run. The values of C_j were calculated by following an identical procedure except that in this case no solid material was fluidized in the system. A heat balance for such a system with a blank run gave the following equation:

$$C_j L \frac{dT_{j,\,avg.}}{d\theta} = W_g C_{p_f} (T_1 - T_2) + W_j C_{p_f} (T_{j1} - T_{j2}) - \left(\frac{k_i}{L_i}\right) A_{ins.} \Delta T_{ins.} \qquad (63)$$

where $\left(\frac{k_i}{L_i}\right)$ had a value of $0.0048 \frac{Btu}{min\ ft^2\ °F}$.

The value of $\frac{dT_{j,\,avg.}}{d\theta}$ was evaluated by measuring the slope of the tangent to the curve at a time interval (θ) of 60 minutes. The curve was obtained by plotting $T_{j,\,avg.}$ values against θ from Table C-1, Appendix C.

The value of C_j was obtained from equation (63) by making the appropriate substitutions. Such a calculation is shown in Appendix C.

Having thus determined the heat capacity of the jacket hardware, C_j, the other terms of equation (61) were evaluated as follows:

(i) $T_{j,\,avg.}$ was calculated at different time intervals for each run. Such a calculation is shown in Table 2 for a particular run.

(ii) Calculated values of $T_{j,\ avg.}$ were then plotted against time in minutes (θ). Figure 12 shows some such characteristic plots.

(iii) Slopes of tangents to each of the characteristic curves $\frac{dT_{j,\ avg.}}{d\theta}$ were measured at the middle portion of a particular run, usually after 60 minutes.

(iv) Bed expanded height, L_{ex}, was determined separately from a transparent column under similar conditions to the 2 and 4 inch metal columns. For each bed settled height, a set of expanded bed heights for different flow rates and particle size were determined. A set of such data is shown in Figure 13.

(v) The term $W_j\ C_{p_f}\ (T_{j1} - T_{j2})$ was calculated from the inlet and outlet jacket temperatures.

(vi) $q_{ins.}$ was calculated from the temperature drop across the insulation layer, and the cross-sectional area corresponding to the expanded bed height. Appendix A shows such a calculation.

Having determined q_l and $(1 - n)$ as described above, U was calculated for the particular run from equation (55) by making appropriate substitutions. The dependence of U on the superficial fluid flow velocity, particle diameter, bed settled height, thermal conductivity and solid density was studied. All the results of the data and a sample calculation is shown in Appendix A.

Table II Data for Evaluating $T_{j,\ avg.}$

Run No. h3

0	(5)	(11)	(12)	T_j	T_s	T_w	$\Delta T_{ins.}$	$T_{j,\ avg.}$
0	131.0	132.5	151.0	138.0	169.5	129.0	52.0	145.0
10	151.0	146.0	168.0	155.0	183.0	146.0	69.0	160.0
20	169.5	166.0	178.0	171.2	196.5	166.0	89.0	177.5
30	179.5	176.0	185.0	180.2	173.0	179.5	102.5	176.3
40	189.5	183.0	189.5	213.0	190.0	113.0	113.0	197.6
50	196.5	186.0	191.0	191.2	220.0	193.0	116.0	202.2
60	200.0	190.0	194.5	194.8	223.0	200.0	123.0	207.3
70	203.0	193.0	196.5	197.5	223.0	200.0	123.0	207.5
80	206.5	193.0	196.5	198.7	228.0	206.5	129.5	212.9
90	206.5	194.5	196.5	199.2	225.0	206.5	129.5	211.8
100	208.0	201.0	196.5	201.8	226.5	208.0	131.0	213.4
110	210.0	196.0	198.0	201.3	223.0	210.0	133.0	213.0

Note: T_j is the arithmetic average of thermocouples (5), (11) and (12).

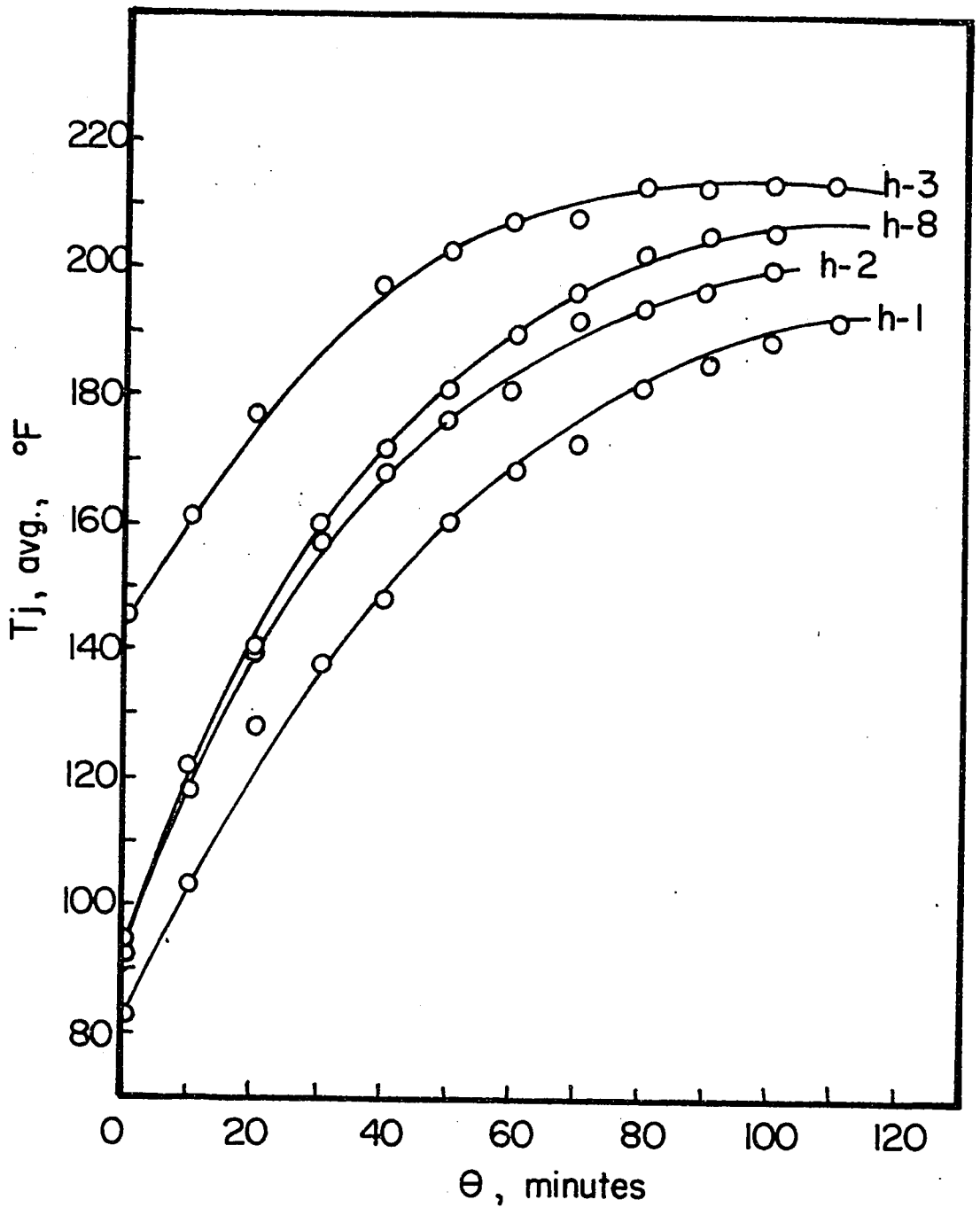

Fig. 12 $T_{j,\ avg.}$ - Time curves of a few runs

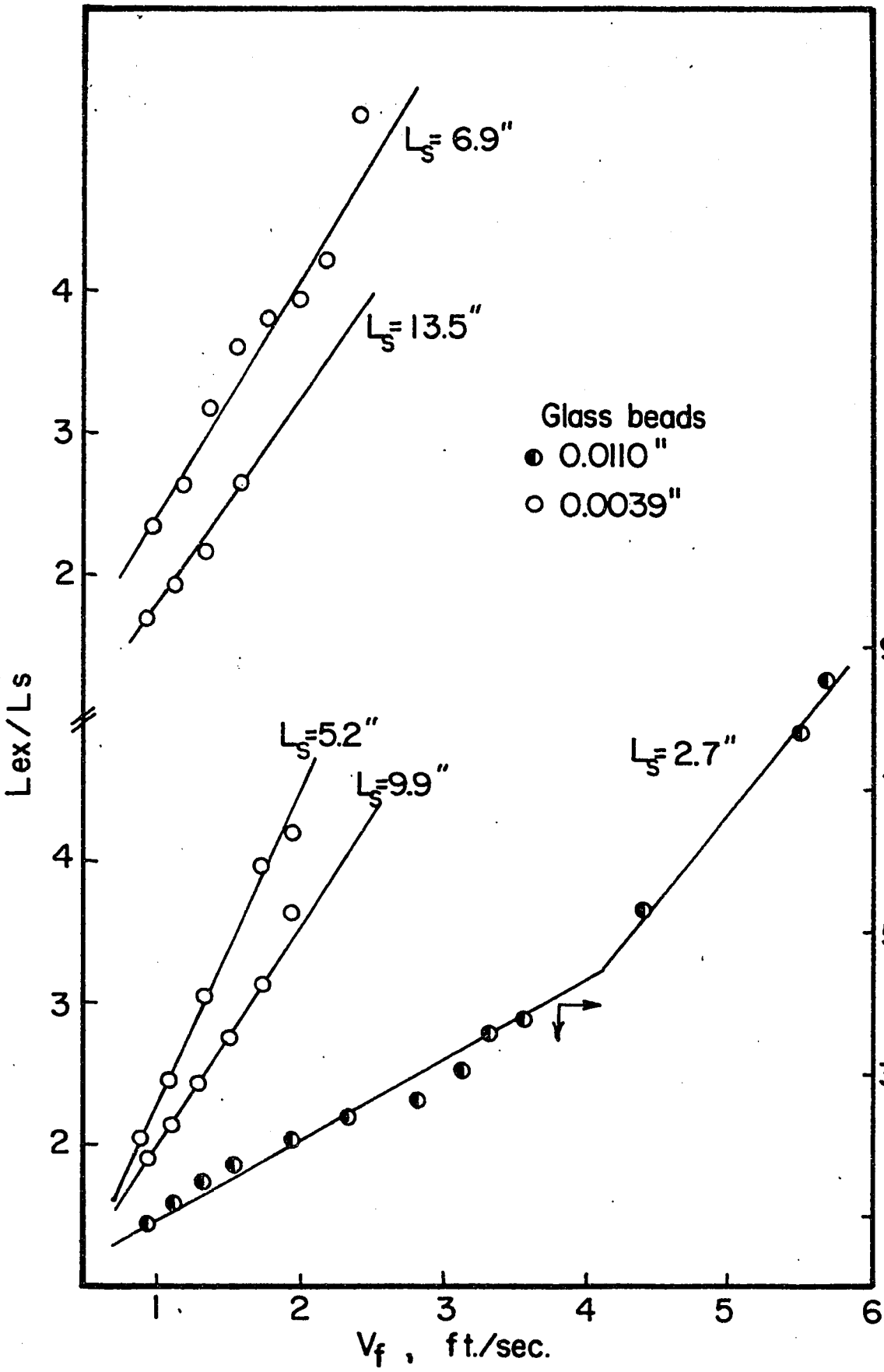

Fig. 13 L_{ex}/L_s versus fluid superficial velocities

VI CORRELATION

All the well known heat transfer equations for forced convection have been invariably derived from dimensional analysis. They are generally of the form

$$h = a \left(\frac{L}{D_t}\right)^{m} \left(\frac{DG}{\mu}\right)^{n'} \left(\frac{C_p \mu}{k}\right)^{p} (\Omega_1)^{q} (\Omega_2)^{r} \qquad (64)$$

where a is a constant; and m, n', p, q, r are exponential terms to the various functions.

In case of gas-solid fluidised systems, since the number of variables are several, the constant and the exponential terms are generally evaluated by a graphical method instead of the algebraic method. In this particular study the variables involved, in combination with U, are formed into the following dimensionless numbers:

$$Nu = \frac{UD_p}{\mu_f} ; \frac{L_s}{D_t} ; \frac{D_s}{D_t} ; \frac{\rho_s}{\rho_f} ; \frac{k_s}{k_f}$$

$$Re = \frac{D_p V_f \rho_f}{\mu_f} ; \quad Pr = \frac{C_{p_f} \mu_f}{k_f}$$

Experimental results were correlated by using the functional relationship:

$$Nu = \text{function } (Re, Pr, L_s, D_p, k_s, \rho_s) \qquad (65)$$

Equation (65) can be correlated only when the variables are made dimensionless. While Prandtl number is in itself dimensionless, L_s and D_p

were converted into the dimensionless form of L_s/D_t and D_p/D_t by dividing each by D_t, where D_t is the diameter of the tube or the reactor. The physical properties, k_s and ρ_s of the solid were reduced into the dimensionless form k_s/k_f and ρ_s/ρ_f. Thus equation (65) was converted to the form:

$$(Nu)\,(Pr)^x \left(\frac{L_s}{D_t}\right)^m \left(\frac{D_p}{D_t}\right)^{n'} \left(\frac{k_s}{k_f}\right)^p \left(\frac{\rho_s}{\rho_f}\right)^q = \text{function (Re)} \qquad (66)$$

For a single sample, one particle diameter, at various bed-settled heights, all the terms, except $(Nu)\,(Pr)^x$ and (L_s/D_t) on the left hand side of equation (66) are constant. The value of x, exponential to Prandtl number, was evaluated by the method of trial and error and found to be 0.4. The plot which gave the best correlation of $(Nu)\,(Pr)^x$ to Re for the various bed settled height parameter is shown in Figure 16.

Bed-Settled Height

The exponent m in equation (66) was determined by cross plotting the settled bed heights of Figure 16 for different Reynolds numbers, that is, by plotting the (L_s) as abscissa against $(U\,D_p/\mu_f)\,(C_{p_f}\,\mu_f/k_f)^{-0.4}$ for various parameters of Reynolds number. Such a plot is shown in Figure 17. The slope of the lines of Figure 17 gave the exponential m as -1.324.

The term $(U D_p/\mu_f) (C_{p_f} \mu_f/k_f)^{-0.4} (L_s/D_t)^{1.3}$ was plotted against the modified Reynolds number for glass beads of three different particle sizes, and is shown in Figure 18.

Particle Diameter

The exponent n' to the term (D_p/D_t) in equation (66) was evaluated by cross plotting the values of D_p from Figure 18, obtained for a particular Reynolds number. The particle diameter D_p was plotted as abscissa against $(U D_p/k_f) (C_{p_f} \mu_f/k_f)^{-0.4} (L_s/D_t)^{1.3}$ for various parameters of Reynolds numbers. Figure 19 shows such a plot. The exponent n was thus evaluated to be 4.292 from the slopes of the lines.

In Figure 20, Reynolds numbers have been plotted against the term $(UD_p/k_f) (C_{p_f} \mu_f/k_f)^{-0.4} (L_s/D_t)^{1.3} (\frac{D_p}{D_t})^{-4.3}$ for the various materials fluidized. Most of the experimental points fell on a smooth curve.

Thermal Conductivity

The group $(UD_p/k_f) (C_{p_f} \mu_f/k_f)^{-0.4} (L_s/D_t)^{1.3} (D_p/D_t)^{-4.3} (k_s/k_f)^p$ obtained by interpolation from Figure 21, was plotted against ρ_s/ρ_f for constant Re and for $p = 1.7, 2, 4$ correspondingly. Such a plot is shown in Figure 21. The best value of p giving a linear relationship occurred at $p = 4$. It would also be seen (Figure 22) that when data

$(UD_p/k_f)\,(C_p\,\mu_f/k_f)^{-0.4}\,(L_s/D_t)^{1.3}\,(D_p/D_t)^{-4.3}\,(k_p/k_f)^4$ was plotted using the exponential value of 4 for $(k_s/k_f)^4$, most of the data points fell on a smooth curve.

Solid Density

The value of exponential p was accepted as 4, and the term $(k_s/k_f)^4$ incorporated into the ordinate of Figure 22. $(UD_p/k_f)\,(C_{p_f}\,\mu_f/k_f)^{-0.4}\,(L_s/D_t)^{1.3}\,(D_p/D_t)^{-4.3}\,(k_s/k_f)^4$ values were plotted against ρ_s/ρ_f for the various solid material fluidised. Such a plot is shown in Figure 23. A value of 7.796 was obtained for exponential term q from the slope of the lines.

The final correlation is shown in Figure 24.

The physical and thermal properties of the fluid were evaluated at the average temperature of the run, while those of solids were supplied by the manufacturer, applicable for the temperature range used in the present investigation.

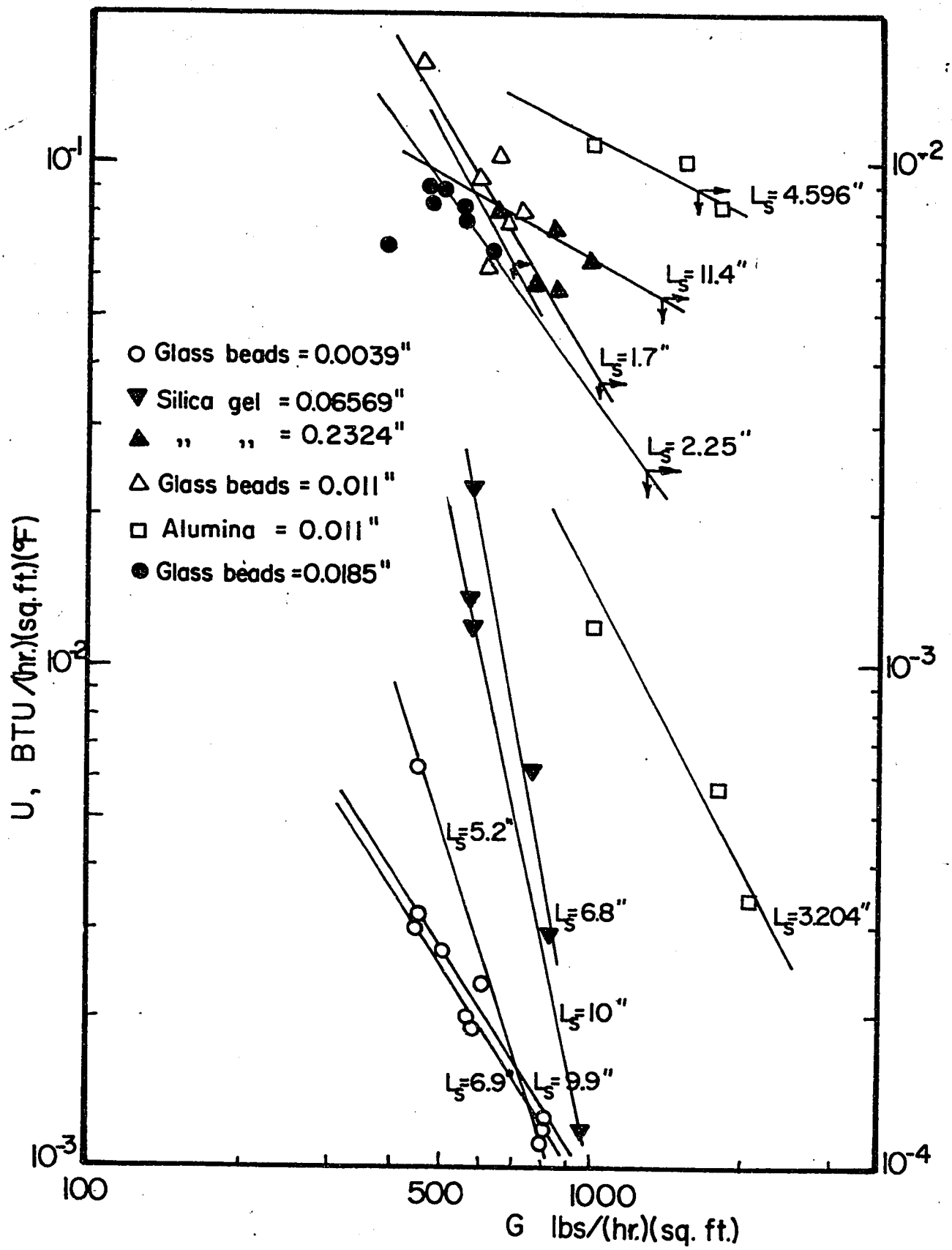

Fig. 14 Effect of mass velocity on heat transfer coefficient

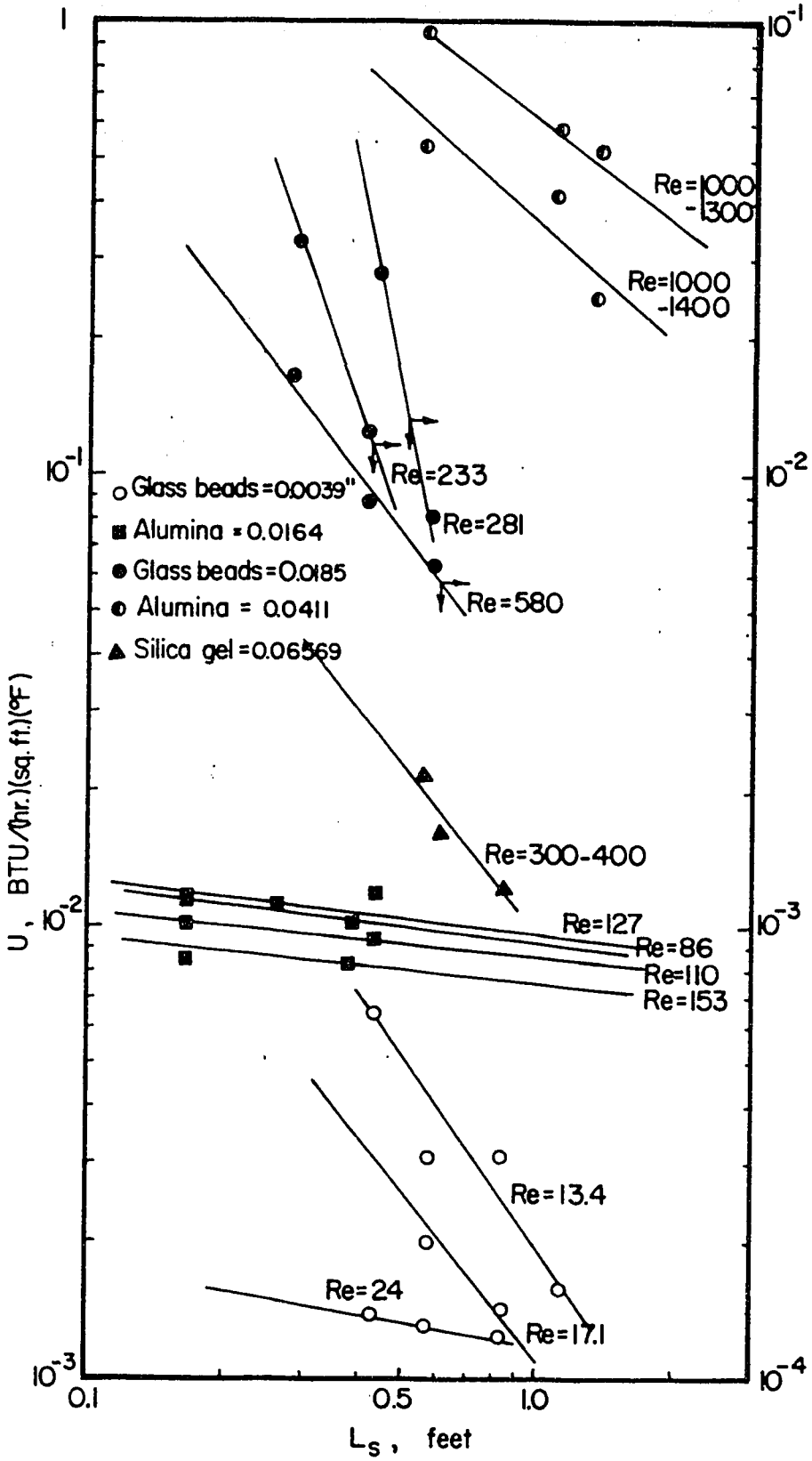

Fig. 15 Effect of bed-settled height on heat transfer coefficient

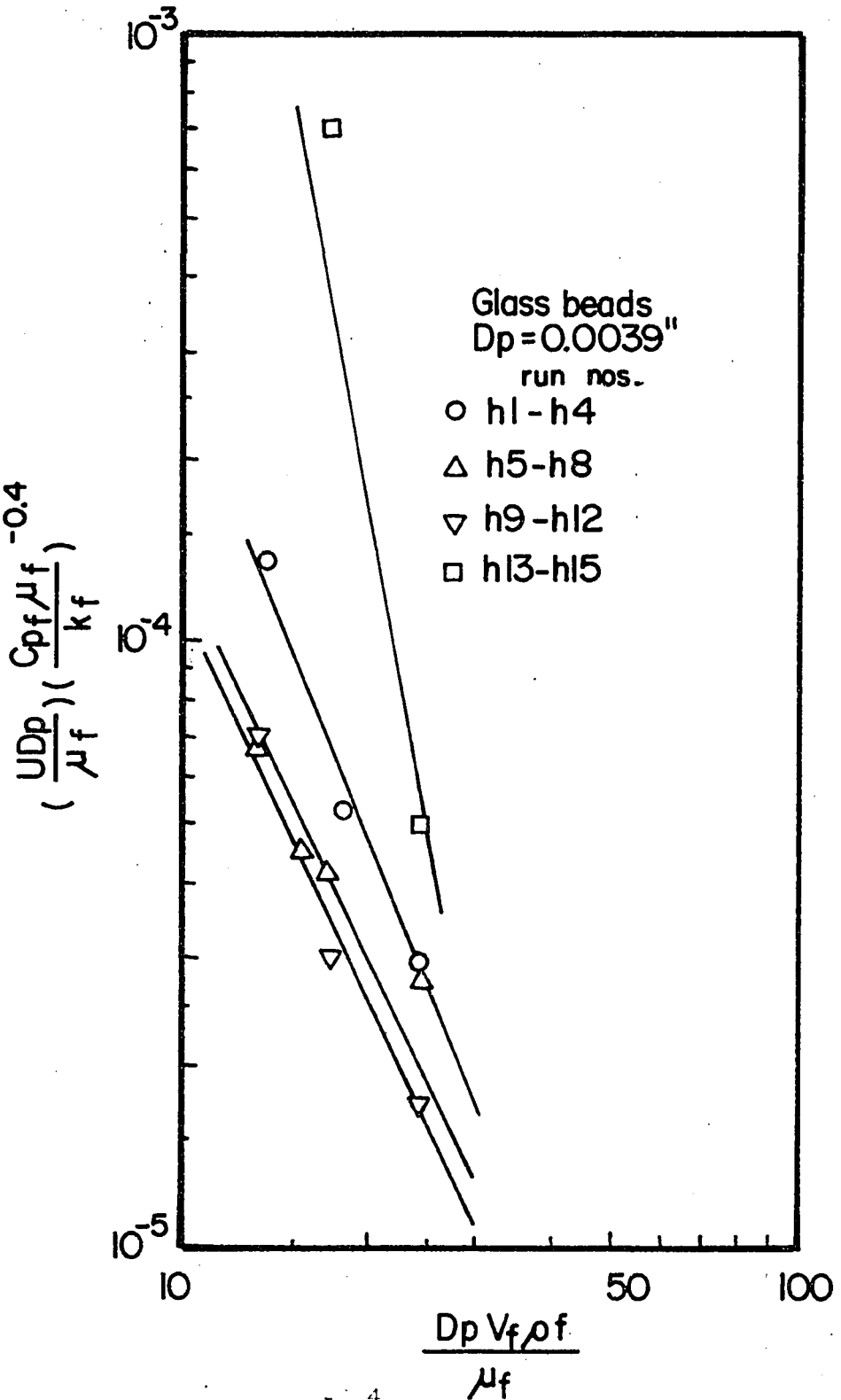

Fig. 16 $\left(\frac{U D_p}{\mu_f}\right)\left(\frac{C_{p_f} \mu_f}{k_f}\right)^{-0.4}$ versus $\left(\frac{D_p V_f \rho_f}{\mu_f}\right)$ for glass beads at constant D_p, different L_s

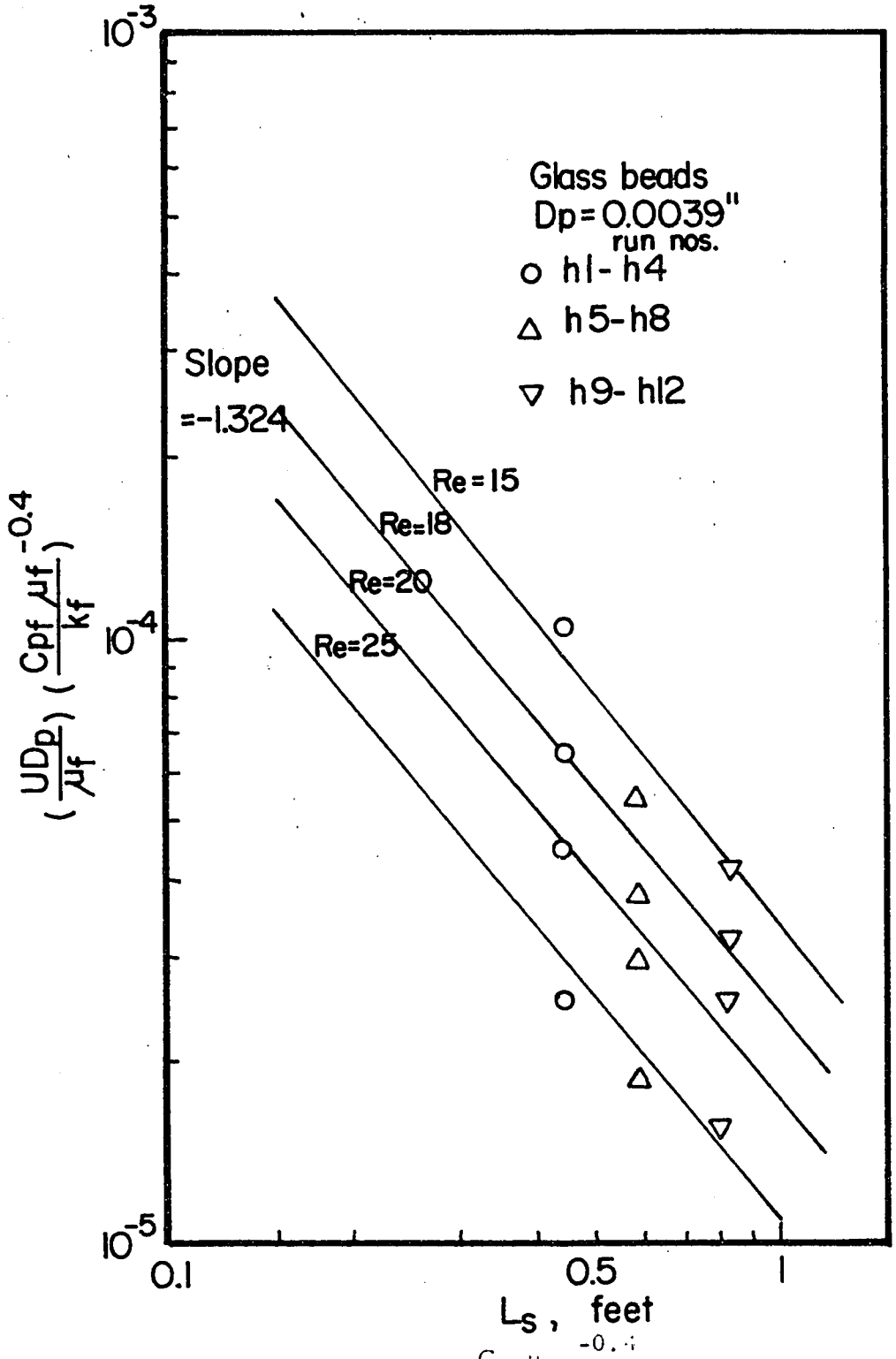

Fig. 17 Dependency of $(\frac{UD_p}{\nu_f})(\frac{C_{p_f}\mu_f}{k_f})^{-0.4}$ on L_s at various constant Reynolds number for glass beads

Fig. 18 $\left(\frac{UD_p}{\mu_f}\right)\left(\frac{C_{p_f}\mu_f}{k_f}\right)^{-0.4}\left(\frac{L_s}{D_t}\right)^{1.3}$ versus $\left(\frac{D_p V_f \rho_f}{\mu_f}\right)$

at different particle diameters

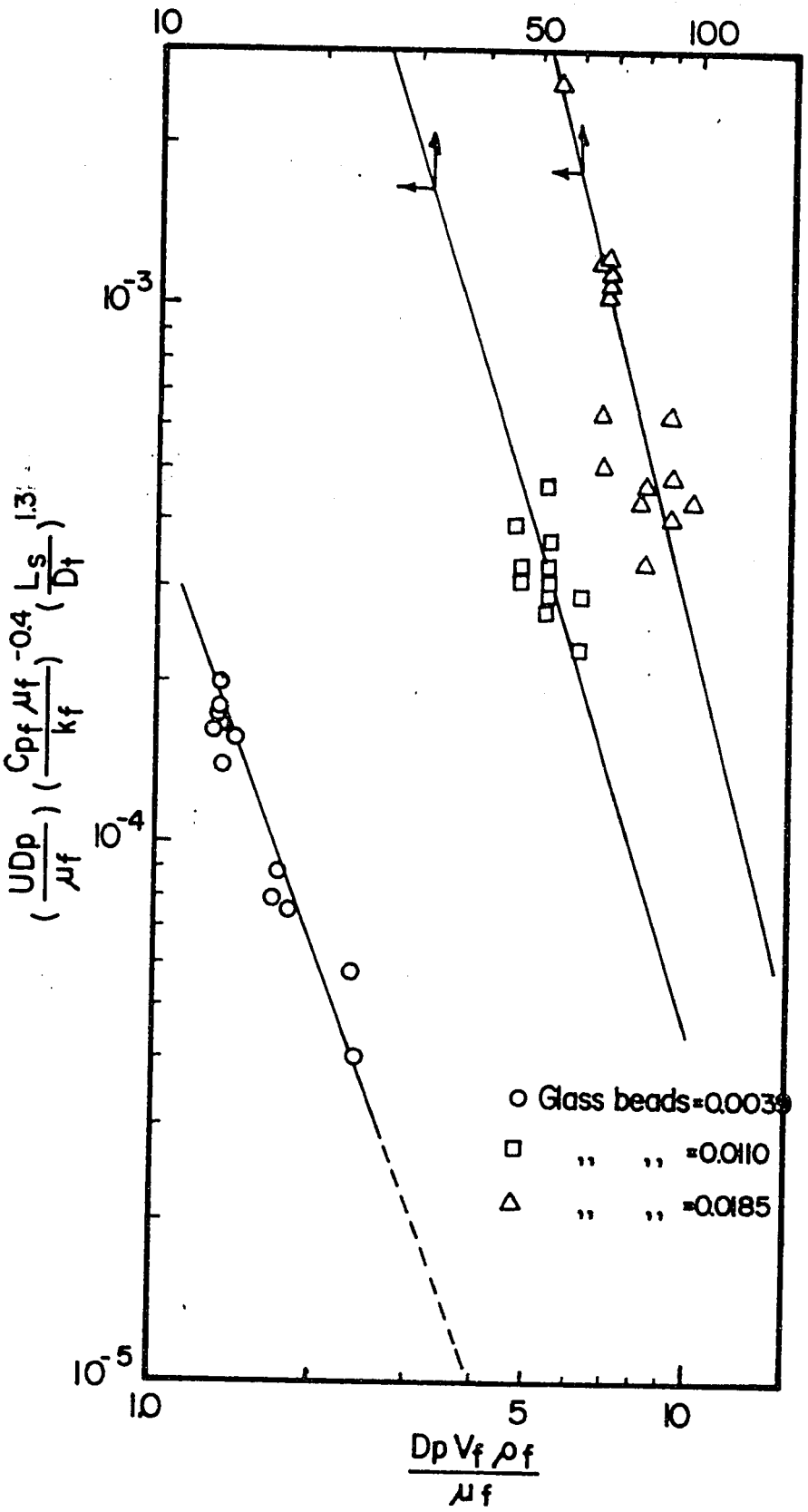
10
50
100
10^{-3}
10^{-4}
10^{-5}
1.0
5
10
$\frac{UDp}{\mu f}\left(\frac{Cpf\,\mu f}{kf}^{-0.4}\right)\left(\frac{Ls}{Df}\right)^{1.3}$
$\frac{Dp\,Vf\,\rho f}{\mu f}$
○ Glass beads=0.0039
□ ,, ,, =0.0110
△ ,, ,, =0.0185

Fig. 19 Dependency of $\left(\frac{UD_p}{\mu_f}\right)\left(\frac{C_{p_f}\mu_f}{k_f}\right)^{-0.4}\left(\frac{L_s}{D_t}\right)^{1.3}$ on D_p

at constant Reynolds number

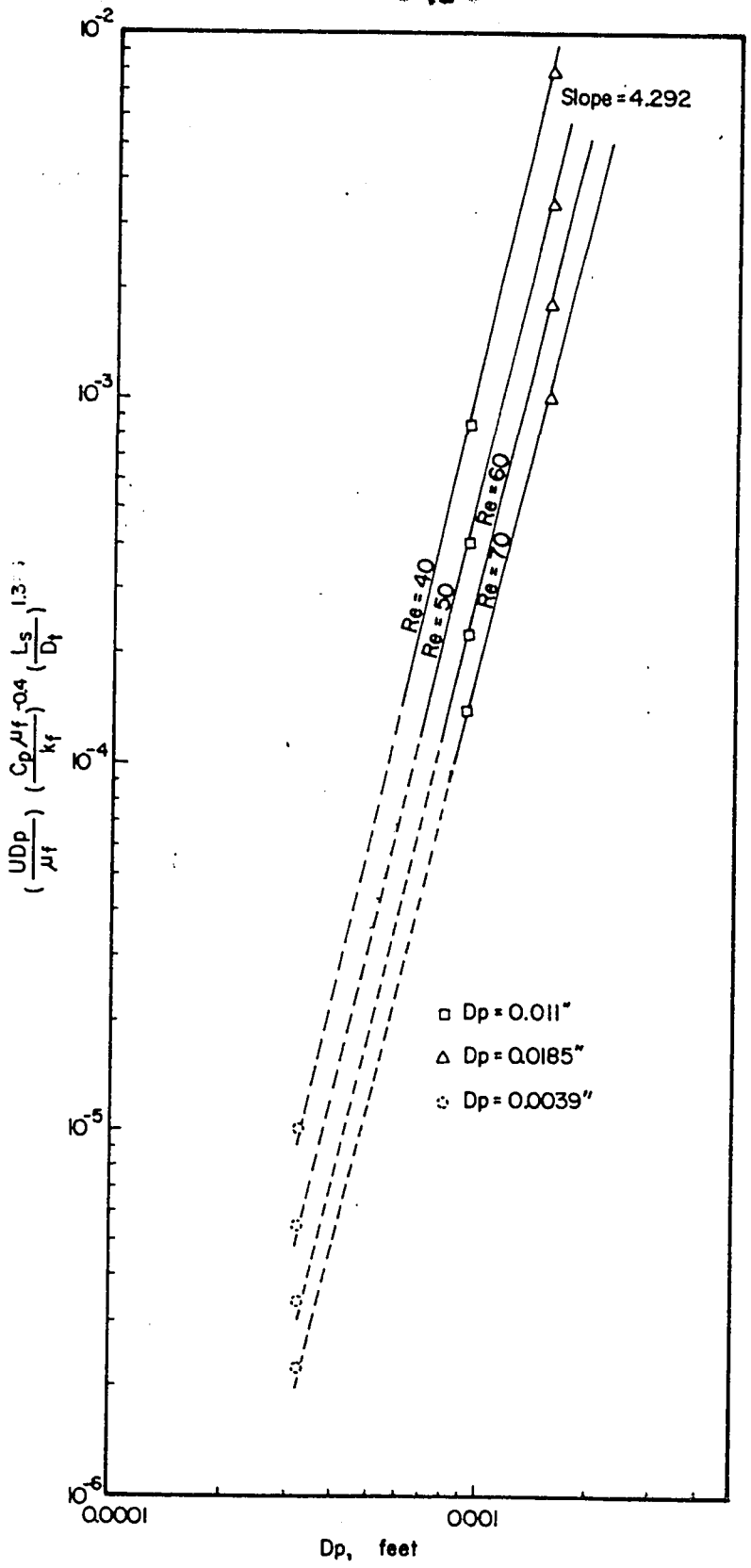
Slope = 4.292
Re = 40
Re = 50
Re = 60
Re = 70
□ Dp = 0.011"
△ Dp = 0.0185"
⁘ Dp = 0.0039"
10^{-2}
10^{-3}
10^{-4}
10^{-5}
10^{-6}
0.0001
0001
Dp, feet
$(\frac{UDp}{\mu f})(\frac{Cp\mu f}{kf})^{-0.4}(\frac{Ls}{Dt})^{1.3}$

Fig. 20 $\left(\frac{UD_p}{k_f}\right)\left(\frac{C_{p_f}\mu_f}{k_f}\right)^{-0.4}\left(\frac{L_s}{D_t}\right)^{1.3}\left(\frac{D_p}{D_t}\right)^{-4.3}$ versus

Reynolds numbers

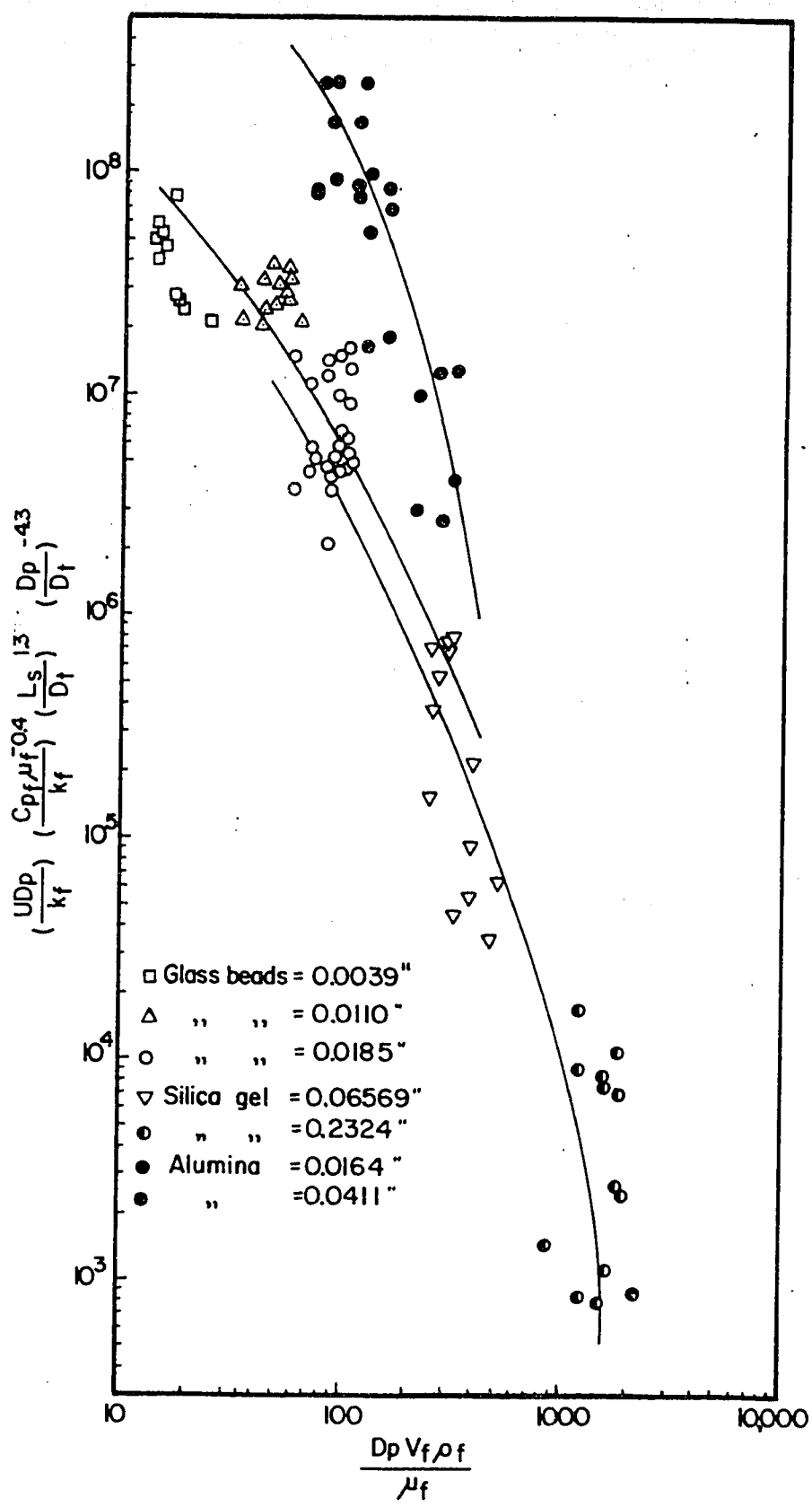
10^8
10^7
10^6
10^5
10^4
10^3
$\left(\frac{UDp}{k_f}\right)\left(\frac{C_{pf}\mu_f^{0.4}}{k_f}\right)\left(\frac{L_s}{D_t}\right)^{1.3}\left(\frac{Dp}{D_t}\right)^{-.43}$
□ Glass beads = 0.0039"
△ " " = 0.0110"
○ " " = 0.0185"
▽ Silica gel = 0.06569"
◐ " " = 0.2324"
● Alumina = 0.0164"
● " = 0.0411"
10
100
1000
10,000
$\frac{Dp\,V_f\rho_f}{\mu_f}$

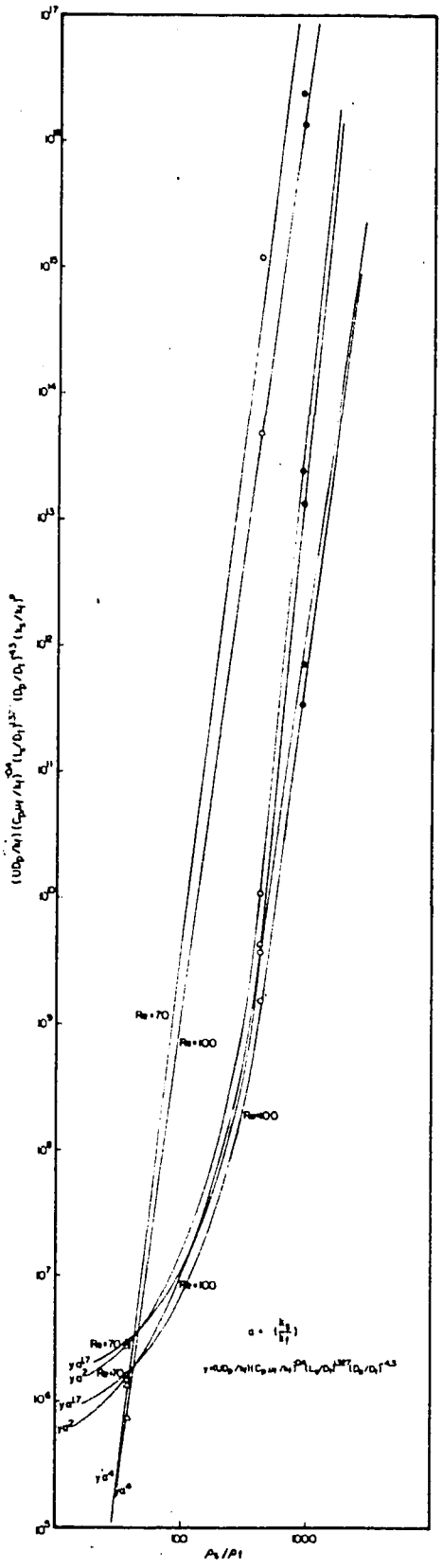

Fig. 21 Evaluation of the exponent of $(\frac{h_m}{k_f})$, p

Fig. 22 $\left(\frac{UD_p}{k_f}\right)\left(\frac{C_{p_f}\mu_f}{k_f}\right)^{-0.4}\left(\frac{L_s}{D_t}\right)^{1.3}\left(\frac{D_p}{D_t}\right)^{-4.3}\left(\frac{k_s}{k_f}\right)^{4}$ versus Reynolds numbers

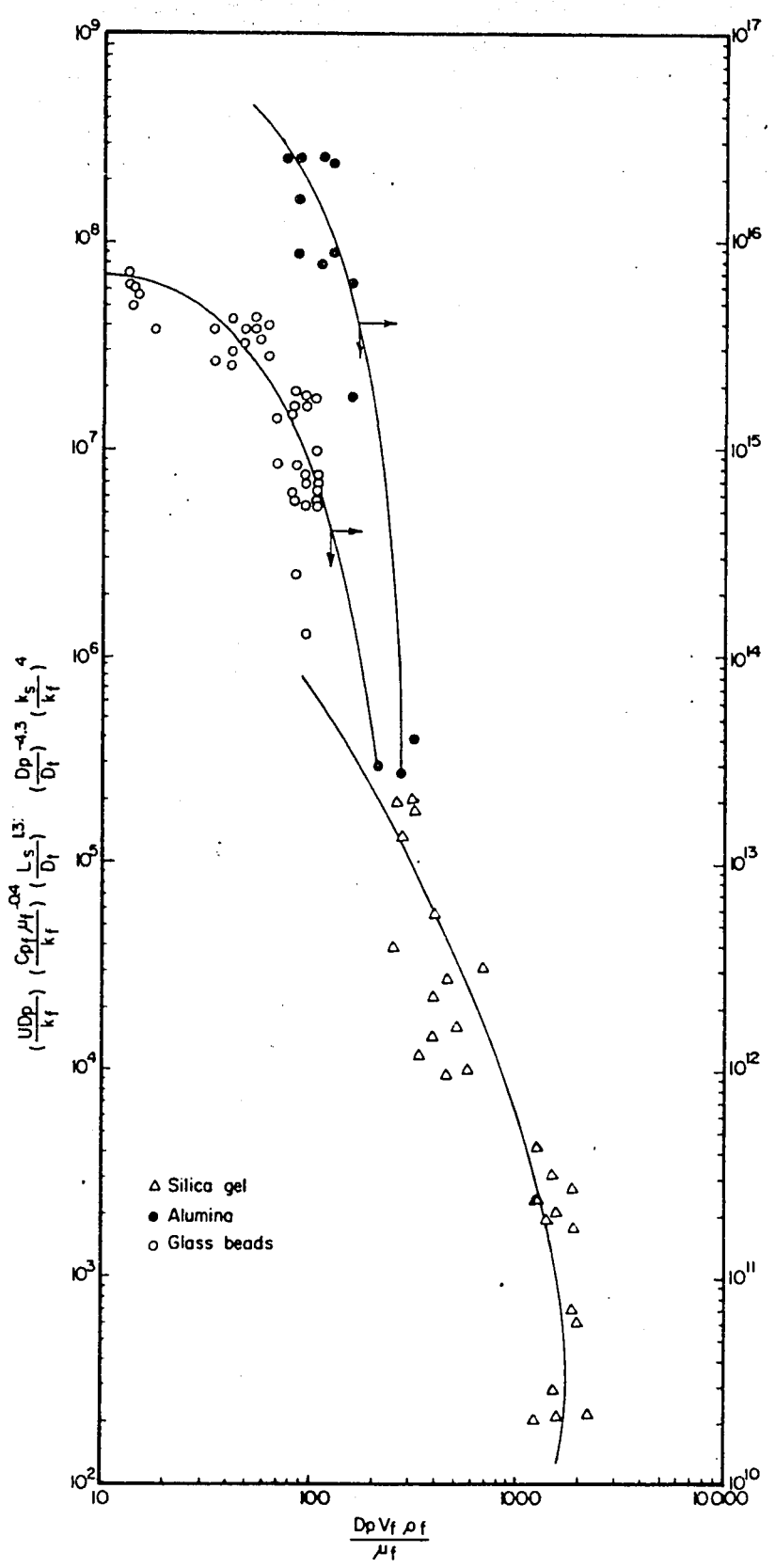
10^9
10^8
10^7
10^6
10^5
10^4
10^3
10^2
10^{17}
10^{16}
10^{15}
10^{14}
10^{13}
10^{12}
10^{11}
10^{10}
10
100
1000
10000
$\left(\frac{UDp}{k_f}\right)\left(\frac{C_{pf}\mu_f}{k_f}\right)^{.04}\left(\frac{L_s}{D_t}\right)^{1.3}\left(\frac{Dp}{D_t}\right)^{-4.3}\left(\frac{k_s}{k_f}\right)^4$
$\frac{Dp\,V_f\,\rho_f}{\mu_f}$
△ Silica gel
● Alumina
○ Glass beads

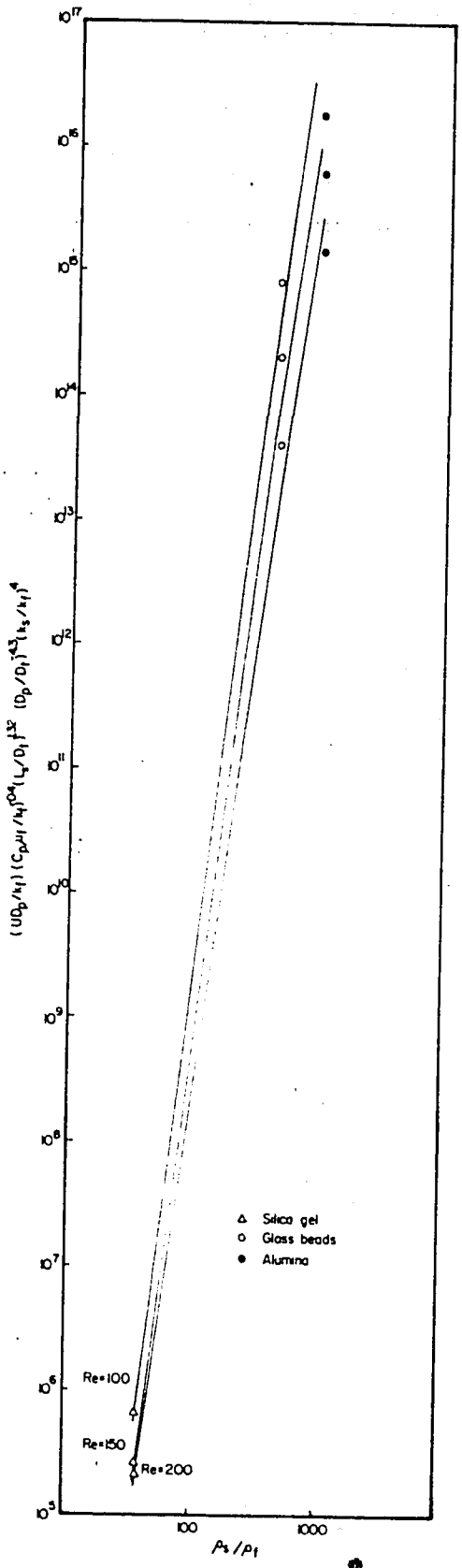

Fig. 23 Evaluation of the exponent of $(\frac{\rho_s}{\rho_f})$, q

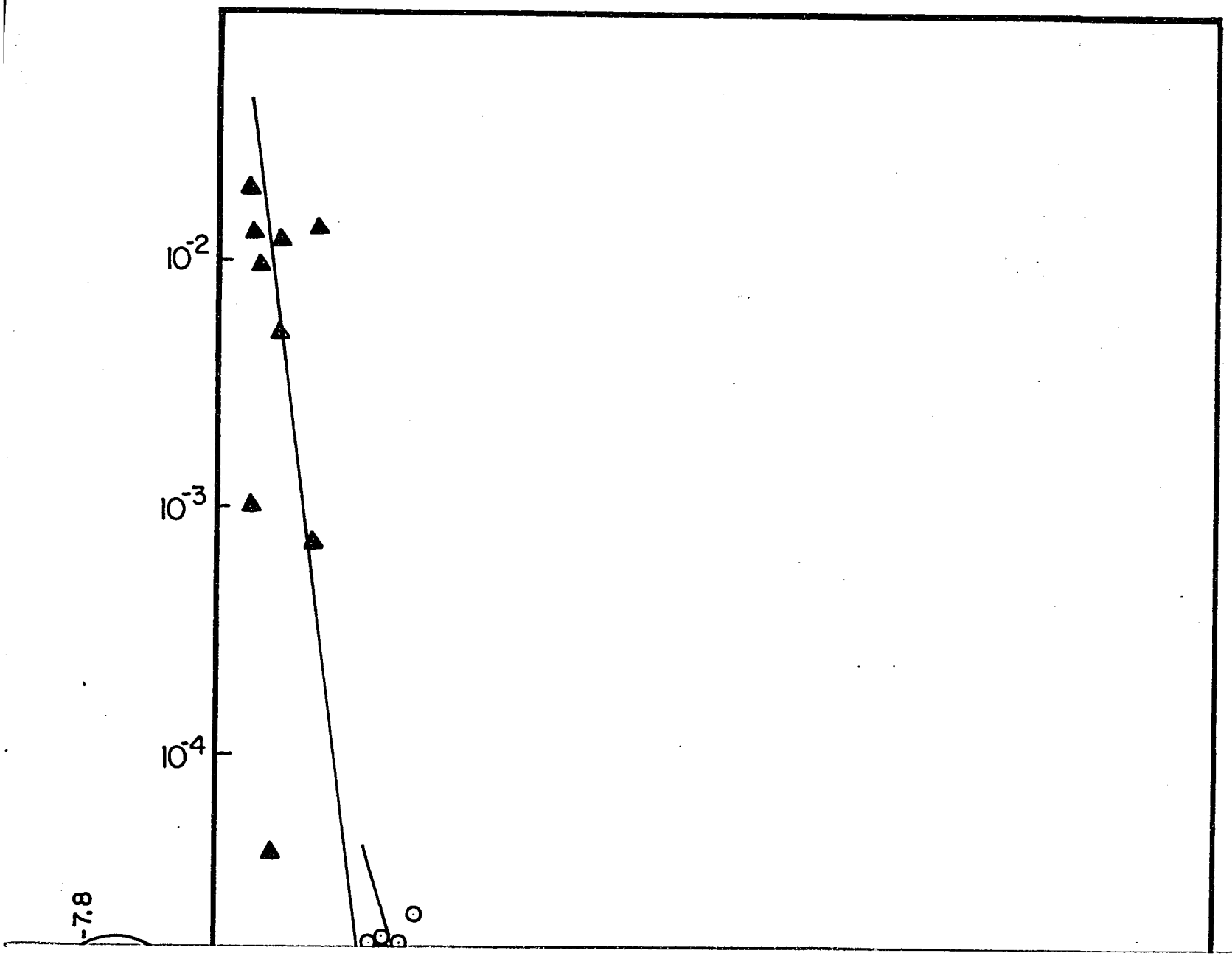
10^{-2}
10^{-3}
10^{-4}
-7.8
O

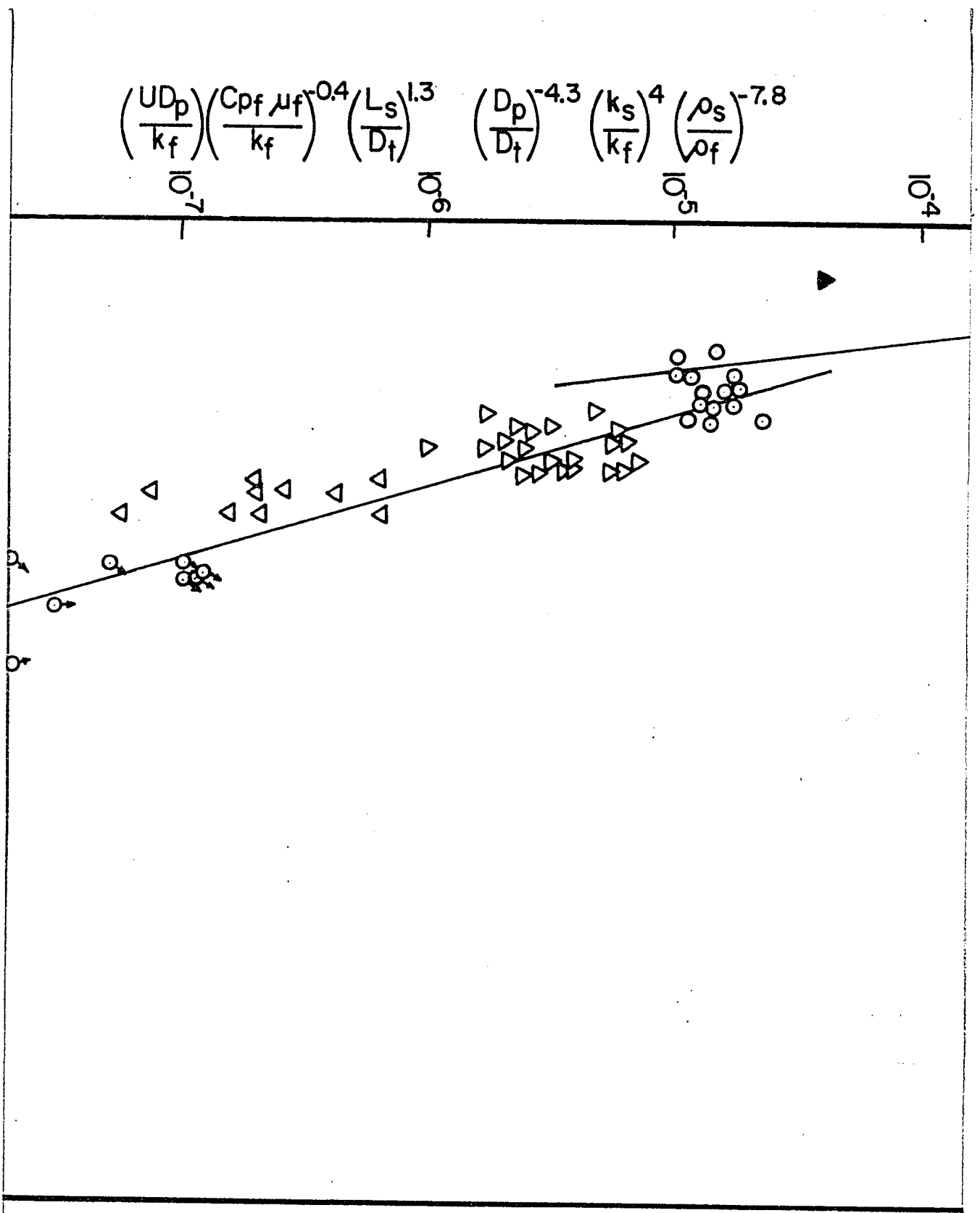
$\left(\frac{UD_p}{k_f}\right)\left(\frac{C_{pf}\mu_f}{k_f}\right)^{-0.4}\left(\frac{L_s}{D_t}\right)^{1.3}\left(\frac{D_p}{D_t}\right)^{-4.3}\left(\frac{k_s}{k_f}\right)^{4}\left(\frac{\rho_s}{\rho_f}\right)^{-7.8}$
10^{-7}
10^{-6}
10^{-5}
10^{-4}

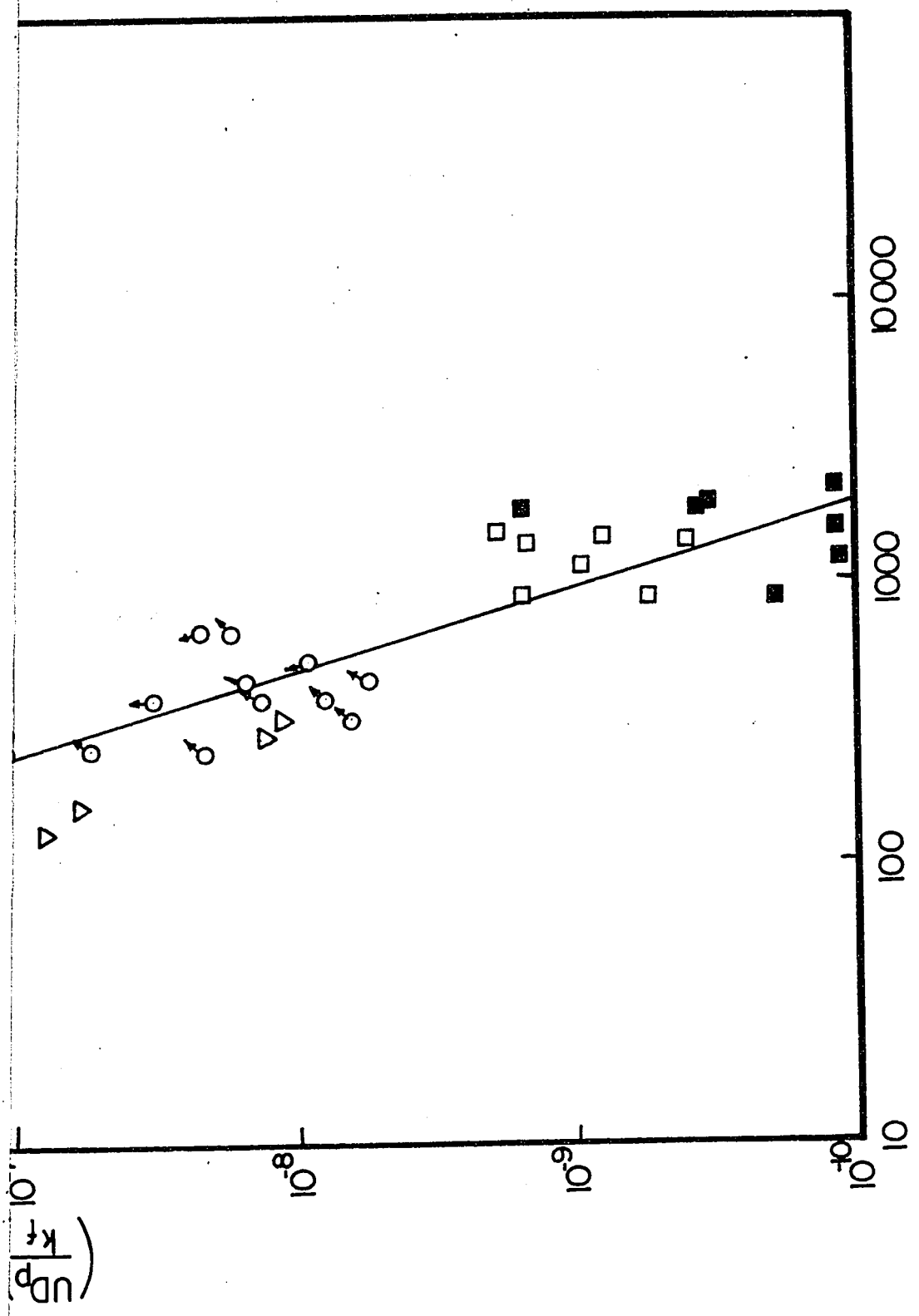

Fig. 24 Final Correlation

LEGEND FOR FIGURE 24

▲	glass beads	0.0039	inch
△	glass beads	0.0185	inch
⊙	glass beads	0.0110	inch
□	alumina	0.0411	inch
▽	alumina	0.0164	inch
♂	silica gel	0.06569	inch
▩	silica gel	0.2324	inch

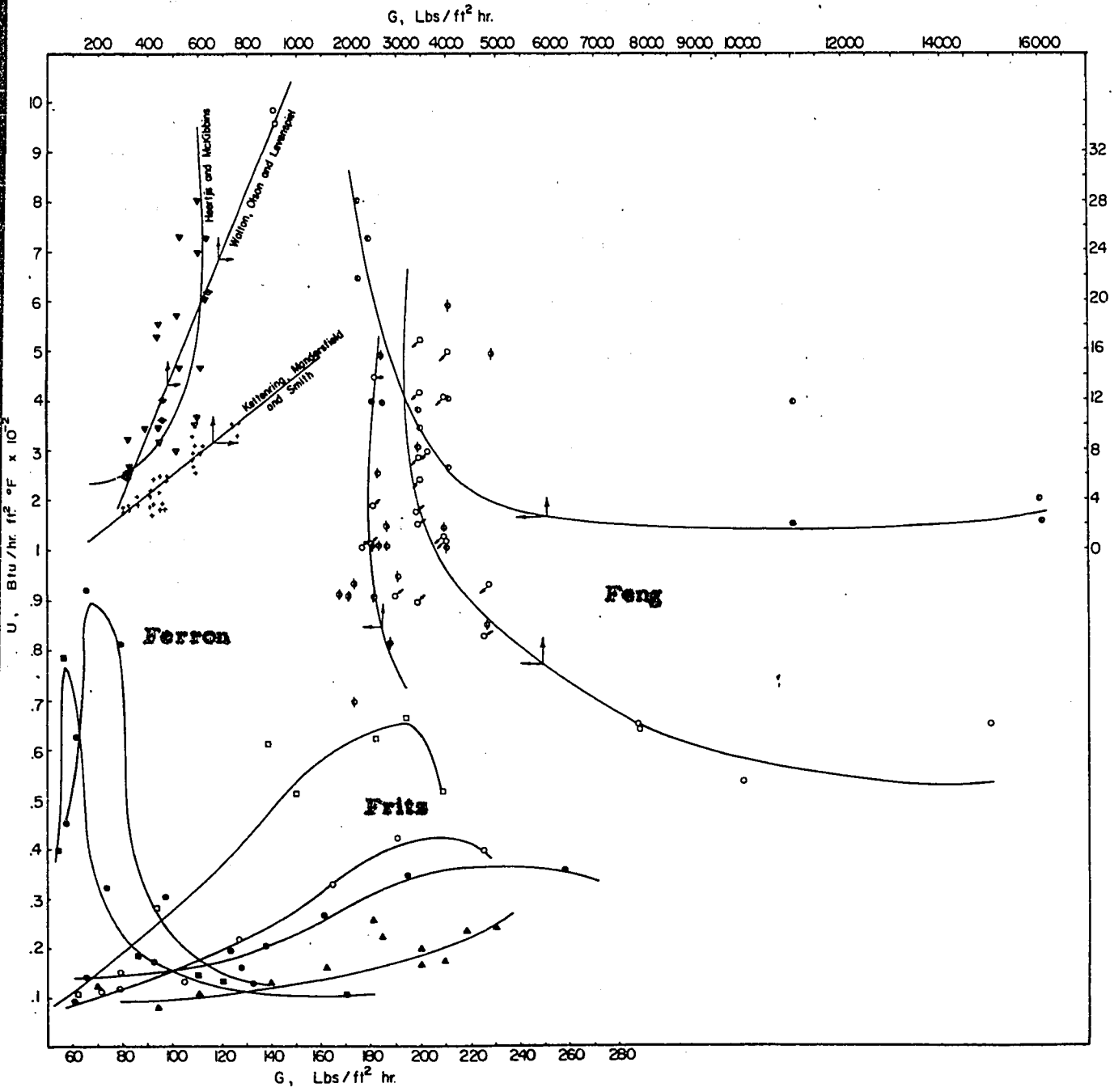

Figure 25 Comparison of Results

VII DISCUSSIONS

In order to simplify the calculations and derive a satisfactory correlation for heat transfer in terms of the parameters of the solid-fluid system, certain assumptions generally have to be made. The following three such assumptions were made in order to make the derivation of the correlation more realistic and simpler.

(1) The Prandtl numbers of the gases do not vary significantly over the temperature range studied.

(2) Temperature gradients within the particles are negligible compared with the film gradients.

(3) Sufficient particle mixing occurs, so that any time the temperature of the solid is uniform throughout the bed.

Although the thermal properties of gases, like specific heat, viscosity and thermal conductivity increase with temperature, the Prandtl number, $C_{p_f} \mu_f / k_f$, shows little variation with temperature. The value of $C_{p_f} \mu_f / k_f$ calculated at any single temperature serves sufficiently well for the solution of problems involving the same gas at another temperature within reasonable proximity.

The section on correlation follows the usual dimensionless numbers approach. Although it is not the best method employed, so far it is the most appropriate at the moment for the kind of data involved.

The prandtl number, although it does not vary significantly when only air is used, has been introduced in order to facilitate the use of the correlation in the future for different gases. It will very much enhance convenience in the future.

There is neither any data nor any technique available to measure the temperature gradients within single particles of smaller diameters. Since the particle diameters were very small, it has been assumed that the temperature gradients within the particles are negligible as compared to the surface film gradients.

It has been found by several investigators, Table G-1, and experimentally in the course of present investigations, Figure G-1, that temperature gradients existed at different bed heights and at radial locations in the bed within the threshold of the expanded bed height. However, the gradients were so small that they were considered insignificant, and thus negligible. Furthermore, it was recognized that there was a great deal of turbulence in the bed as a result of which the temperature would normally get equalized.

The bed temperature, which in this case also means solid temperature, is still a matter of sufficient controversy. Ketterering, Manderafield and Smith (33) assumed that the bed temperature was uniform and equal to the temperature of the gas leaving the fluidized bed. However, in the present investigation,

it was found that a screened thermocouple placed at the exit of the fluidizing column, showed considerable variations from temperatures indicated by thermocouples located right within the threshold of expanded bed height. Furthermore, even if the assumption was justified, it was found that the exit temperature T_2, was most uncertain and inaccurate to be measured.

Walton and Levenspiel (34) reported minimum and maximum heat transfer coefficients. If the bed temperature was assumed to be equal to that of a bare thermocouple immersed in the bed, the heat transfer coefficients thus calculated represented maximum limiting values. If the equilibrium temperature of the exit air was assumed as the bed temperature, the calculated heat transfer coefficient would be the minimum limiting value. The temperature indicated by a bare thermocouple has been considered to give an intermediate value between that of the solid and fluid, therefore the first assumption would be in contradiction to this. The second assumption encountered the same shortcoming as those of Kettenring.

Wamsley and Johanson (41) did not measure the bed temperature but calculated it from the time-temperature history curves of the inlet and outlet gas temperatures. Since the outlet temperature of the gas was uncertain, the values propagated from the curves would

also be uncertain, specially when no heat loss was corrected for.

Heertjes and McKibbins used bare thermocouples to indicate the temperature of the bed; again here the temperature indicated an intermediate value.

Rozental and Shakhova (45) used a bare thermocouple to indicate the temperature of the solid. The thermocouples were placed at different heights of the fluidised threshold. Again this gave an intermediate value between that of solid and fluid.

In order to circumvent the difficulties encountered by others, space-averaged solid temperature, T_s, was used in the present investigation. This temperature has been taken from screened thermocouples immersed in the fluidised threshold. This avoided the possibility of errors due to collision of cooler particles from the lower regions of the bed with the sensing element. The temperature of solids was thus assumed to be in equilibrium with the surrounding fluid.

For gas temperature, Kettenring, et al. used a bare thermocouple. Such a measurement is likely to give much erroneous results, since the sensing element of the thermocouple was in contact with the moving particles all the time. Such indicated temperature, thus could not be the true gas temperature.

Walton and Levenspiel used a suction thermocouple to measure the temperature of the gas, whereby a direct contact of the particles with the sensing elements was avoided. The fluid velocity traversing past the sensing elements would generally be much higher than the fluid velocity of the entire bed. Such higher velocities or turbulence would reduce the thickness of the boundary layer film at the surface of the thermocouple. A considerable part of the total energy of the gas stream would be in the form of kinetic energy and not all of this would be converted to thermal energy in the boundary layer around the thermocouple junction. As a result, the temperature indicated by the thermocouple would be lower than the suction stream temperature. Furthermore, the flow pattern in the suction stream would not be the true representative of the flow pattern in the fluidised stream.

Wamsley and Johanson measured the gas temperatures at the inlet and the outlet of the apparatus. Since the outlet temperature was not taken at the expanded bed height, it would not be truly representative of the gas temperature.

Rosental and Shakhova used a bare thermocouple to measure the inlet temperature of the gas. This temperature was not space-averaged and thus was not representative of the gas in the fluidised bed.

For the present investigation, although turbulence was assumed to have occurred and equalized the temperature of the bed, complete mixing was unlikely to have happened. A flow pattern of two phases, a dense phase and a dilute phase, was then assumed. The inlet temperature could easily be measured, but not the outlet gas temperature, as it would be shown later that the outlet temperature T_2 (Appendix F) could not be located properly. Therefore it was decided to evaluate the value of T_2 mathematically. Since the gas flow was not completely mixed, the temperature driving force would be

$$\Delta T = \frac{(T_1 - T_s) + (T_2 - T_s)}{2} \qquad (51)$$

Basically, the unsteady state method is not new, the present study does not claim it to be so. Other authors have chosen to use integrated equations for plotting their data whereas the present work has chosen to use the differential form. It has been shown experimentally and theoretically in Appendix E that by tedious calculations, there has been essentially no difference in the expected answer between that of an integrated form and a differential one.

In a recent review, Barker (44) has pointed out that the definition of T used by Watson and Ferron has yielded

an irrelevant heat transfer coefficient and thus resulted in U which is really not basic. It has also been pointed out that the total area of the bed was not effective in transfering heat - only a small, undetermined fraction of particles in the bed was actually involved in the heat transfer process. So far, area for heat transfer as well as the temperature driving force are still controversial matters as far as the fluidised bed is concerned. Due to the tremendous amount of turbulence in a fluidised bed, there is no way of telling as to what portion carries heat and what does not; although even common sense would suggest that only a small amount is involved in heat transfer. Furthermore, at the initial stage of heat transfer perhaps only a fraction of the entire solid bed is involved in the process, but it is a fact that eventually the entire bed is heated and all the particles are thus involved in the heat transfer.

The present investigation is a combination of most of the merits of other people and thus suggests a more appropriate alternative comparatively.

Also, in the same review, the work of Shakhova (45) [The information for this reference was actually derived from a cross reference by Rosental (46)] seems to have obtained the merits of Barker among all works compared. However, the paper of Rosental (46) does not provide any information as to how the area for heat transfer was used.

Fortunately, another reference of Shakhova and Rychkov (47) was cited. The two papers of Shakhova appeared at different time intervals. The earlier paper of Shakhova (45) was a dissertation of thesis in 1954 whereas the latter (47) is a joint publication in a Russian journal at a later date. Surprisingly enough, Shakhova (47) actually used the entire surface area of fluidized bed as the heat transfer area. Perhaps assuming that a different surface area was used in the first paper (45), but if one were to refer to the dates of the work done and publication of references (45) (47) respectively, it would not be difficult to realize that the same author had used two different definitions for the area in question. Since the joint publication (47) was published much later, it is very likely that Shakhova herself had chosen the entire area of particles to be more appropriate for the definition. The definition for such an area therefore is still a matter of opinion.

Some attempts were made to measure T_2 for the present system. It would appear at first thought that the most reliable method would be to use a transparent column for fluidization process. At the beginning of this investigation, a plexiglass column was tried. It was found that particles clustered and adhered to the column walls and hot junctions of the thermocouples inside the column due to the generation of static electricity. Humidification was next tried to avoid static

electricity. An error was introduced by such a modification due to heat loss on account of adsorption. The use of a transparent column for fluidisation process was therefore ruled out, and a metal column subsequently used.

Due to the opaque nature of the metal column used for fluidizing experiments, the expanded bed height in the column could not be observed visually. Hence the measurement of temperature at the threshold of expanded bed height, (T_2), by placing thermocouples at these locations, was considered highly inaccurate.

However, some experiments were carried out by locating the thermocouples in the metal column at distances equal to expanded bed heights, calculated from a transparent glass column. The glass column was identical in design to the metal column, which has been used in the course of fluidisation work. Results thus obtained are given in Appendix F. The results indicated that there was a gradual change of temperature along the length of the column, and not an abrupt one, which would have indicated that the temperature at the threshold of expanded bed height, T_2, was being measured. Thus T_2 could not be measured properly.

Since the thickness of the insulation was thin, it was treated as a thin surface skin of a poor conductor (44) and the heat lost through the insulation, $q_{ins.}$ was assumed to be the flow of heat across the thickness of the insulation in a steady state. An energy equation (68), was first written and the different terms of the equation were then evaluated experimentally; the temperature of the insulation along the length (height of the fluidised bed), and at different angles of the column remained constant. The temperature at different radial positions were also measured. The derivation of the equation (67)

$$q_{ins.} = k_{(ins.)} A_{(ins.)} \frac{\Delta T_{(ins.)}}{\Delta r} \tag{67}$$

used in calculation, from the ordinary energy equation

$$\rho C_p \frac{dT}{d\theta} = k \nabla^2 T \tag{68}$$

and

$$\rho C_p \frac{dT}{d\theta} = - \nabla \cdot q \tag{69}$$

is given in Appendix D.

In connection with the attention given to the insulation, a few words of comments may be added here to the last paragraph of page 9 of this thesis.

The different jackets improvised were by no means a perfect solution to a steady state system; it is only a compromise in a certain manner wherein the heat input and heat output were more or less maintained constant. The heat transferred to the solid and from solid to fluid is still in itself transient and when such is treated as steady state it only concludes a compromise. It is therefore more relevant and convincing to assume an unsteady state heat transfer. This is why an unsteady state heat transfer has been adopted for the present investigation.

The correction terms of heat losses were very difficult to achieve. It has been done by taking account of all the contributing factors. Questions may be raised as to the validity of the assumptions made on material properties and consequently doubt the correctness of the result and thereby introduce some uncertainty in the result. The author is very much aware of this from the very beginning, but there is no other alternative except to take all the precautions and make the best possible assumptions. However, errors are bound to come in, uncertainties are expected in every aspect of work. Thus a certain magnitude of error in the form of $\pm\ q_1$ has been incorporated into the evaluation of results.

Incidentally, questions may arise as to what experimental evidence there is to justify the assumption that the correct result is really obtained by using the data at θ (time) = 60 mins. Referring back to Table E-1 again, although U is expected tos be a function of θ, it was found, in the course of the experiments, that there was actually a slight variation of U with time. It would also be seen that the values of U were higher and inaccurate at the start of a run due to the rapidly changing experimental conditions and slightly negative at the end of the run due to small temperature differences. A question would arise here as to what value of time would be most appropriate and most convenient to use. At first it would seem that an average, either arithmetic or integral, of th e entire run would be most convenient, but in view of the fact that the variation and thus the error involved (0.00003798 and -0.0000022 for start and end of a run respectively as shown by Table E-1) in the beginning and end of a run are too great in magnitude, the error brought forward in such a manner would be too big in the final result. As an alternative, some authors have assumed the average of the middle 50% to be the most acceptable value. This too was only assumed. For the present investigation, the value at θ = 60 min. has been found to be very close to that of the average of the middle 50% portion of the run. It is thus reasonable to accept the value at θ = 60 min. for values of U.

The design of the transparent column and the heat transfer column were identical; the operating pressures were maintained the same in both cases; in the beginning of the experimental works, a few test runs were performed, the bed level measuring runs were performed in such a way as to preheat the gases to the temperature of the actual runs, it was found that there was a slight difference in the two sets of data (on the average), that is, a set collected from a heated stream expanded height and a set collected from the unheated stream. The result came out to be practically the same, consequently no temperature conditions were corrected and no further runs with temperature adjustments performed.

For the present investigation, the particles used in fluidisation have been assumed essentially to be spherical. For glass beads, all references have given their shapes to be spherical, it is therefore assumed the same for the present investigation. For silica gel most of the references have presented them as microspheres and thus approximately assumed to be spherical. However, Leva has given an approximate range of silica gel's shape factor to be 0.7 to 0.9. For alumina, most references have given them to be granular and thus approximately assumed to be spherical.

Shape factor is a derived number. According to Leva (18), shape factors are determined by pressure drop test and the equation to be used is

$$f_m = \frac{\Delta p\, D_p\, \phi_s^2\, g_c\, \epsilon^3}{2 u_o^2\, L\, \rho_F\, (1-\epsilon)^2} = 100\ \left(\frac{D_p\, u_o\, \rho_F}{\mu}\right)^{-1.0} \qquad (69a)$$

Since f_m is a derived term, ϕ_s is also a derived number. ϕ_s is in itself most likely inaccurate. Perhaps that is one of the reasons so many authors assumed ϕ_s for silica gel and alumina to be microspheres.

Calculated results and correlations are given in Figures 14 and onward. It would be seen from Figure 14 that U was inversely proportional to G for different samples. Figure 16 shows that the fluid superficial velocity, or alternatively, the mass flow rate or Reynolds number affected the heat transfer coefficient values extensively. According to the film theory, it is expected that a film of gas moves with a particle. The motion of a particle in a fluidised bed being much at random, results in the outer surface of the gas film surrounding the particle becoming thermally in equilibrium, with the temperature of the fluidising gas after the particle moves towards the area, where most of the heat exchange takes place. Heat will then further penetrate towards the particle by thermal conduction. The

height of the bed where heat exchange takes place is only a very small portion of the bed. The motion of the particle is so fast that the contact and residence time of the particle in the shallow heat transfer region of the bed is extremely short. Therefore, the depth of the penetration of heat into the particle is very small. When the particle leaves the hot zone, part of the heat continues to flow towards the particle but the remainder is transferred back into the stream of the gas, partly by conduction and partly as a result of attrition of the outer layers of the gas film. Since the heat capacity of the gas film is very low, the amount of heat transferred to the particles would be small and comparatively less than that transferred in a steady state system. In such a process, Reynolds number is important since it influences the thickness of the gas film, the velocity of the particles and rate of heat transfer into and out of the gas film.

Figure 15 shows the relationships between U and bed settled heights with Reynolds numbers as the parameters. Unless otherwise specified, the Reynolds number refers to the modified Reynolds numbers, which are based on particle diameters, instead of column diameter. The heat transfer coefficient decreased with increasing bed settled height. The data is consistent with some published works of Fritz, Wamsley and Johanson. The interpretation

to the phenomena of the inverse proportionality between U and bed settled heights could be explained in the following manner.

The increase in bed settled height means an increase in the amount of fluidized materials and hence an increase in the heat transfer surface area. If the inlet temperature were kept constant and hence the quantity of heat to be transferred were constant, which actually happened in this case, then U would certainly be inversely proportional to bed settled heights.

The variation of U with the particle diameter, where U is expressed in terms of Nusselt number is shown in Figure 19. U increased as particle diameter increased. This is consistent with the findings of Wamsley (41). Frits (42) and Ferron (43) both used only one sample of one single particle size. Hence no direct comparison could be made with their works. Theoretically, by considering equation (70)

$$A_t = \frac{6 W_s}{\rho_s D_p} \tag{70}$$

with $$D_p = \frac{1}{\sum \frac{X_i}{D_{pi}}} \tag{71}$$

where X_i = weight fraction of D_{pi} particles

D_{pi} = diameter of the x_i fraction particles

it would be expected that the larger the particle sizes, D_p, the smaller would be the surface area A_t. Also, from an empirical point of view, the larger the particle sizes, the lesser would be the number of particles in the same weight of sample (had the sample consisted of small particle sizes) and the entire surface area of solids would be smaller. Since U is inversely proportional to the surface area, the result is that U would increase with increased particle sizes.

The experimental data covered a wide range of Reynolds numbers extending from 10 to 2200. Since the entire range was very wide for accurate correlations, it was broken into two ranges; 10 to 100 and as to 2200. The following final correlations were obtained:

i) For Reynolds number 10 to 60:

$$\left(\frac{UD_p}{k_f}\right) = 0.08 \left(\frac{C_{p_f}\mu_f}{k_f}\right)^{0.4} \left(\frac{L_s}{D_t}\right)^{-1.3} \left(\frac{D_p}{D_t}\right)^{4.3} \left(\frac{k_s}{k_p}\right)^{-4} \left(\frac{\rho_s}{\rho_f}\right)^{7.8} \left(\frac{D_p V_f \rho_f}{\mu_f}\right)^{-6.1}$$

ii) For Reynolds number 60 to 2200:

$$\left(\frac{UD_p}{k_f}\right) = (0.0011) \left(\frac{C_{p_f}\mu_f}{k_f}\right)^{0.4} \left(\frac{L_s}{D_t}\right)^{-1.3} \left(\frac{D_p}{D_t}\right)^{4.3} \left(\frac{k_s}{k_p}\right)^{-4} \left(\frac{\rho_s}{\rho_f}\right)^{7.8} \left(\frac{D_p V_f \rho_f}{\mu_f}\right)^{-3.1}$$

The physical properties of the solids were evaluated at the average gas temperature. The average diameter of the particles was evaluated

by equation (71). Based on the assumption that particles were spherical in nature, heat transfer area was calculated by standard procedures. Gas mass velocities were calculated on the basis of cross-sectional area of the empty column.

Figure (25) shows a comparison of the present investigation with those of others. The present data are much lower than those of Kettenring, et al.; Heertjis, et al.; and Waltonet al.; this is perhaps due to the difference in the method used in measuring the temperature and the approach made. However, though the present data seems to be little higher, it has the same trend as those of Fritz and Ferron. The data of Fritz and Ferron were obtained for one fluidising material only, namely alumina-silica catalysts. The present data includes a variety of sizes of glass beads. The difference between the beads and other materials was the almost complete absence of friction. The beads, when rubbed between the fingers, felt like a lubricant with very little frictional drag. It is possible that in a fluidized bed this would result in a freer movement with no effective intermeshing of particles. Since no attempt has been made to introduce any shape factor, it is consequently expected that present data should yield higher values of U.

The error in measuring rates of flow of gases by the rotameters was within $\pm$ 2%, screening errors in particle diameter analysis amounted to $\pm$ 3%. The evaluation of q_1 propagated an error of about $\pm$ 2%. The uncertainty involved in the temperature measurement was approximately $\pm$ 4%.

The correlation of the entire range is found in Figure 24.

VIII CONCLUSIONS AND RECOMMENDATIONS

The fluid flow for this investigation was patterned after the two phase flow theory, a dense phase characterized by high concentration of solid and low concentration of gas; and a dilute phase by low concentration of solid and high concentration of gas. Since it was impossible to obtain the local coefficients of either phase, a space-averaged over-all heat transfer coefficient (U) was found most appropriate for such a system.

The order of magnitude of the space-averaged heat transfer coefficients in the present investigation are low compared to others such as Kettenring, Wamsley and some others; but are quite in line with those of Ferron and Fritz. This is attributed to the way the coefficient is being defined.

The over-all coefficient was inversely proportional to the bed-settled height and directly proportional to the particle size. The influence of the thermal conductivities of the solids was also investigated. It was found that U was inversely proportional to the thermal conductivities of the solids.

The over-all coefficient was also found to be inversely proportional to the Reynolds number but directly proportional to the solid densities.

It is hereby recommended that further investigation of variables be carried out, such as using different gases to vary the Prandtl number; use of fluidizing materials bearing wider range of specific heats. It is also important that a new technique be developed so as to measure the true temperature of the solid. So far, there is no research done that could be called as truly unsteady state or steady state; a radio active disintegration process would be highly recommended for a truly unsteady state process.

IX NOMENCLATURE

a	=	surface area per unit volume, sq. ft./cu. ft.
A	=	surface area of arbitrarily shaped particle, sq. ft.
A_i	=	point surface area, sq. ft.
$A_{ins.}$	=	cross-sectional area for heat transfer in the insulation, sq. ft.
A_p	=	surface area of a single particle, sq. ft.
A_t	=	surface area of the entire solid bed, sq. ft.
$C_{i,\ avg.}$	=	heat capacity of the insulation jacket and reactor hardware per inch height of the column, Btu/(° F) (in. L)
$C_{ins.}$	=	specific heat of insulation, Btu/(lb.-mass) (° F)
C_r	=	specific heat of reactor hardware, Btu/(lb.-mass) (° F)
$C_{i,\ ins.}$; $C_{i,\ j}$; $C_{i,\ r}$	=	heat capacity of insulation, jacket hardware respectively, per inch of column height, Btu/(° F) (in. L)
C_{p_f}	=	specific heat of fluid, Btu/(lb.-mass) (° F)
C_{p_s}	=	specific heat of solid, Btu/(lb.-mass) (° F)
D_p	=	particle diameter, ft.
D_t	=	tube diameter, ft.
f	=	modified friction factor, dimensionless
g_c	=	conversion factor, (ft.) (lb.-mass)/(lb.-force) (sec) (sec)
G_f	=	fluid mass velocity, (lbs)/(hr) (sq. ft.)
G_{mf}	=	fluid mass velocity for minimum fluidization, (lbs)/(hr) (sq. ft.)

G_s = mass velocity of solids, (lbs.)/(hr) (sq. ft.)

h = heat transfer coefficient, Btu/(hr) (sq. ft.) (°F)

h_i = point heat transfer coefficient, Btu/(hr) (sq. ft.) (°F)

h_{ir} = heat transfer coefficient at the inner radius of the tube, Btu/(hr) (sq. ft.) (°F)

h_o = heat transfer coefficient at the outer radius of the tube, Btu/(hr) (sq. ft.) (°F)

h_p = single particle heat transfer coefficient Btu/(hr) (sq. ft.) (°F)

k = thermal conductivity, Btu/(hr) (sq. ft.) (°F/ft.)

k_f = thermal conductivity of fluid, Btu/(hr) (sq. ft.) (°F/ft.)

k_i = point thermal conductivity of fluid, Btu/(hr) (sq. ft.) (°F/ft.)

$k_{ins.}$ = thermal conductivity of the insulation, Btu/(hr) (sq. ft.) (°F/ft.)

k_m = thermal conductivity of fluidizing medium, Btu/(hr) (sq. ft.) (°F/ft.)

k_s = thermal conductivity of the solid, Btu/(hr) (sq. ft.) (°F/ft.)

K = coefficient of permeability, ml^2/(dyne) (sec)

l = length of tube, ft.

L = column height from the bottom of the bed, ft.

L_e = bed height when expansion sets in, ft.

L_{ex} = expanded bed height, in.

$L_{ins.}$ = thickness of the insulation, ft.

L_{mf} = bed height at point of minimum fluidization ft.

L_o = thickness of a porous structure, cm.

L_s = bed-settled height, ft.

n	=	dimensionless temperature
n_1	=	state-of-flow factor, dimensionless
n'	=	exponent, dimensionless
Nu	=	Nusselt number, dimensionless
q	=	rate of heat transfer, Btu/hr
q_i	=	point heat transfer, Btu/hr
$q_{ins.}$	=	rate of heat lost through the insulation, Btu/(hr)
q_r	=	radial rate of heat transfer, Btu/(hr)
q_t	=	vertical rate of heat transfer, Btu/(hr)
Q	=	rate of heat transfer, Btu/hr.
r	=	radius of a particle, ft.
r_i	=	inner radius of the tube, ft.
r_m	=	logarithmic mean radius, ft.
r_o	=	outer radius of the tube, ft.
Re	=	modified Reynolds Number, dimensionless
S	=	cross-sectional area of tube, sq. ft.
t	=	temperature, °F
T	=	temperature, °F
T_f	=	temperature of fluid, °F
T_s	=	temperature of the solid, °F
$T_{j,\ avg.}$	=	mean temperature of the room, jacket reactor hardware and insulation, °F
T_{room}	=	room temperature, °F

T_1 = inlet temperature, °F

T_2 = outlet temperature, °F

T_{1f} = inlet temperature of fluid, °F

T_{2f} = outlet temperature of fluid, °F

T_{j1} = inlet temperature of fluid in the jacket, °F

T_{j2} = outlet temperature of fluid in the jacket, °F

T_{1s} = inlet temperature of solid stream, °F

T_{2s} = outlet temperature of solid stream, °F

u = average rate of flow through porous structure, ml/sec

U = space-averaged over-all heat transfer coefficient, Btu/(hr) (sq. ft.) (°F)

U_n = over-all heat transfer coefficient in pneumatic system, Btu/(hr) (sq. ft.) (°F)

V_f = superficial fluid velocity, ft./sec.

V_{mf} = superficial fluid velocity required for minimum fluidization, ft./sec.

W_g = fluid flow rate, lbs./hr

W_j = fluid flow rate in the jacket, lbs./hr

W_s = weight of solid fluidized, lbs.

x = film thickness

x_i = point film thickness, ft.

$\bar{x}_i$ = average film thickness, ft.

X = weight fraction, dimensionless

X_i = weight fraction of particle passing through i opening of screen

Greek Letters

α	=	constant, dimensionless
δ	=	particle roughness, dimensionless
δ_p	=	boundary layer thickness, ft.
ΔP	=	pressure drop, lbs./sq. ft.
ΔP_e	=	pressure drop when expansion of bed sets in, lbs./sq. ft.
ΔT	=	temperature difference between solid and fluid °F
ΔT_a	=	arithmetic mean temperature difference, °F
ΔT_i	=	point temperature difference °F
$\Delta T_{ins.}$	=	temperature difference across the insulation, °F
ϵ	=	bed voidage fraction, dimensionless
ϵ_e	=	bed-voidage fraction at point when expansion sets in, dimensionless
ϵ_{mf}	=	bed-voidage fraction at point of minimum fluidization, dimensionless
θ	=	time, minutes
μ_f	=	fluid viscosity, lbs./hr sec.
π	=	constant, dimensionless
ρ_f	=	fluid density, lb./cu. ft.
ρ_s	=	solids density, lb./cu. ft.
Σ	=	summation of, dimensionless
ϕ	=	function of, dimensionless
ϕ_1, ϕ_2	=	dimensionless parameters
Ψ	=	particle shape factor, dimensionless

X BIBLIOGRAPHY

1. Phillips, W.A. and Bulteel, J.G., English patent 23045, Oct. 5, 1910.

2. Zenz, F.A. and Othmer, D.F., Fluidization and Fluid Particle Systems, Reinhold Publishing Corporation, New York, (1960).

3. D'Arcy, H.P.G., "Les Fontaines Publiones de la Ville de Dijon" V. Delmont Paris (1856).

4. Coulson, J.M., Transt. Inst. Chem. Engrs. (London), Dec. Issue, 1949.

5. Schwartz, C.E., Ind. Eng. Chem., 45, 1209 (1953).

6. Cooling, L.F., Chem. and Ind. (London), 43, 892 (1951).

7. Martin, J.J., McCabe, W.L. and Monrad, C.C., Chem. Eng. Progr., 47, 91 (1951).

8. Van Heerden, C.C., Appl. Chem. (London), 2, Suppl. Issue, 57 (1952).

9. Blake, C.F., Trans. Am. Inst. Chem. Engrs., 14, 415 (1922).

10. Carman, P.C., Trans. Inst. Chem. Engrs. (London), 15, 150 (1937); J. Soc. Chem. Ind. (London), 57, 225 (1938).

11. Bakhmeteff, B.A. and Feodoroff, N.V., J. Appl. Mechanics, 4, A 97 (1937).

12. Oman, A.O. and Watson, K.M., Natl. Petrol. News, 36, R795 (1944).

13. Chilton, T.H. and Colburn, A.P., Ind. Eng. Chem., 23, 913 (1931).

14. Daniels, L.S., Pet. Ref., 25, 435 (1946).

15. Parent, J.D., Yagol, N. and Steiner, G.S., Chem. Eng. Progr., 43, 429 (1947).

16. Wilhelm, R.H. and Kwauk, M., Chem. Eng. Progr., 44, 201 (1948).

17. Leva, M., Weintraub, M., Grummer, M., Pollchik, M., and Storch, H.H., U.S. Bur. Miners Bull., 504 (1951).

18. Leva, M., "Fluidisation", McGraw-Hill Book Company Inc., N.Y. (1959).

19. Leva, M., Weintraub, and Grummer, M., Chem. Eng. Progr., 45, 563-572 (1949).

20. Heerden, C. Van, Nobel, A.P.P., and Krevelen, D.W. Van, Chem. Eng. Sci., 1 (2) 51 - 66 (1951).

21. Heerden, C. Van, Novel, A.P.P., and Krevelen, D.W. Van, Ind. Eng. Chem., 45, 1237 - 1242 (1953).

22. Wicke, E. and Fetting, F., Chem. Ingr. Tech., 26 (6) 301 - 309 (1954).

23. Leva, M., Weintraub, M., and Grummer, M., Chem. Eng. Progr., 45, 563 - 572 (1949).

24. Agarwal, O.P., and Storrow, J.A., Chem. and Industry (London), 321 - 324 (1951).

25. Baerg, A., Klassen, J., and Gishler, P.E., Can. J. Research, F28, 287 - 307 (1950).

26. Toomey, R.D. and Johnstone, H.F., Chem. Eng. Progr. Symposium Ser. 5, 49, 51 - 63 (1953).

27. Vreedenberg, H.A., J. Appl. Chem. (London) 2 (Suppl. Issue 1) 526 - 533 (1952).

28. Koble, R.A., Ademino, J.H., Bartkus, E.P. and Corrigan, T.E., Chem. Eng., 58, 174 (1951).

29. Farbar, L., and Morley, M.J., Ind. Eng. Chem., 49, 1143 (1957).

30. Richardson, J.F., and Ayers, P., Trans. Instn. Chem. Engrs., 37, 314 - 321 (1959).

31. Johnstone, H.F., Pigford, R.L., and Chapin, J.H., Trans. Am. Inst. Chem. Engrs., 37, 95 (1941).

32. Zens, F.A., and Othmer, D.F., Fluidization and Fluid Particle System, p. 421 - 423, Reinhold Publishing Corporation, N.Y. (1960).

33. Kettenring, K.N., Manderefield, E.L., and Smith, J.M., Chem. Eng. Progr., 46, 139 (1950).

34. Walton, J.S., Olson, R.S., and Levenspiel, O., Ind. Eng. Chem., 44, 1474 - 1480 (1952).

35. Heertjes, P.M., and McKibbins, S.W., Chem. Eng. Sci., 5, 161 (1956).

36. Heertjes, P.M., de Boer, H.G.S., and De Haas Van Dorser, A.H., Chem. Eng. Sci., 2, 97 (1953).

37. Anton, J.R., Ph.D. Dissertation, State University of Iowa.

38. Richardson, J.F., and Ayers, P., Trans. Inst. of Chem. Engrs., 37, 314 - 322 (1959).

39. Frantz, J.F., Chem. Eng. Progr., 57, 35 - 42 (1961).

40. Sunkoori, N.R., and Kaparthi, R., Chem. Eng. Sci., 12, 166 (1960).

41. Wamsley, W.W., and Johanson, L.N., Chem. Eng. Progr., 50, 347 (1954).

42. Fritz, J.C., Ph.D. Dissertation, Louisiana State University (1958).

43. Ferron, J.R., Ph.D. Dissertation, University of Wisconsin (1961).

44. Barker, J.J., I.E.C. 57, 33 - 39 (1965).

45. Shakhova, N.A., Candidate Dissertation, Moscow Institute of Chemical Equipment, 1954.

46. Rozental, E.O., "Heat and Mass Transfer in the Fluidized State", Teplo-i Massoobmen V Prestses. Isparemiya. Akad. Nauk SSSR Energet. Inst. 1958, 87.

47. Shakhova, N.A., Rychkov, A.I., "Heat Transfer in a Fluidized Bed", Trudy Moskov. Inst. Khim Mashynostroeniya 12, 119 (1957).

48. Carslaw, H.S., and Jaeger, J.C., Conduction of Heat in Solids, p. 20, Clarendon Press, Oxford (1959).

49. Rowe, P.N. and Henwood, G.A., Trans. Instn Chem. Engrs, 39, 43 (1961).

50. Wace, P.F. and Burnett, S.J., Trans Instn Chem. Engrs, 39, 168 (1961).

51. Sutherland, J.P., Vasilatos, G., Kubota, H. and Osberg, G.L., A.I.Ch.E. Journal, 9, 437 (1963).

52. Ziegler, E.N. and Brazelton, W.T., Ind. Eng. Chem. Process Design and Development, 2, 276 (1963).

53. Anonymous, Chem. Eng. Sc., 19, 319 (1964).

54. Shibler, B.K. and Martin, D.A., U.S. Bureau of Mines Report 6209 (1963).

55. Frantz, J.E., Chem. Eng., September 17, 161 (1962), October 1, 89 (1962), October 29, 103 (1962).

56. Rowe, P.N., Trans. Instn Chem. Engrs 39, 175 (1961).

57. Adler, I.L. and Happel, J., Preprint 105, A.I. Ch. E. Symposium, December 2-7, 1961.

58. Romero, J.B. and Johnson, L.N., Preprint 77, A.I.Ch. E. Symposium, December 2-7, 1961.

59. Lewis, W.K., Gilliland, E.R. and Lang, P.M. Preprint 104, A.I.Ch. E. Symposium, December 2-7, 1961.

XI APPENDICES

Appendix A

Sample Calculations and Data

Sample Calculations

The basic equations to be used in the calculations are:

$$U = \frac{2 W_g C_{p_f}}{A_t} \left(\frac{1 - n}{1 + n}\right) - \frac{2 q_1}{A_t (1 + n)(T_1 - T_s)} \qquad (55)$$

$$(1 - n) = \frac{W_s C_s \frac{d T_s}{d \theta}}{W_g C_{p_f} (T_1 - T_s)} + \frac{q_1}{W_g C_{p_f} (T_1 - T_s)} \qquad (57)$$

$$q_1 = C_j L_{ex} \frac{d T_{j,\,avg.}}{d \theta} - W_j C_{p_f} (T_{j1} - T_{j2}) + q_{ins.} \qquad (61)$$

for run No. D-6

Materials used: Glass beads, $D_p = 0.0185"$

$W_s = 1.59$ lbs.

$W_g = 1.026$ lbs.

$C_{p_s} = 0.27$ Btu/(lb-mass) °F

$C_{p_f} = 0.24$ Btu/(lb-mass) °F

$T_1 = 181°F$

$T_{j1} = 150°F$

$T_{j2} = 142.5°F$

$T_s = 163°F$

$C_j = 0.275$ Btu/(°F) (in. L) (empirical value)

$\left(\frac{k}{L}\right) = 0.0048 \frac{\text{Btu}}{(\text{min.})(\text{ft.}^2)\,°F}$ (empirical value)

$L_{ex} = 5.41$ in.

$A_{ins.} = 0.825$ sq. ft.

$$\Delta T_{ins.} = 62^\circ F$$

$$A_t = 67.949 \text{ sq. ft.}$$

$$\frac{dT_s}{d\theta} = 0.45\ ^\circ F/(\text{min.})$$

$$\frac{dT_{j,\,avg.}}{d\theta} = 0.507\ ^\circ F/(\text{min.})$$

for q_1, using equation (61):

$$C_j L_{ex} \frac{dT_{j,\,avg}}{d\theta} = (0.275)(5.41)(0.507) = 0.7539 \frac{\text{Btu}}{\text{min.}}$$

$$W_j C_{p_f} (T_{j1} - T_{j2}) = (0.463)(0.24)(150 - 142.5) = 0.825 \frac{\text{Btu}}{\text{min.}}$$

$$q_{ins.} = \left(\frac{k}{L}\right)_{ins.} A_{ins.} \Delta T_{ins.} = (0.0048)(0.875)(67)$$

$$= 0.2455 \frac{\text{Btu}}{\text{min.}}$$

therefore

$$q_1 = C_j L_{ex} \frac{dT_{j,\,avg.}}{d\theta} - W_j C_{p_f} (T_{j1} - T_{j2}) + q_{ins.}$$

$$= 0.7539 - 0.825 + 0.2455 = 0.1744 \frac{\text{Btu}}{\text{min.}}$$

for (1 - n):

$$\frac{W_s C_{p_s} \frac{dT_s}{d\theta}}{W_g C_{p_f} (T_1 - T_s)} = \frac{(1.59)(0.27)(0.45)}{(1.026)(0.24)(181 - 163)} = 0.0359$$

$$\frac{q_1}{W_g C_{p_f} (T_1 - T_s)} = \frac{0.1744}{(1.026)(0.24)(181 - 163)} = 0.0377$$

$$(1 - n) = \frac{W_s C_{p_s} \frac{dT_s}{d\theta}}{W_g C_{p_f} (T_1 - T_s)} + \frac{q_1}{W_g C_{p_f} (T_1 - T_s)}$$

$$= 0.0359 + 0.0377 = 0.0736$$

$$U = \frac{2 W_g C_{p_f}}{A_t} \left(\frac{1 - n}{1 + n}\right) - \frac{2 q_1}{A_t (1 + n) (T_1 - T_s)}$$

$$= \frac{2 (1.026) (0.24)}{67.949} \left(\frac{0.0736}{1.926}\right) - \frac{2 (0.1744)}{67.949 (1.926) (20.25)}$$

$$= 2 (0.000144 - 0.000074)$$

$$= 0.00014 \frac{\text{Btu}}{\text{min. ft.}^2 \cdot F} = 0.0084 \frac{\text{Btu}}{\text{hr. ft.}^2 \cdot F}$$

Table A-1 Data for Sample Calculations

θ min.	T_e °F	T_j °F	$T_{ins.}$ °F	$T_{j,\ avg.}$ °F
0				
10	126	99	22	106.5
20	139	109	32	117.9
30	147	117.5	40.5	126.5
40	153.5	124	47	132
50	159	131	54	140
60	163	139	62	146.9
70	167	142.5	65.5	150
80	169.5	146	69	153
90	171.5	153	76	158
100	173	153	76	159
110	174.5	156	79	161
120	175	163	86	165.5

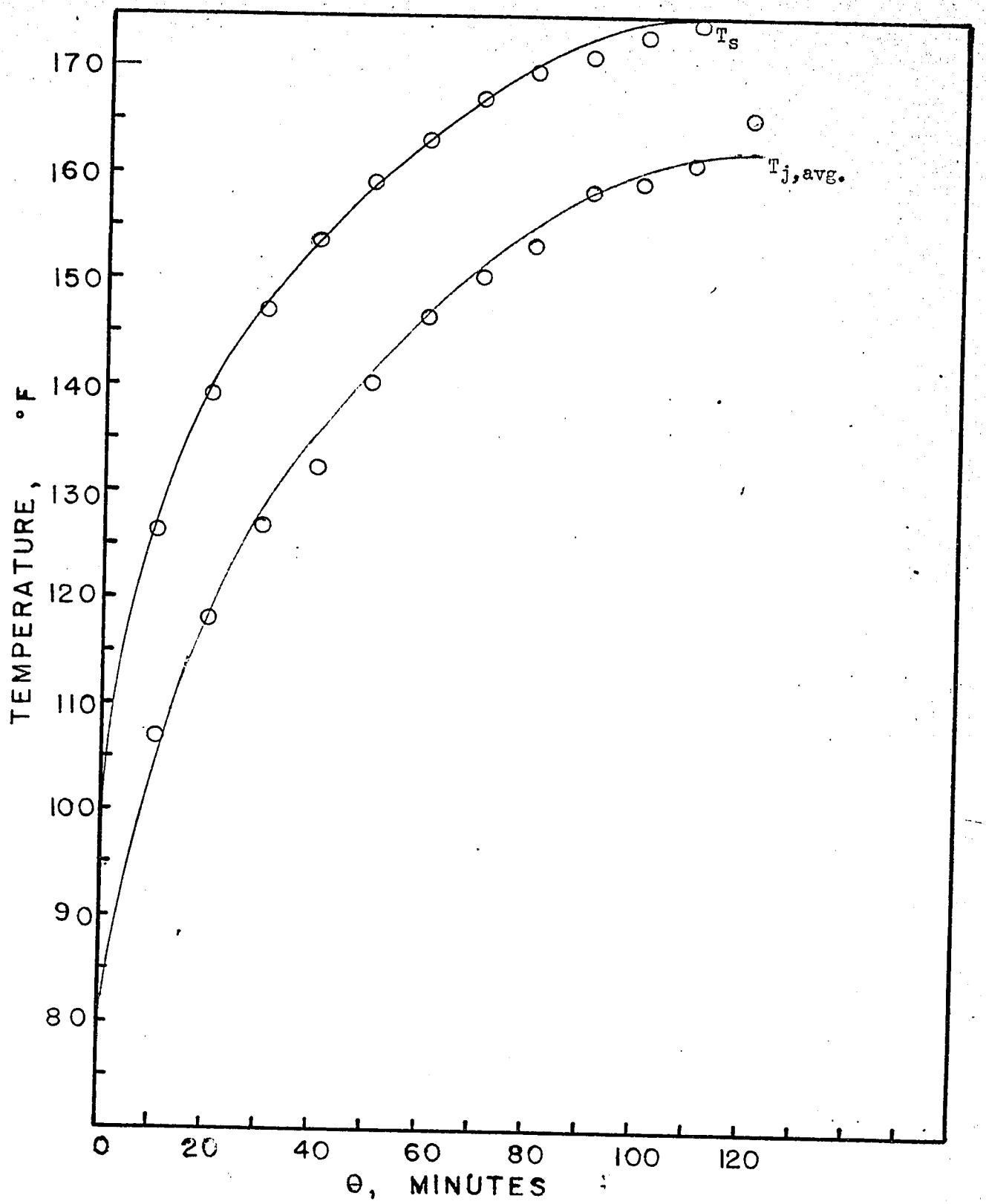

Fig. A-1 Temperature-time curve for sample calculations

Tables A-2 to A-11

Heat Transfer Coefficients, Rates of Fluid Flow and Bed-Settled Heights to Bed Diameter Ratio Data

Table A-2 4-in. Column, Glass beads, D_p = 0.0039"

Run No.	W_g	$\frac{L_s}{D_t}$	U
h1	0.646	1.30	0.00630
h2	0.826	1.30	0.00139
h3	1.162	1.30	0.00136
h4	0.879	1.30	0.00238
h5	0.646	1.725	0.00306
h6	0.826	1.725	0.00197
h7	1.162	1.725	0.00128
h8	0.771	1.725	0.00204
h9	0.646	2.02	0.00313
h10	0.826	2.02	0.00139
h11	1.162	2.02	0.00122
h12	0.713	2.02	0.00276
h13	0.646	3.375	0.00156
h14	0.826	3.375	0.00262

Table A-3 4-in. Column, Silica gel, D_p = 0.06569"

Run No.	W_g	$\frac{L_s}{D_t}$	U
h15	0.818	1.700	0.02303
h16	1.087	1.700	0.00625
h17	1.190	1.700	0.00297
h18	0.713	1.700	0.01076
h19	0.826	2.500	0.01200
h20	0.813	2.500	0.01370
h21	0.749	2.500	0.00920
h22	1.340	2.500	0.00127
h23	0.657	0.850	
h24	0.879	0.850	0.00323
h25	1.034	0.850	0.00394
h26	1.215	0.850	0.00268
h27	1.550	0.850	0.01116
h28	0.659	0.438	-0.02682
h29	1.034	0.438	0.01602
h30	1.370	0.438	0.01088
h31	1.783	0.438	0.02125

Table A-4 4-in. Column, Silica gel, D_p = 0.2324"

Run No.	W_g	$\frac{L_s}{D_t}$	U
h32	0.932	0.425	0.00947
h33	1.215	0.425	0.00946
h34	1.448	0.425	0.02851
h35	1.680	0.425	0.01001
h36	0.657	0.425	0.01592
h37	0.932	0.875	-1.77210
h38	1.215	0.875	0.00487
h39	1.384	0.875	0.01171
h40	1.836	0.875	
h41	1.370	1.950	0.01650
h42	1.650	1.950	0.02670
h43	0.765	1.950	0.48580
h44	0.932	2.850	0.00843
h45	1.190	2.850	0.00735
h46	1.384	2.850	0.00641
h47	1.655	2.850	
h48	0.932	3.750	0.01096
h49	1.190	3.750	0.00534
h50	1.370	3.750	
h51	1.680	3.750	
h52	0.713	3.750	

Table A-5 4-in. Column, Alumina, $D_p = 0.0164"$

Run No.	W_g	$\frac{L_s}{D_t}$	U
h53	1.115	0.126	
h54	1.293	0.126	0.01272
h55	1.454	0.126	0.01292
h56	2.141	0.126	0.01247
h57	2.586	0.126	0.01404
h58	1.196	0.498	0.01012
h59	1.454	0.498	0.01153
h60	1.858	0.498	0.01020
h61	2.182	0.498	0.01166
h62	2.424	0.498	0.00840
h63	1.454	0.801	0.01146
h64	1.858	0.801	0.00506
h65	2.161	0.801	0.00348
h66	2.586	0.801	0.00576
h67	1.454	1.149	0.01104
h68	1.858	1.149	0.01109
h69	2.586	1.149	0.00840
h70	2.182	1.149	0.01044
h71	1.858	1.302	0.00930
h72	2.161	1.302	0.01212
h73	2.586	1.302	0.00930

Table A-6 4-in. Column, Alumina, $D_p = 0.0411"$

Run No.	W_g	$\frac{L_s}{D_t}$	U
h74	1.454	0.175	0.03131
h75	1.858	0.175	0.02564
h76	2.182	0.175	0.04211
h77	1.454	0.498	0.02552
h78	1.858	0.498	0.03132
h79	2.182	0.498	0.03336
h80	2.586	0.498	0.01896
h81	1.454	0.849	0.12564
h82	1.858	0.849	
h83	2.161	0.849	
h84	2.586	0.849	
h85	1.858	0.849	
h86	2.161	0.849	
h87	2.586	0.849	

Table A-7 4-in. Column, Glass beads, D_p = 0.011"

Run No.	W_g	$\frac{L_s}{D_t}$	U
c6	0.709	0.675	0.00504
c7	0.557	0.675	
c8	0.826	0.675	0.00492
c9	0.979	0.675	0.00780
c10	1.114	0.675	0.00648
c11	1.266	0.675	0.00552
c12	0.645	0.675	0.00732
c13	0.768	0.675	0.00828
c14	0.890	0.675	0.00636
c15	1.013	0.675	0.00720
c16	1.151	0.675	0.00708
c17	0.734	0.675	0.00576
c18	0.852	0.675	0.00936
c19	0.969	0.675	0.00792
c20	1.101	0.675	
c21	0.824	0.675	0.12624
c22	0.938	0.675	0.00864
c23	1.066	0.675	0.01116
c24	0.794	0.675	0.00792
c25	0.903	0.675	0.01128
c26	1.026	0.675	0.00816

Table A-7 (Cont.)

Run No.	W_g	$\frac{L_s}{D_t}$	U
c27	0.777	0.675	0.00756
c28	0.884	0.675	0.00684

Table A-8 4-in. Column, Glass beads, D_p = 0.0185"

Run No.	W_g	$\frac{L_s}{D_t}$	U
d1	0.850	0.563	0.00698
d2	1.027	0.563	0.00916
d3	1.207	0.563	0.00907
d4	1.373	0.563	0.01088
d5	1.540	0.563	0.01124
d6	1.026	0.563	0.00840
d7	1.208	0.563	0.00936
d8	1.374	0.563	0.00829
d9	1.543	0.563	0.01544
d10	1.208	0.563	0.00689
d11	1.026	0.563	0.00848
d12	1.543	0.563	0.00856
d13	1.026	0.563	0.01050
d14	1.208	0.563	0.00931
d15	1.374	0.563	0.01152
d16	1.543	0.563	0.01020
d17	1.026	0.563	0.00958
d18	1.208	0.563	0.00901
d19	1.374	0.563	0.00984

Table A-8 (Cont.)

Run No.	W_g	$\frac{L_s}{D_t}$	U
d20	1.543	0.563	
d21	1.208	0.563	0.00385
d22	1.026	0.563	0.01310
d23	1.374	0.563	0.01306
d24	1.543	0.563	0.01083
d25	1.208	1.187	0.00848
d26	1.374	1.187	0.00679
d27	1.543	1.187	0.00907
d28	1.026	1.187	
d29	1.026	1.187	0.00817

Table A-9 4-in. Column, Glass beads, D_p = 0.0185"

Run No.	W_g	$\frac{L_s}{D_t}$	U
e1	1.208	1.187	0.00979
e2	1.374	1.187	0.01093
e3	1.543	1.187	0.01171
e4	1.026	1.187	0.00920
e5	1.208	1.187	0.00423
e6	1.374	1.187	
e7	1.543	1.187	0.01110
e8	0.848	1.187	0.01036
e9	1.026	1.187	0.00856
e10	1.208	1.187	0.00896
e11	1.450	1.187	0.01066
e12	1.547	1.187	0.01053
e13	0.848	1.187	0.02016
e14	1.026	1.187	0.00865
e15	1.208	1.187	0.00895
e16	1.374	1.187	0.00979
e17	1.543	1.187	0.00866
e18	0.848	1.187	
e19	1.026	1.187	0.00957

Table A-9 (Cont.)

Run No.	W_g	$\frac{L_s}{D_t}$	U
e20	1.208	1.187	0.01065
e21	1.374	1.187	0.01035
e22	1.543	1.187	0.00867
e23	0.848	1.187	0.00704
e24	0.848	1.187	0.00805
e25	1.026	1.187	0.00434
e26	1.208	1.187	0.00866
e27	1.374	1.187	0.00796
e28	1.535	1.187	0.00717
e29	0.848	1.187	0.00711

Table A-10 2-in. Column, Glass beads, D_p = 0.0185"

Run No.	W_g	$\frac{L_s}{D_t}$	U
h88	0.848	1.698	0.03276
h89	1.115	1.698	0.00888
h90	1.374	1.698	0.41580
h91	2.141	1.698	0.01650
h92	0.848	2.598	0.01232
h93	1.026	2.598	0.02859
h94	2.020	2.598	0.00654
h95	1.026	3.498	0.00635
h96	1.374	3.498	0.00537
h97	2.157	3.498	0.00806
h98	1.454	4.398	0.00886

Table A-11 2-in. Column, Silica gel, D_p = 0.06569" (h99 - h102, h113 - h115); Alumina, D_p = 0.0411" (h103 - h112)

Run No.	W_g	$\frac{L_s}{D_t}$	U
h99	2.161	3.60	0.00799
h100	1.454	3.60	0.00299
h101	2.424	3.60	0.01066
h102	1.454	6.750	0.00678
h113	1.454	7.080	0.00180
h114	1.858	7.080	0.00409
h115	2.182	7.080	0.00262
h103	2.586	3.240	0.05293
h104	1.454	3.240	0.94964
h105	2.161	3.240	
h106	2.586	3.240	
h107	1.858	6.480	0.05916
h108	2.161	6.480	0.01620
h109	2.42	6.480	0.04163
h110	1.858	7.980	-0.10640
h111	2.161	7.980	0.02442
h112	2.586	7.980	0.02442

Tables A-12 to A-21

Temperature Data

Table A-12 4-in. Column, Glass beads, D_p = 0.0039"

Run No.	T_1	T_s	T_{j1}	T_{j2}	T_j	$\Delta T_{ins.}$
h1	225.0	176.0	176.0	166.0	169.3	83.3
h2	249.5	194.5	185.5	181.0	148.2	101.0
h3	269.0	223.0	194.5	200.0	194.8	123.0
h4	256.0	206.5	183.0	174.5	184.0	109.0
h5	228.0	181.0	173.0	168.0	169.0	83.6
h6	244.0	196.5	188.0	183.0	183.6	100.6
h7	262.5	210.0	193.0	193.0	190.2	114.2
h8	248.5	199.5	191.0	184.5	185.2	105.7
h9	234.5	179.5	178.0	168.0	170.0	90.1
h10	251.0	200.0	188.0	186.0	185.0	101.0
h11	267.5	211.5	191.0	186.0	190.0	117.5
h12	244.5	193.0	179.5	180.0	176.8	98.5
h13	234.5	168.0	168.0	160.0	162.5	89.0
h14	254.0	198.0	186.0	186.0	183.8	109.0

Table A-13 4-in. Column, Silica gel, D_p = 0.06569"

Run No.	T_1	T_s	T_{j1}	T_{j2}	T_j	$\Delta T_{ins.}$
h15	257.5	243.0	169.5	179.5	170.6	97.8
h16	266.0	243.0	183.0	200.0	186.3	117.8
h17	272.5	242.5	181.0	200.0	185.6	115.9
h18	251.0	243.0	186.0	181.0	181.0	92.4
h19	256.0	241.0	174.5	179.5	173.3	100.8
h20	261.0	232.5	181.0	186.0	180.0	109.8
h21	261.0	241.0	176.0	183.0	175.6	104.2
h22	254.0	251.0	176.0	179.5	175.0	96.2
h23	239.5	236.0	166.0	154.5	159.0	79.3
h24	254.0	233.0	179.5	183.0	177.8	102.8
h25	262.5	243.0	176.0	190.0	177.3	96.0
h26	266.0	246.0	181.0	193.0	182.3	111.0
h27	275.5	261.0	191.0	220.0	193.0	126.0
h28	249.5	249.0	176.0	170.0	170.3	84.2
h29	266.0	259.0	184.5	201.0	187.8	100.3
h30	275.5	264.0	181.0	207.0	187.6	119.5
h31	278.5	270.0	191.0	220.0	199.0	125.8

Table A-14 4-in. Column, Silica gel, D_p = 0.2324"

Run No.	T_1	T_s	T_{j1}	T_{j2}	T_j	$\Delta T_{ins.}$
h32	266.0	266.0	178.0	190.0	179.0	100.3
h33	272.5	272.0	184.5	200.0	186.8	111.3
h34	273.0	275.0	176.0	203.0	183.3	113.3
h35	279.0	277.0	178.0	205.0	190.0	123.6
h36	249.0	247.5	179.5	173.0	174.0	86.6
h37	262.5	266.0	173.0	196.0	185.0	111.2
h38	276.0	269.0	176.0	191.0	178.8	105.4
h39	275.5	272.0	180.0	206.5	185.8	115.4
h40	283.5					
h41	285.5	283.5	186.0	227.0	198.7	137.7
h42	283.5	280.0	184.5	227.0	196.5	137.2
h43	257.5	256.0	176.0	183.0	174.5	92.5
h44	267.5	266.0	169.5	193.0	175.2	109.0
h45	275.5	272.5	186.0	213.0	191.7	127.7
h46	278.5	277.0	161.0	203.0	174.0	120.6
h47	280.5	279.0	191.0	227.0	200.8	140.6
h48	261.0	259.0	186.0	203.0	184.2	109.4
h49	272.5	269.0	188.0	213.0	193.7	127.4
h50	278.5	278.5	183.0	223.0	195.3	139.4
h51	279.0	272.0	193.0	228.0	216.3	147.4
h52	249.5		178.0	179.5		92.1

Table A-15 4-in. Column, Alumina, D_p = 0.0164"

Run No.	T_l	T_s	T_{j1}	T_{j2}	T_j	$\Delta T_{ins.}$
h53	249.0	241.0	190.0	188.0	186.0	108.5
h54	252.5	243.0	183.0	186.0	180.7	111.4
h55	262.0	244.5	186.0	196.5	186.2	103.1
h56	270.5	259.0	178.0	207.0	186.0	119.7
h57	275.5	267.5	190.0	220.0	196.7	117.9
h58	257.5	246.0	173.0	183.0	172.3	89.8
h59	267.0	257.5	183.0	198.0	189.1	102.6
h60	264.0	262.5	183.0	203.0	186.3	101.8
h61	269.0	264.0	181.0	210.0	188.5	116.5
h62	282.0	275.5	180.0	216.5	189.8	128.2
h63	267.5	259.0	174.5	196.0	180.2	109.2
h64	277.0	271.0	179.0	208.0	186.7	98.1
h65	280.5	239.0	186.0	218.0	194.5	109.7
h66	282.0	277.0	181.0	222.0	193.0	103.6
h67	259.0	246.0	178.0	193.0	180.3	111.2
h68	275.5	266.0	109.0	127.5	190.3	110.4
h69	275.0	274.0	183.0	220.0	193.7	116.9
h70	277.0	272.0	176.0	213.0	186.3	115.5
h71	269.0	262.5	176.0	210.0	185.3	111.8
h72	276.0	272.0	186.0	220.0	195.7	125.8
h73	279.0	274.0	180.0	216.0	189.7	113.6

Table A-16 4-in. Column, Alumina, D_p = 0.0411"

Run No.	T_1	T_s	T_{j1}	T_{j2}	T_j	$\Delta T_{ins.}$
h74	269.0	251.0	186	206.5	190.8	125.9
h75	272.0	262.5	193	216.0	199.7	132.4
h76	266.0	259.0	176	180.0	175.3	99.4
h77	259.0	259.0	173	180.0	176.0	90.6
h78	266.0	252.5	180	191.0	180.3	96.8
h79	269.0	257.5	196	203.0	196.3	103.4
h80	272.5	259.0	183	198.0	187.0	112.4
h81	266.0	262.5	190	203.0	193.0	108.8
h82						
h83	272.5	256.0	190	206.5	193.7	103.8
h84	272.0	259.0	190	208.0	193.6	113.2
h85	272.0	257.0	196	213	200.0	
h86	272.0	256.0	198	210.0	201.0	122.6
h87	275.5					

Table A-17 2-in. Column, Glass beads, D_p = 0.0185"

Run No.	T_l	T_s	T_{j1}	T_{j2}	T_j	$\Delta T_{ins.}$
h88	220.0	208	190.0	178.0	182.7	
h89	238.0	236	190.0	198.0	193.0	27.8
h90	249.0	244	180.0	186.0	182.3	27.3
h91	190.0	190	156.0	169.0	161.7	29.8
h92	228.0	211	169.5	174.5	171.3	26.5
h93	239.0	230	180.0	183.0	181.0	31.4
h94	266.0	259	184.5	193.0	188.5	37.6
h95	239.0	215	178.0	183.0	179.7	26.7
h96	252.5	236	186.0	190.0	187.3	25.4
h97	269.0	256	196.0	196.0	195.0	19.4
h98	259.0	246	191.0	193.0	190.0	19.3

Table A-18 2-in. Column, Silica gel, D_p = 0.06569" (h99 - h102, h113 - h115); Alumina, D_p = 0.0411" (h103 - h112)

Run No.	T_1	T_s	T_{j1}	T_{j2}	T_j	$\Delta T_{ins.}$
h99	266.0	261	181.0	184.5	183.3	15.1
h100	254.0	243.0	186.0	194.5	190.2	28.1
h101	270.5	266.0	200.0	203.0	201.0	22.2
h102	259	249.0	188.0	193.0	190.3	
h113	262.5	252.5	200.0	205.0	202.7	29.3
h114	269.0	262	196.0	200.0	198.7	17.8
h115	272.5	266	206.5	210.0	207.8	24.3
h103	259.0	249.0	188.0	191.0	189.0	
h104	262.5	256.0	195.0	201.0	196.3	
h105	270.0	266.0	198.0	200.0	198.0	19.5
h106	272.0	269.0	203.0	206.0	204.0	37.0
h107	262.5	252.5	184.5	186.0	184.3	26.7
h108	269.0	259.0	203	206.5	204.2	21.1
h109	275.5	266.0	205.0	208.0	206.0	22.2
h110	269.0	256.0	198.0	200.0	198.0	15.7
h111	272.5	259.0	198.0	196.0	196.7	
h112	272.5	262.5	200.0	196.0	197.3	23.2

Table A-19 4-in. Column, Glass beads, D_p = 0.011"

Run No.	T_1	T_s	T_{j1}	T_{j2}	T_j	$\Delta T_{ins.}$
c6	128.5	118.0	114.5	111.0	112.1	21.9
c7	124.5	125.2	118.5	110.0	114.8	23.9
c8	132.5	124.0	117.0	114.0	115.0	26.8
c9	134.0	127.6	117.0	120.5	118.2	27.3
c10	136.0	128.6	118.0	116.0	116.0	24.2
c11	137.5	133.0	119.0	123.5	120.0	36.6
c12	159.5	148.0	135.0	123.0	129.3	42.4
c13	166.0	155.6	139.0	136	137.0	51.0
c14	165.0	152.6	132.5	131	130.8	44.9
c15	165.0	153.4	139.0	137.5	137.5	51.9
c16	179.5	171.0	129.0	144	132.3	63.8
c17	186.0	173.0	153.0	151	151.1	66.5
c18	186.0	171.0	141.0	142.5	139.8	52.8
c19	188.5	176.0	150.0	151.0	149.0	67.2
c20	203.0	195	157.0	169.0	159.0	82.5
c21	198.0	192.5	170.0	166.0	166.0	82.4
c22	210.0	193.0	154.0	159.5	153.2	67.9
c23	216.5	206.5	166.0	176.0	167.5	85.4
c24	223.0	200.0	155.0	160.0	153.7	75.8

Table A-19 (Cont.)

Run No.	T_1	T_s	T_{j1}	T_{j2}	T_j	$\Delta T_{ins.}$
c25	228.0	210.0	166.0	174.5	167.2	90.8
c26	230.0	212.0	163.0	170.0	162.0	87.8
c27	241.0	216.0	169.5	173.0	167.5	91.1
c28	244.0	224.0	178	181.0	175.0	102.6

Table A-20 4-in. Column, Glass beads, D_p = 0.0185"

Run No.	T_1	T_s	T_{j1}	T_{j2}	T_j	$\Delta T_{ins.}$
d1	158.5	139.5	127.5	121.5	123.0	43.6
d2	161.0	147.5	131.0	130.0	129.0	46.7
d3	167.0	150.5	125.5	127.5	124.0	48.6
d4	169.5	156.5	129.5	132.5	128.5	54.1
d5	173.5	160.5	132.0	139.0	132.5	55.5
d6	181.0	163.0	150.0	142.5	144.8	62.0
d7	184.0	167.0	151.0	147.5	147.2	65.5
d8	187.5	173.0	153.0	151	149.3	71.0
d9	196.5	187.5	149.5	159.5	150.3	44.2
d10	205	184.0	168.0	163.5	163.0	86.4
d11	199.5	176.5	159.5	156	155.0	81.5
d12	212.5	189.5	162	162.0	159.0	79.6
d13	215.0	186.5	164.5	161.0	160.5	73.0
d14	217.0	189.0	163.0	159.5	157.8	77.8
d15	222.5	199.0	169.5	172.0	167.0	90.5
d16	225.0	200.5	163.0	170.0	162.0	87.5
d17	231.5	199.0	173.0	173.0	170.6	90.8
d18	238.5	210.8	173.0	173.0	169.7	87.8
d19	240.0	215.0	181.0	184.5	178.3	97.5

Table A-20 (Cont.)

Run No.	T_1	T_s	T_{j1}	T_{j2}	T_j	$\Delta T_{ins.}$
d20						
d21	254.5	219.0	183.0	183.0	179.6	107.0
d22	248.5	222.0	180.0	181.0	177.3	97.0
d23	261.5	232.5	186.0	188.5	181.3	114.5
d24	263.0	240.0	190.0	203	190.6	120.6
d25	165.5	145.0	132.5	132.5	130.0	54.0
d26	168.5	152.5	137.5	139.0	136.0	31.0
d27	172.0	154.5	136.0	137.5	134.0	60.8
d28	163.5	147.5	163.0	137.5	149.3	63.5
d29	200.5	176.0	169.5	159.5	162.8	77.2

Table A-21 4-in. Column, Glass beads, D_p = 0.0185"

Run No.	T_1	T_s	T_{j1}	T_{j2}	T_j	$\Delta T_{ins.}$
e1	203.0	179.0	166.0	158.5	159.6	79.3
e2	204.5	182.5	172.0	161.0	163.0	82.8
e3	211.5	191.0	175.5	173.0	171.0	92.5
e4	179.5	154.5	149.5	139.5	142.8	61
e5	185.0	166.5	153.0	149.5	148.8	65.1
e6			149.5	149.5	146.5	69.5
e7	192.5	172.0	151.0	151.0	147.6	74.3
e8	213.0	185.0	169.5	163.0	163.6	84
e9	213.0	183.0	168.0	158.5	160.3	75.5
e10	218.5	192.0	171.0	169.5	167.0	84.2
e11	218.5	194.0	174.5	169.5	168.3	87.2
e12	226.0	199.5	161.0	171.0	161.3	92.8
e13	224.5	191.0	177.5	169.5	171.0	89
e14	230.5	201.0	171.0	167.0	165.8	87.8
e15	235.0	201.5	178.0	174.5	171.8	94.3
e16	241.5	213.5	180.0	190.0	179.8	13.9
e17	244.0	216.0	178.5	186.0	176.8	100.4
e18						
e19	241.5	206.0	179.5	176.0	173.8	92.2
e20	249	214.0	179.5	183.0	176.1	103.8

Table A-21 (Cont.)

Run No.	T_1	T_s	T_{j1}	T_{j2}	T_j	$\Delta T_{ins.}$
e21	255.0	223.0	184.5	191.0	182.2	105.4
e22	258.0	227.0	183.0	93.0	183.0	112.5
e23	241.0	204.0	183.0	183.0	179.7	99.0
e24	256.0	208.0	186.0	178.0	177.8	88.6
e25	261.0	220.0	184.5	185.0	179.6	102.8
e26	274.0	236.5	191.0	203.0	192.3	124.8
e27	276.0	236.5	186.0	200.0	186.3	117.5
e28	281.0	248.0	195.5	213.0	198.2	134.5
e29	265.0	215.5	188.0	183.0	181.3	102.6

Table A-22 4-in. Column, Expanded Bed Height Data

Material: Alumina, D_p = 0.0411"

u ft/sec	L_{ex}/L_s			
	L_s = 0.7"	L_s = 2"	L_s = 3.4"	L_s = 4.1"
3.728		1.175	1.265	1.256
4.008		1.375	1.500	1.488
4.288	1.786	1.45	1.706	1.707
4.661		1.625		
4.940	2.00	1.775	1.912	2.00
5.966	3.143	2.175	2.412	2.402
6.618	3.571	2.60	2.706	2.744

Table A-23 4-in. Column, Expanded Bed Height Data

Material: Glass beads, D_p = 0.0185"

u ft/sec	L_{ex}/L_s		
	L_s = 2.25"	L_s = 4.75"	L_s = 6.8"
0.95	1.155	1.189	1.082
1.142	1.333	1.347	1.195
1.332	1.533	1.501	1.318
1.522	1.671	1.697	1.445
1.715	1.849	1.838	1.567
1.905	1.982	1.964	1.626
2.100	2.146	2.048	1.784
2.290	2.368	2.328	1.965
2.470	2.576	2.339	2.034
2.670	2.724	2.490	2.147
2.860	2.844	2.581	2.259
3.045	2.991	2.759	2.376
3.25	3.168	2.842	2.426
3.43	3.271	2.905	2.494

Table A-24 4-in. Column, Expanded Bed Height Data

Material: Silica gel, $D_p = 0.06569"$

u ft/sec	L_{ex}/L_s				
	$L_s = 1.7"$	$L_s = 3.5"$	$L_s = 7.8"$	$L_s = 11.4"$	$L_s = 15"$
3.728			1.154	1.053	1.100
4.008			1.410	1.316	1.47
4.288	1.294	1.257	1.603	1.579	1.600
4.661	1.471	1.486	1.795	1.842	1.830
4.940		1.657	2.115	2.061	2.27
5.313	1.765	1.771	2.308	2.456	2.40
5.593		2.00	2.436	2.587	
5.966	2.059	2.143	2.692	2.982	
6.618		2.286	2.949	3.158	
6.898			3.205		
7.271	2.647				

Table A-25 4-in. Column, Expanded Bed Height Data

Material: Alumina, D_p = 0.0164"

u ft/sec	L_{ex}/L_s				
	L_s = 0.5"	L_s = 2"	L_s = 3.2"	L_s = 4.6"	L_s = 5.2"
1.957		1.3	1.187	1.217	
2.367	1.20	1.4	1.312	1.217	
2.777		1.55	1.468	1.326	
2.982	3.00				
3.169		1.675	1.734	1.478	1.385
3.356	4.40	1.850	1.906	1.685	1.635
4.287			2.50	2.228	2.115
4.986	7.00	3.05	2.968	2.608	2.308
5.966		4.875	3.515	2.826	2.98
6.664		5.125	3.984		
6.851				3.261	3.173

Table A-26 4-in. Column, Expanded Bed Height Data

Material: Glass beads, D_p = 0.0039"

u ft/sec	L_{ex}/L_s			
	L_s = 5.2"	L_s = 6.9"	L_s = 9.9"	L_s = 13.5"
0.932	2.115	2.32	1.92	1.70
1.139	2.500	2.61	2.12	1.93
1.342	3.07	3.19	2.42	2.15
1.547	3.07	3.62	2.73	2.67
1.752	4.04	3.77	3.13	
1.957	4.23	3.91	3.64	
2.162	4.23	4.20		
2.368	4.23	5.22		

Table A-27 4-in. Column, Expanded Bed Height Data

Material: Silica gel, $D_p = 0.06569"$

u ft/sec	L_{ex}/L_s		
	$L_s = 1.75"$	$L_s = 6.8"$	$L_s = 10"$
2.367		1.110	1.15
2.572		1.324	1.30
2.777	1.257	1.434	1.475
2.982		1.654	1.612
3.169	1.371	1.801	1.775
3.355	1.571	1.853	1.875
3.728	1.657	2.059	2.20
4.008	1.886	2.353	2.55
4.287		2.574	2.85
4.660	2.229	2.757	3.20
4.986		2.941	
5.313	2.800	3.015	
5.966	3.029		
6.664		3.272	
6.851	3.314		

Tables A-28 to A-37

Solid Weights, Slopes, Heat Transfer

Surface Area and $q_{ins.}$ Data

Table A-28 4-in. Column, Glass Beads, $D_p = 0.0039"$

Run No.	W_s	$\frac{dT_s}{d\theta}$	$\frac{dT_{j,\,avg.}}{d\theta}$	A_t	$q_{ins.}$
h1	3.307	0.769	0.781	652.3	1.341
h2	3.307	0.700	0.688	652.3	1.626
h3	3.307	0.331	0.419	652.3	1.978
h4	3.307	0.606	0.663	652.3	1.754
h5	4.409	0.756	0.756	869.6	1.951
h6	4.409	0.606	0.675	869.6	2.643
h7	4.409	0.550	0.731	869.6	2.999
h8	4.409	0.770	0.750	869.6	2.774
h9	6.614	0.831	0.856	1304.5	2.374
h10	6.614	0.644	0.688	1304.5	2.666
h11	6.614	0.594	0.650	1304.5	3.099
h12	6.614	0.794	0.613	1304.5	2.599
h13	8.819	0.769	0.556	1739.5	2.329
h14	8.819	0.900	0.713	1739.5	2.853

Table A-29 4-in. Column, Silica Gel, $D_p = 0.06569"$

Run No.	W_s	$\frac{dT_s}{d\theta}$	$\frac{dT_{j,\,avg.}}{d\theta}$	A_t	$q_{ins.}$
h15	2.205	0.438	0.906	284.6	0.755
h16	2.205	0.529	0.856	284.6	1.305
h17	2.205	0.513	0.600	284.6	1.429
h18	2.205	0.369	0.650	284.6	0.604
h19	3.307	0.444	0.800	426.8	1.205
h20	3.307	0.638	0.844	426.8	1.915
h21	3.307	0.506	0.756	426.8	1.050
h22	3.307	0.525	0.750	426.8	2.310
h23	1.102	0.350	0.612	142.2	0.179
h24	1.102	0.500	0.656	142.2	0.345
h25	1.102	2.475	0.700	142.2	0.401
h26	1.102	0.362	0.512	142.2	0.725
h27	1.102	0.528	0.762	142.2	0.871

Table A-29 (Cont.)

Run No.	W_s	$\frac{dT_s}{d\theta}$	$\frac{dT_{j,\,avg.}}{d\theta}$	A_t	$q_{ins.}$
h28	0.551	0.400	0.763	71.1	0.182
h29	0.551	0.325	0.593	71.1	0.301
h30	0.551	0.380	0.625	71.1	0.466
h31	0.551	0.308	0.581	71.1	0.628

Table A-30 4-in. Column, Silica Gel, $D_p = 0.2324"$

Run No.	W_s	$\frac{dT_s}{d\theta}$	$\frac{dT_{j,\,avg.}}{d\theta}$	A_t	$q_{ins.}$
h32	0.551	0.350	0.631	20.1	0.226
h33	0.551	0.291	0.643	20.1	0.320
h34	0.551	0.275	0.556	20.1	0.381
h35	0.551	0.160	0.668	20.1	0.474
h36	0.551	0.537	0.800	20.1	0.146
h37	1.102	0.379	0.556	40.1	0.523
h38	1.102	0.225	0.675	40.1	0.622
h39	1.102	0.250	0.808	40.1	0.765
h40	1.102	0.133		40.1	
h41	2.205	0.037	0.550	80.2	2.571
h42	2.205	0.201	0.613	80.2	3.084
h43	2.205	0.463	0.800	80.2	0.990
h44	3.307	0.244	0.613	120.3	2.233
h45	3.307	0.214	0.600	120.3	3.555

Table A-30 (Cont.)

Run No.	W_s	$\frac{dT_s}{d\theta}$	$\frac{dT_{j,\ avg.}}{d\theta}$	A_t	$q_{ins.}$
h46	3.307	0.200	0.450	120.3	3.879
h47	3.307	0.075	0.450	120.3	5.488
h48	4.409	0.369	0.75	160.1	1.979
h49	4.409	0.231	0.675	160.1	3.023
h50	4.409	0.213	0.425	160.1	3.853
h51	4.409	0.175	0.487	160.1	5.076
h52	4.409	0.488	0.744	160.1	1.295

Table A-31 4-in. Column, Alumina, $D_p = 0.0164''$

Run No.	W_s	$\frac{dT_s}{d\theta}$	$\frac{dT_{j,\,avg.}}{d\theta}$	A_t	$q_{ins.}$
h53	0.551	0.680		11.8	0.06981
h54	0.551	0.7875	0.61	11.8	0.1124
h55	0.551	0.738	0.700	11.8	0.1383
h56	0.551	0.525	0.594	11.8	0.3296
h57	0.551	0.364	0.481	11.8	0.4322
h58	1.653	0.763	0.738	35.3	0.2087
h59	1.653	0.713	0.681	35.3	0.2801
h60	1.653	0.438	0.638	35.3	0.3433
h61	1.653	0.438	0.706	35.3	0.5354
h62	1.653	0.400	0.700	35.3	0.7257
h63	2.755	0.571	0.663	58.8	0.3320
h64	2.755	0.471	0.738	58.8	0.5680
h65	2.755	0.200	0.988	58.8	0.7420
h66	2.755	0.313	0.825	58.8	0.8439

Table A-31 (Cont.)

Run No.	W_s	$\frac{dT_s}{d\theta}$	$\frac{dT_{j,\,avg.}}{d\theta}$	A_t	$q_{ins.}$
h67	3.858	0.643	0.738	82.3	0.4582
h68	3.858	0.463	0.613	82.3	0.6174
h69	3.858	0.319	0.563	82.3	0.9632
h70	3.858	0.400	0.638	82.3	0.7811
h71	4.409	0.433	0.738	94	0.8914
h72	4.409	0.417	0.663	94	1.1681
h73	4.409	0.286	0.438	94	1.2671

Table A-32 4-in. Column, Alumina, $D_p = 0.0411"$

Run No.	W_s	$\frac{dT_s}{d\theta}$	$\frac{dT_{j,\,avg.}}{d\theta}$	A_t	$q_{ins.}$
h74	0.551	0.679	0.713	4.7	0.0596
h75	0.551	0.463	0.650	4.7	0.1112
h76	0.551	0.244	0.563	4.7	0.1125
h77	1.653	0.368	0.556	14.1	0.1385
h78	1.653	0.375	0.650	14.1	0.2108
h79	1.653	0.375	0.593	14.1	0.2785
h80	1.653	0.250	0.488	14.1	0.3754
h81	2.755	0.275	0.381	23.4	0.4313
h82	2.755	0.621	0.675	23.4	
h83	2.755	0.375	0.606	23.4	0.3780
h84	2.755	0.306		23.4	0.4939
h85	3.306	0.450	0.6375	28.1	0.0758
h86	3.306	0.500	0.6500	28.1	0.4463
h87	3.306	0.500	0.6500	28.1	

Table A-33 2-in. Column, Glass Beads, $D_p = 0.0185''$

Run No.	W_s	$\frac{dT_s}{d\theta}$	$\frac{dT_{j,\,avg.}}{d\theta}$	A_t	$q_{ins.}$
h88	1.102	0.3060	0.6250	45.86	0.7110
h89	1.102	0.0940	0.4563	45.86	0.2533
h90	1.102	0.5130	0.5875	45.86	0.2319
h91	1.102	0.2250	0.4875	45.86	0.1687
h92	1.653	0.3190	0.5125	68.79	0.2237
h93	1.653	0.2690	0.5125	68.79	0.2360
h94	1.653	0.1190	0.5813	68.79	0.2809
h95	2.205	0.2875	0.5500	91.71	0.2405
h96	2.205	0.1625	0.4813	91.71	0.0998
h97	2.205	0.1833	0.5438	91.71	0.2925
h98	2.756	0.1750	0.5063	114.6	0.2634

Table A-34 2-in. Column, Silica Gel, D_p = 0.06569"

(h99 - h102, h113 - h115); Alumina, D_p = 0.0411"

Run No.	W_s	$\frac{dT_s}{d\theta}$	$\frac{dT_{j,\,avg.}}{d\theta}$	A_t	$q_{ins.}$
h99	0.55	0.1250	0.4500	71.11	0.3795
h100	0.55	0.1687	0.5688	71.11	0.7063
h101	0.55	0.1167	0.5000	71.11	0.5582
h102	0.992	0.2313	0.6125	128.02	
h113	1.102	0.1313	0.3375	142.21	0.7362
h114	1.102	0.1125	0.5125	142.21	0.4472
h115	1.102	0.1000	0.4438	142.21	0.6105
h103	0.551	0.1500	0.5500	4.69	
h104	0.551	0.1500	0.5375	4.69	
h105	0.551	0.0875	0.5250	4.69	0.4901
h106	0.551	0.1167	0.5438	4.69	0.9299
h107	1.102	0.1125	0.5375	9.376	0.6713

Table A-34 (Cont.)

Run No.	W_s	$\frac{dT_s}{d\theta}$	$\frac{dT_{j,\,avg.}}{d\theta}$	A_t	$q_{ins.}$
h108	1.102	0.0812	0.4812	9.376	0.5304
h109	1.102	0.1429	0.6125	9.376	0.5582
h110	1.433	0.2375	0.5063	12.19	0.3948
h111	1.433	0.2643	0.5750	12.19	
h112	1.433	0.1375	0.3500	12.19	0.5833

Table A-35 4-in. Column, Glass Beads, D_p = 0.011"

Run No.	W_s	$\frac{dT_s}{d\theta}$	$\frac{dT_{j,\,avg.}}{d\theta}$	A_t	$q_{ins.}$
c6	1.872	0.1990	0.263	131.1	0.1314
c7	1.872	0.0925	0.175	131.1	0.1195
c8	1.872	0.1475	0.214	131.1	0.1876
c9	1.872	0.1650	0.240	131.1	0.1911
c10	1.872	0.1680	0.263	131.1	0.1936
c11	1.872	0.0887	0.190	131.1	0.3294
c12	1.872	0.3230	0.456	131.1	0.2544
c13	1.872	0.2600	0.344	131.1	0.3570
c14	1.872	0.2680	0.239	131.1	0.3592
c15	1.872	0.3030	0.281	131.1	0.4671
c16	1.872	0.1610	0.331	131.1	0.5742
c17	1.872	0.2310	0.400	131.1	0.4655
c18	1.872	0.3900	0.563	131.1	0.4224
c19	1.872	0.2730	0.413	131.1	0.5376

Table A-35 (Cont.)

Run No.	W_s	$\frac{dT_s}{d\theta}$	$\frac{dT_{j,\,avg.}}{d\theta}$	A_t	$q_{ins.}$
c20	1.872	0.2380	0.388	131.1	0.7425
c21	1.872	0.2880	0.250	131.1	0.6592
c22	1.872	0.438	0.619	131.1	0.6111
c23	1.872	0.238	0.375	131.1	0.7686
c24	1.872	0.5250	0.694	131.1	0.6064
c25	1.872	0.525	0.581	131.1	0.7264
c26	1.872	0.375	0.544	131.1	0.7902
c27	1.872	0.550	0.707	131.1	0.7288
c28	1.872	0.425	0.607	131.1	0.8208

Table A-36 4-in. Column, Glass Beads, $D_p = 0.0185''$

Run No.	W_s	$\frac{dT_s}{d\theta}$	$\frac{dT_{j,\,avg.}}{d\theta}$	A_t	$q_{ins.}$
d1	1.590	0.3884	0.4570	67.95	0.1474
d2	1.590	0.3086	0.3380	67.95	0.1849
d3	1.590	0.3527	0.4500	67.95	0.2214
d4	1.590	0.3251	0.4560	67.95	0.2776
d5	1.590	0.321	0.3940	67.95	0.3159
d6	1.590	0.450	0.5070	67.95	0.2455
d7	1.590	0.4055	0.4500	67.95	0.2984
d8	1.590	0.3167	0.4570	67.95	0.3643
d9	1.590	0.3040	0.3750	67.95	0.2514
d10	1.590	0.3223	0.4312	67.95	0.3937
d11	1.590	0.3909	0.5625	67.95	0.3227
d12	1.590	0.4403	0.6437	67.95	0.4531
d13	1.590	0.5062	0.6437	67.95	0.2891

Table A-36 (Cont.)

Run No.	W_s	$\frac{dT_s}{d\theta}$	$\frac{dT_{j,\,avg.}}{d\theta}$	A_t	$q_{ins.}$
d14	1.590	0.5167	0.6375	67.95	0.3545
d15	1.590	0.4876	0.6125	67.95	0.4643
d16	1.590	0.4733	0.4642	67.95	0.4977
d17	1.590	0.6790	0.6750	67.95	0.3595
d18	1.590	0.5724	0.7312	67.95	0.4000
d19	1.590	0.5667	0.6625	67.95	0.5003
d20	1.590	0.5750			
d21	1.590	0.5058	0.5750	67.95	0.4876
d22	1.590	0.6050	0.6928	67.95	0.3841
d23	1.590	0.8667	0.7562	67.95	0.5875
d24	1.590	0.4897	0.6625	67.95	0.6859

Table A-37 4-in. Column, Glass Beads, $D_p = 0.0185''$

Run No.	W_s	$\frac{dT_s}{d\theta}$	$\frac{dT_{j,\,avg.}}{d\theta}$	A_t	$q_{ins.}$
d25	3.233	0.375	0.4575	138.15	0.5256
d26	3.233	0.258	0.1800	138.15	0.3131
d27	3.233	0.304	0.3715	138.15	0.6709
d28	3.233	0.4025	0.5310	138.15	0.5078
d29	3.233	0.4380	0.4968	138.15	0.6174
e1	3.233	0.5207	0.6593	138.15	0.7300
e2	3.233	0.533	0.6187	138.15	0.8346
e3	3.233	0.4025	0.4406	138.15	0.1026
e4	3.233	0.4711	0.5375	138.15	0.4878
e5	3.233	0.363	0.4437	138.15	0.5996
e6	3.233			138.15	

Table A-38 Particle Size Analysis

Material: Silica Gel

D_{pi}	X_i	X_i/D_{pi}	$\sum X_i/D_{pi}$	D_p
0.1320"	0.0140	0.1061		
0.0937"	0.2710	2.8922		
0.0661"	0.5180	7.8366		
0.0555"	0.1338	2.4108		
0.0465"	0.0817	1.7420		
0.0394"	0.0092	0.2335		
			15.2212	0.06569"
0.2230"	0.0363"	0.16278		
0.15700"	0.0421"	0.26821		
0.13200"	0.1936"	1.46666		
0.11100"	0.2525"	2.27477		
0.09370"	0.0676"	0.72145		
0.07800"	0.0319"	0.40897		
			4.30284	0.2324"

Table A-39 Particle Size Analysis

Determination of Average Particle Diameter D_p

Material: Alumina

D_{pi}	X_i	X_i/D_{pi}	$\sum X/D_{pi}$	D_p
0.0555"	0.70	12.61		
0.0331"	0.25	7.53		
0.0165"	0.25	15.15		
0.0098"	0.25	25.51		
			60.83	0.0164"
0.0555"	0.80	14.39		
0.0331"	0.10	3.02		
0.0165"	0.08	4.85		
0.0098"	0.02	2.04		
			24.31	0.0411"

Appendix B

Evaluation of $T_{j, avg.}$

$T_{j,\ avg.}$ is a complicated combination of several kinds of temperature readings related by an equation arrived at empirically. To derive the equation for $T_{j,\ avg.}$, $C_{i,\ avg.}$ must first be evaluated. $C_{i,\ avg.}$ is here taken to be the simple arithmetic sum of the specific heat capacity per inch of the reactor and jacket hardware and that of the insulation. It is represented by the following equation:

$$C_{i,\ avg.} = C_{i,\ ins.} + C_{i,\ j} + C_{i,\ r} \qquad \text{(B-1)}$$

From literature:

		4" column	2" column	
$C_{ins.}$	=	0.157	0.157	$\frac{\text{Btu}}{\text{lb.-mass}}$
C_j	=	0.136	0.136	$\frac{\text{Btu}}{\text{lb.-mass}}$
C_r	=	0.136	0.136	$\frac{\text{Btu}}{\text{lb.-mass}}$

Multipying each by its weight per inch of the column gave:

		4" column	2" column	
$C_{i,\ ins.}$	=	0.0120	0.00799	$\frac{\text{Btu}}{(^\circ\text{F})\ (\text{in.})}$
$C_{i,\ j}$	=	0.3400	0.12240	$\frac{\text{Btu}}{(^\circ\text{F})\ (\text{in.})}$
$C_{i,\ r}$	=	0.2175	0.04150	$\frac{\text{Btu}}{(^\circ\text{F})\ (\text{in.})}$

Assuming the air heat capacity to be negligible, and expressing each of the above in terms of percentages:

		4" column	2" column
$C_{i,\ ins.}$	=	2.1%	4.65%
$C_{i,\ j}$	=	59.8%	71.20%
$C_{i,\ r}$	=	38.2%	24.10%

$T_{j,\ avg.}$ can be represented by the following equation:

$$T_{j,\ avg.} = \frac{C_{i,\ ins.}}{C_{i,\ avg.}} \left(T_{room} + \frac{\Delta T_{ins.}}{2}\right) + \frac{1}{2} \left(\frac{C_{i,\ j}}{C_{i,\ avg.}}\right) \left[\frac{5}{3} \left(T_{room} + \Delta T_{ins.}\right) + \frac{1}{3}\ T_j\right] + \frac{C_{i,\ r}}{C_{i,\ avg.}}\ (T_s) \qquad \text{(B-2)}$$

where

(i) $T_{room} + \frac{\Delta T_{ins.}}{2}$ represents the temperature of the insulation

(ii) $\frac{1}{2} \left[\frac{5}{3}\ (T_{room} + \Delta T_{ins.}) + \frac{1}{3}\ T_j\right]$ is the mean temperature of the jacket wall

(iii) T_s is taken as the temperature of the reactor wall.

For (ii), it is the sum of the inner and outer temperature of the jacket wall divided by 2. The temperature drop across the jacket wall is found to be $\frac{1}{3}\ (T_j - T_{room} - \Delta T_{ins.})$. The derivation for $\frac{1}{3}$ $(T_j - T_{room} - \Delta T_{ins.})$ is as follows:

Heat conduction in a thick walled tube is:

$$Q = \frac{2\pi r_m l}{\left(\frac{r_m}{r_o h_o}\right) + \frac{(r_o - r_i)}{k} + \left(\frac{r_m}{h_i r_i}\right)} (t_i - t_o) \qquad \text{(B-3)}$$

or

$$(t_i - t_o) = \left(\frac{1}{h_o r_o} + \frac{1}{r_m} \cdot \frac{r_o - r_i}{k} + \frac{1}{h_i r_i}\right) \frac{Q}{2\pi l} \qquad \text{(B-4)}$$

where

r_i: inner radius of the tube

r_o: outer radius of the tube

l: length of tube

h_o: heat transfer coefficient at outer radius

h_i: heat transfer coefficient at inner radius

and r_m is the logarithmic mean radius represented by

$$r_m = \frac{r_o - r_i}{\ln\left(\frac{r_o}{r_i}\right)} \qquad \text{(B-5)}$$

Referring to Figure (B-1) and using equations (B-4) and (B-5), the following equations result

$$\Delta T_{23} = \Delta T_w = \left(\frac{1}{h_3 r_3} + \frac{1}{r_m} \cdot \frac{r_3 - r_2}{k_{23}} + \frac{1}{h_2 r_2}\right) \frac{Q}{2\pi l} \qquad \text{(B-6)}$$

$$\Delta T_{24} = \frac{1}{h_4 r_4} + \sum \frac{1}{r_m} \left(\frac{r_o - r_i}{k}\right) + \frac{1}{h_2 r_2} \quad \frac{Q}{2\pi l} \qquad \text{(B-7)}$$

Equating (B-6) and (B-7)

$$\Delta T_w = \Delta T_{24} \frac{\left(\frac{1}{h_3 r_3} + \frac{1}{r_m} \frac{r_3 - r_2}{k_{23}} + \frac{1}{h_2 r_2}\right)}{\left(\frac{1}{h_4 r_4} + \sum \frac{1}{r_m} \frac{r_o - r_i}{k} + \frac{1}{h_2 r_2}\right)} \qquad \text{(B-8)}$$

For the present system

$r_2 = 3.5"$ $\quad r_3 = 3.75"$ $\quad r_4 = 4.5"$

$h_2 = 50,$ $\quad h_3 = 0.4,$ $\quad h_4 = 0.2$ (McAdams)

$$\sum \frac{1}{r_m} \frac{r_o - r_i}{k} = \left[\frac{1}{r_{m23}} \cdot \frac{r_3 - r_2}{\ln \frac{r_3}{r_2}}\right] + \left[\frac{1}{r_{m34}} \cdot \frac{r_4 - r_3}{\ln \frac{r_4}{r_3}}\right]$$

$$= 13.02$$

$$\frac{1}{h_2 r_2} = 0.072, \quad \frac{1}{h_3 r_3} = 8.6, \quad \frac{1}{h_4 r_4} = 13.3$$

$k_{23} = 34,$ $\quad k_{34} = 0.024$

Substituting into equation (B-8):

$$\Delta T_w = \left(\frac{8.674}{26.96}\right) \Delta T_{24} = 0.323 \left(T_j - \Delta T_{ins.} - T_{room}\right)$$

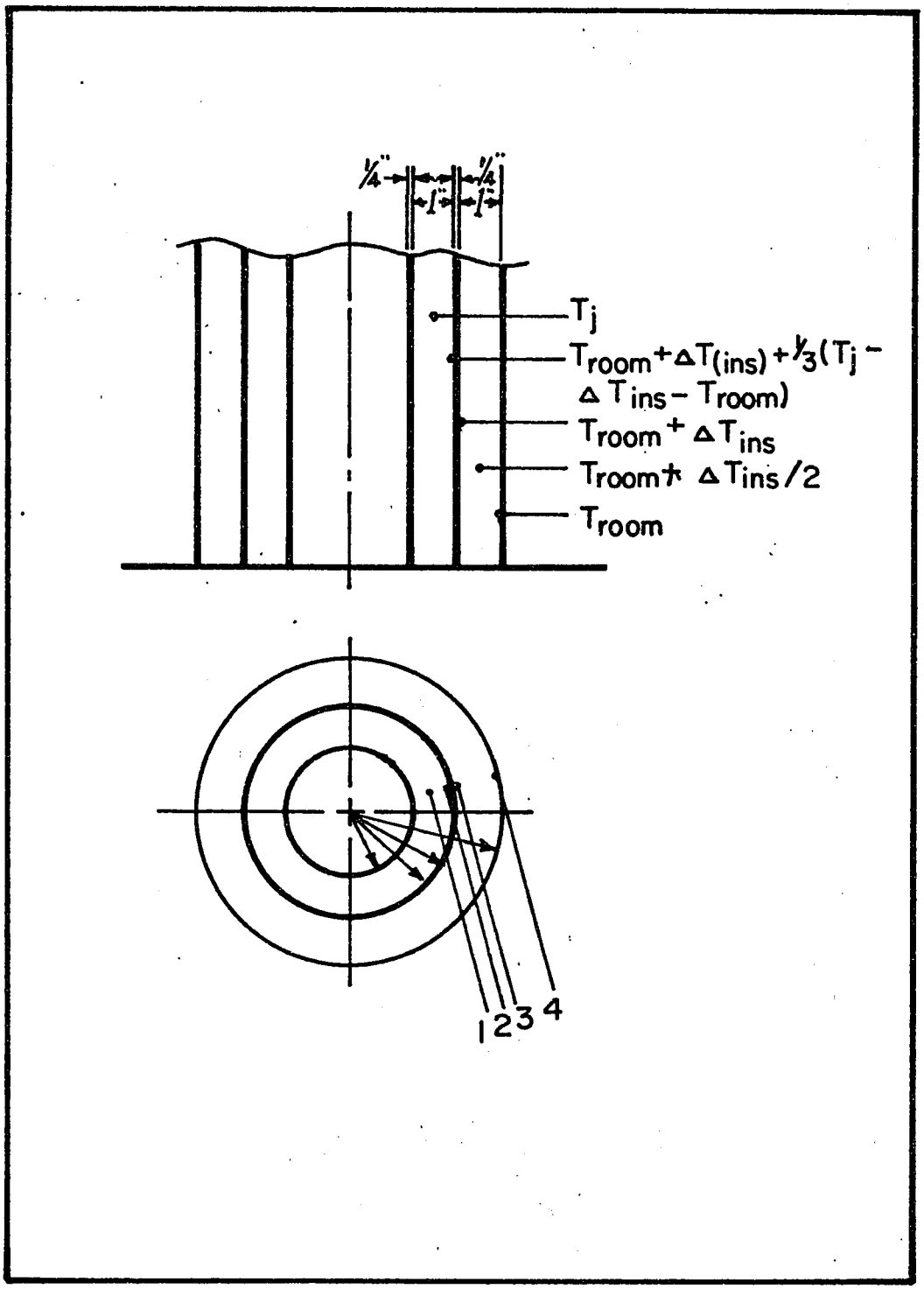

Fig. B-1 Illustration for the derivation of temperature difference across the jacket wall

Appendix C

Evaluation of C_i

Appendix C

A blank run was taken for each column, $T_{j,\ avgs.}$ were evaluated for different time intervals and tabulated on Table C-1. Figure C-1 was then plotted. Slopes $\frac{dT_{j,\ avg.}}{d\theta}$ were then evaluated at the middle portion of the blank runs, giving values of 0.363 and 0.5125 for the 4 inch and 2 inch columns respectively. The rest of the data and evaluation appear below:

		4" column	2" column	
W_g	=	0.85	1.4544	lbs./min.
W_j	=	0.462	0.6556	lbs./min.
C_{P_f}	=	0.2375	0.25	Btu/lb. °F

at θ = 60 min

$T_1 - T_2$	=	24.7	13.5	°F
$T_{j1} - T_{j2}$	=	10.5	8	°F
A_t	=	5.5	5.236	sq. ft.
$\Delta T_{ins.}$	=	93.5	91.5	°F

With $(\frac{k_i}{L_i}) = 0.0048\ (\frac{Btu}{min.\ ft.^2\ °F})$ for both columns, substituting all data into equation (63).

$$C_j = 0.275\ \frac{Btu}{(°F)\ (in.)} \quad \text{(for 4" column)}$$

$$C_j = 0.1594\ \frac{Btu}{(°F)\ (in.)} \quad \text{(for 2" column)}$$

Table C-1

θ	T_s		T_j		T_{jw}		$\Delta T_{ins.}$		$\Delta T_{j,\ avg.}$	
	a	b	a	b	a	b	a	b	a	b
0										
10	218	186	126	151	98	151	19	76	127	164
20	236	192	149	155	118	153	39	78	147	168
30	243	197	164	161	137	157	58	82	162	173
40	243	202	172	166	151	161	72	86	171	177
50	244	206	179	171	163	165	84	90	179	181
60	246	210	185	175	170	168	91.5	94	185	185
70	246	213	186	178	176	172	97	97	189	188
80	246	215	189	181	180	177	101	102	192	192
90	249	217	191	183	183	178	104	103	195	193
100		218		185		180		106		195
110	252	219	193	186	188	182	109	107	199	196

a = data for 2" column

b = data for 4" column

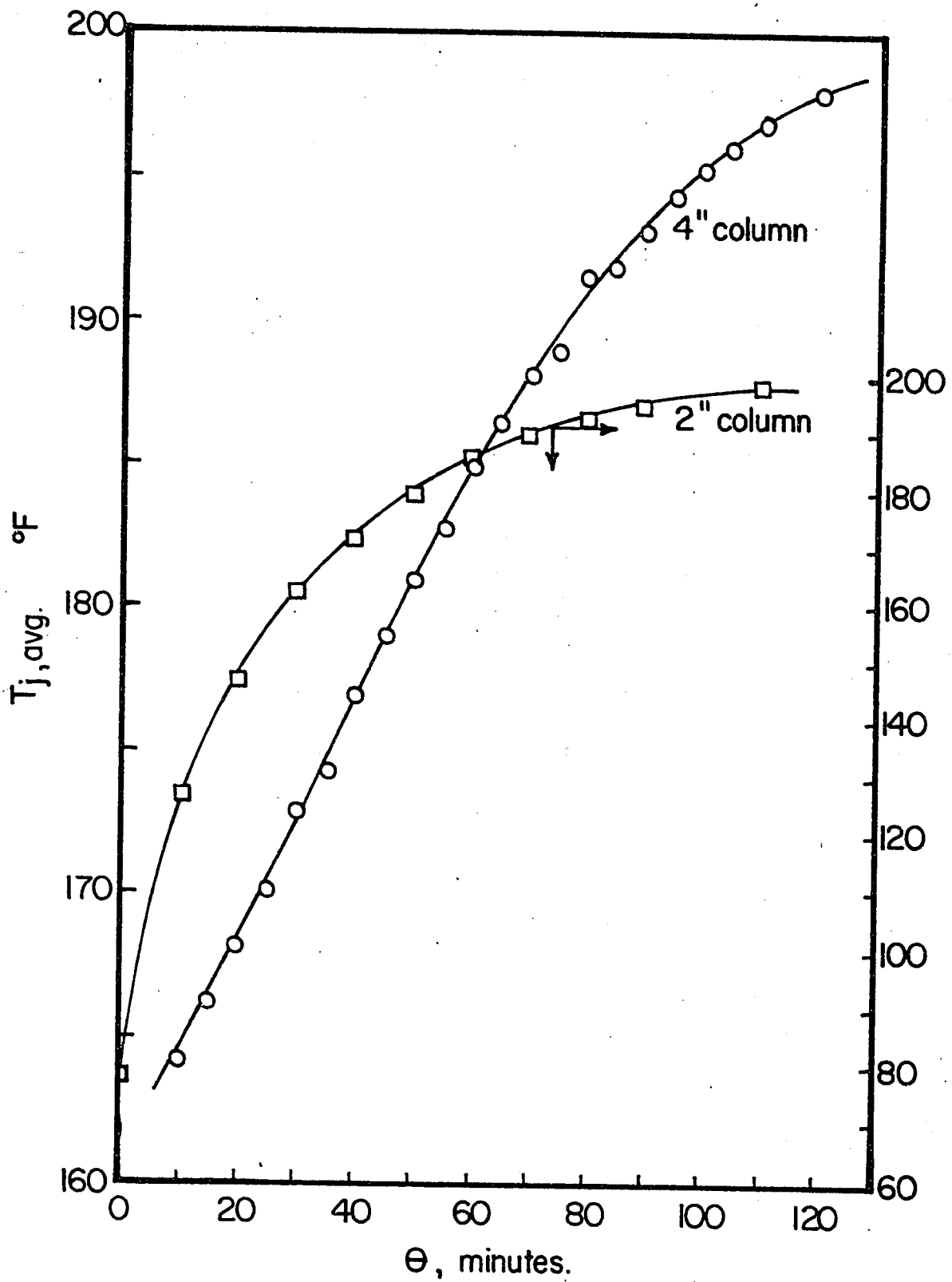

Fig. C-1 $T_{j,\ avg.}$ versus time curve (blank runs)

Appendix D

Derivation of $q_{ins.}$

Derivation of:

$$q_{ins.} = (k_{ins.})\,(A_{ins.})\,\left(\frac{\Delta T_{ins.}}{\Delta r}\right)$$

Start with energy equation:

$$\rho\, C_p \frac{\partial T}{\partial \theta} = k \nabla^2 T \qquad \text{(D-1)}$$

or

$$\rho\, C_p \frac{\partial T}{\partial \theta} = \nabla \cdot q \qquad \text{(D-2)}$$

for cylindrical coordinates

$$\rho\, C_p \frac{\partial T}{\partial \theta} = -\left[\frac{1}{r}\frac{\partial}{\partial r}(r q_r) + \frac{1}{r}\frac{\partial q_r}{\partial a} + \frac{\partial q_z}{\partial Z}\right] \qquad \text{(D-3)}$$

$(\partial q_z/\partial Z)$ and $\left(\frac{\partial q_a}{\partial a}\right)$ of equation (D-3) are negligible. Figure (D-1) and Table (D-1) show that the temperature differences along the height Z, and at different angles a, are very small. Therefore:

$$\rho\, C_p \frac{\partial T}{\partial \theta} = -\frac{1}{r}\,\frac{\partial}{\partial r}(r q_r)$$

$$= -\frac{1}{r}(q_r) - \frac{\partial q_r}{\partial r} \qquad \text{(D-4)}$$

but

$$q_r = -k \frac{\partial T}{\partial r} \qquad \text{(D-5)}$$

$$\rho\, C_p \frac{\partial T}{\partial \theta} = k\left(\frac{1}{r}\right)\left(\frac{\partial T}{\partial r}\right) + k\left(\frac{\partial^2 T}{\partial r^2}\right) \qquad \text{(D-6)}$$

From Carslaw and Jaeger (44), it is justifiable to neglect the term $(\partial T/\partial \theta)$ in the equation of conduction for the case of a thin surface skin of poor conductor. For the present case, the insulating

material is a poor conductor and the insulation is comparatively thin. Equation (D-6) therefore becomes:

$$0 = k\left(\frac{1}{r}\right)\left(\frac{\partial T}{\partial r}\right) + k\left(\frac{\partial^2 T}{\partial r^2}\right) \qquad \text{(D-7)}$$

A special run was taken with thermocouples installed at different axes in the insulation layers of the fluidising column. The results of the temperature measurements are given in Table (D-1). From the data of Table (D-1), the value of $\partial T/\partial r$ and $\partial^2 T/\partial r^2$ were obtained by graphical differentiation. The results are given in Table (D-II). It is realised that the first term of the equation is small compared to the second term and therefore negligible

$$k\frac{\partial^2 T}{\partial r^2} = 0 \qquad \text{(D-8)}$$

Equation (D-8) is based on per unit volume, multiplying it by unit thickness, the temperature distribution per unit cross-sectional area is obtained. Integrating equation (D-8):

$$k\frac{\partial^2 T}{\partial r^2} = 0$$

$$k\frac{dT}{dr} = q_r \qquad \text{(D-9)}$$

Using the method of separation of variables and further integration of equation (D-9) yields:

$$k \int dT = q_r \int dr$$

$$k \quad \Delta T = q_r \, \Delta r$$

or $$q_r = k \frac{\Delta T}{\Delta r} \qquad \text{(D-10)}$$

Multiplying (D-10) by cross-sectional area of heat flow across insulation:

$$q_{ins.} = (k_{ins.}) (A_{ins.}) \left(\frac{\Delta T_{ins.}}{\Delta r}\right) \qquad \text{(D-11)}$$

Table D-I

Thermocouple No.	Temperature, °F
1	142.5
2	116.0
3	100.0
4	146.0
5	119.0
6	95.0
7	149.0
8	149.0
9	105.0
10	196.5
11	196.5
12	196.5

Table D-II

$\theta = 60$

$\frac{r}{r_o}$	$\frac{\partial t}{\partial (\frac{r}{r_o})}$	$\frac{\partial t}{\partial r}$	$\frac{\partial^2 t}{\partial (\frac{r}{r_o})^2}$	$\frac{\partial^2 t}{\partial r^2}$
1.02	783.3	2685	66,666	228,531
1.10	325	1114	7125	24,424
1.16	240	822.7	4500	15,426
1.20	210	719.8	3600	12,340
1.24	150	514	2833	9,711
1.286	107	367	2000	6856

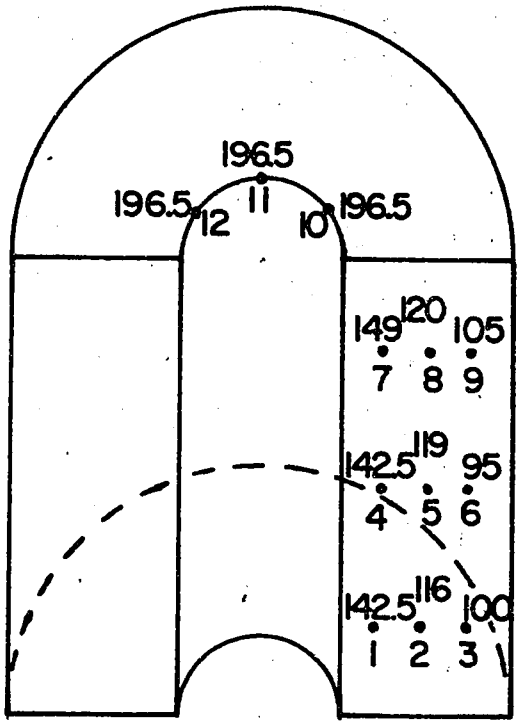

Fig. D-I. Illustration of temperature distribution in determining q_{ins}.

Appendix E

U at Different Time Intervals

A particular calculation was carried out for run h3, where the experimental data are found in Appendix A and calculated results presented in Table E-1.

Table E-1

Calculated Result of Run h3

θ	$\frac{dT_s}{d\theta}$	$T_l - T_s$	$\frac{dT_{j,\,avg.}}{d\theta}$	U
0				
10	1.333	66	1.5333	0.00003798
20	1.080	61.5	1.2400	0.000033446
30	0.850	56	0.9833	0.000028422
40	0.675	54	0.7214	0.000023208
50	0.522	50	0.4125	0.00001891
60	0.331	48	0.4190	0.00001332
70	0.190	47	0.2666	0.00000774
80	0.075	46	0.1538	0.00001066
90	0	47	0.0000	0.000000106
100	-0.05	47	-0.0038	-0.00000176
110	-0.08	49	-0.023	-0.0000022

The value of U at θ = 60 min. is 0.00001332 Btu/hr. ft.^{2} °F, while the arithmetic average value for middle 50% (from θ = 40 min. to θ = 80 min.) of the run is 0.00001476.

Appendix F

T_2 and Expanded Bed Height

In an opaque fluidization vessel, a thermocouple can not be located so as to measure the gas temperature at exactly the top of the bed. To justify this statement, two special runs were conducted. In these runs, thermocouple probes were inserted into the fluidised threshold at different heights of the columns. The temperature profiles of two runs are shown in Figure F-1. The locations of the expanded bed heights are calculated from equations (F-1) and (F-2) and the results shown in Table F-1.

Table F-1

	Run a	Run b	
Sample:	glass beads	alumina	
Weight of Sample:	1500	250	gms
Volumetric flow:	10.5	17.5	$\frac{\text{cu. ft.}}{\text{min.}}$
Bed-Settled Height:	5.2	.5	in.
V_f	2.005	3.342	$\frac{\text{ft.}}{\text{sec.}}$
L_{ex}	1.9913	1.513	ft.

Equations used:

$$\text{a: } \frac{L_{ex}}{L_s} = 2.25\, V_f + 0.1 \qquad \text{(F-1)}$$

$$b: \frac{L_{ex}}{L_s} = 2.433\ V_f - 4.5 \qquad \text{(F-2)}$$

Figures (F-1) and (F-2) do not indicate an abrupt change of temperature at the expanded bed height L_{ex}.

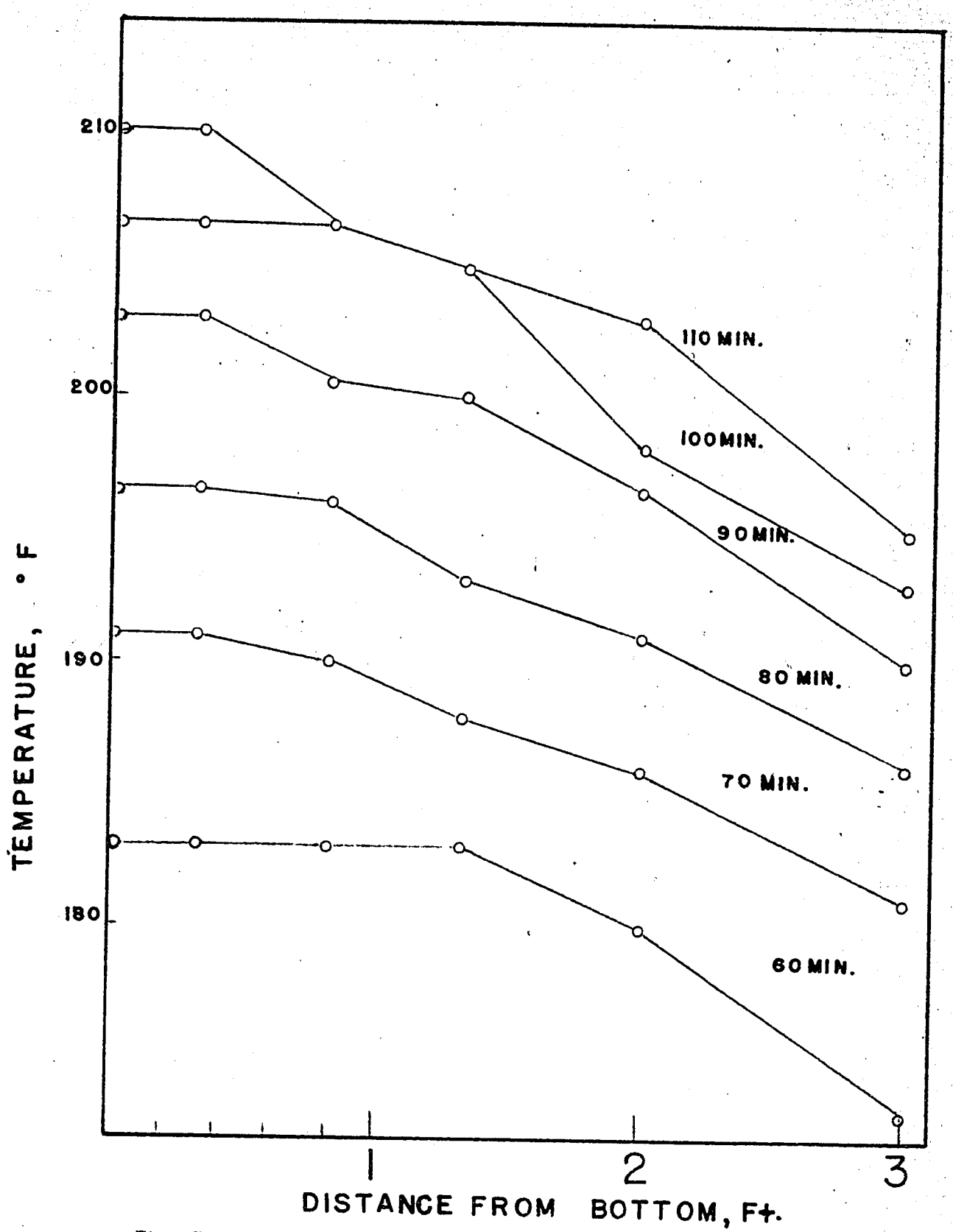

Fig. F-1. Temperature profile along the column height—a

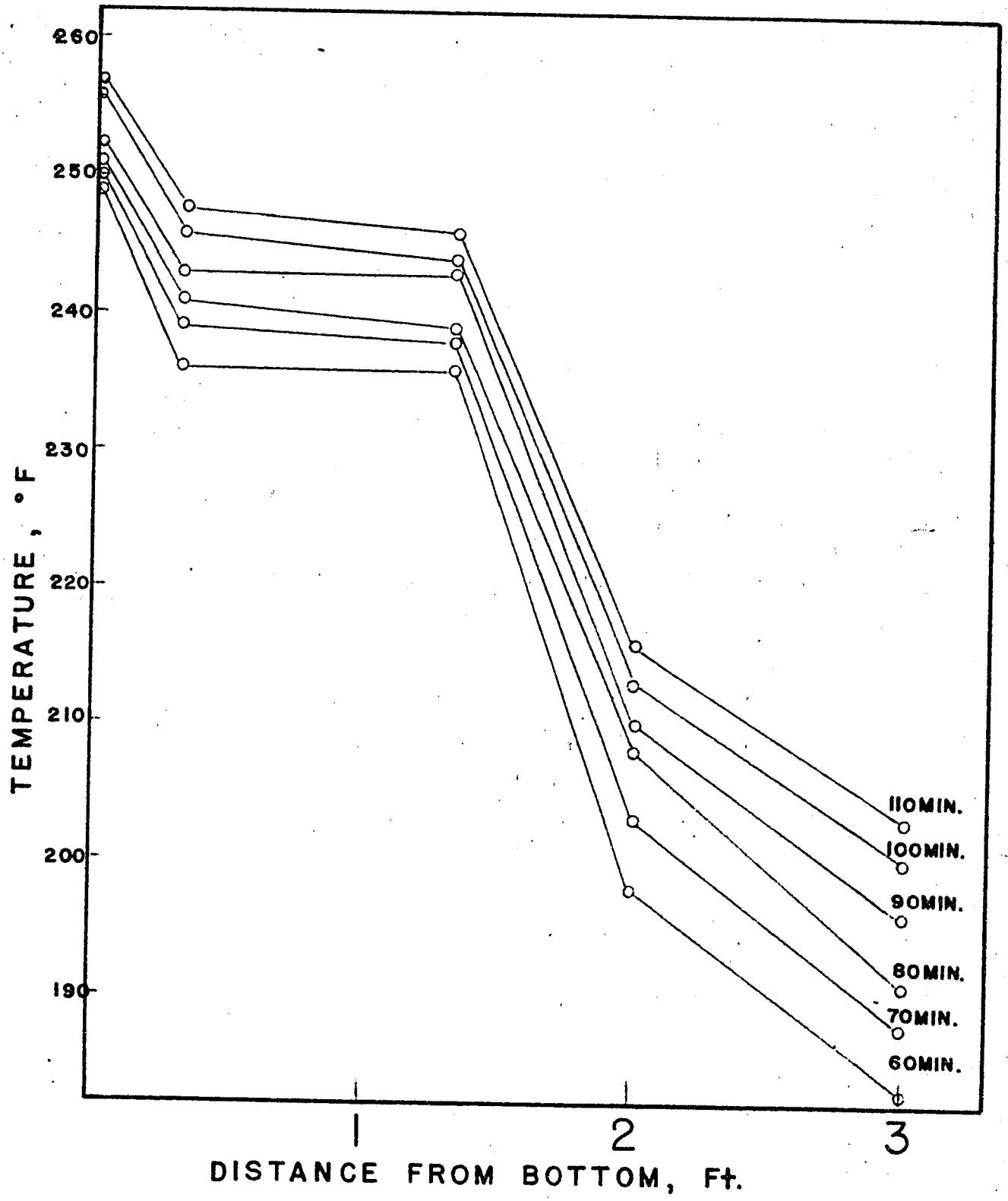

Fig. F-2. Temperature profile along the column height

Appendix G

Temperature Gradients in Fluidised Beds

Table G-1 Temperature Distribution in Fluidized Bed

	Thermocouple Readings, Millivolts* Distance from Center of Tube, in.								
L, in.	+2.0	+1.5	+1.0	+0.5	0.00	-0.5	-1.0	-1.5	-2.0
0.125	1.65	1.65	1.60	1.57	1.60	1.58	1.62	1.70	1.63
	1.50	1.40	1.40	1.34	1.35	1.35	1.35	1.35	1.50
0.225	1.50	1.50	1.42	1.38	1.40	1.42	1.45	1.47	1.48
	1.40	1.35	1.25	1.23	1.22	1.25	1.25	1.25	1.30
0.325	1.35	1.35	1.25	1.25	1.25	1.25	1.28	1.33	1.33
	1.25	1.22	1.16	1.14	1.13	1.14	1.15	1.20	1.27
0.425	1.18	1.20	1.15	1.14	1.10	1.13	1.15	1.19	1.15
	1.18	1.20	1.15	1.15	1.15	1.15	1.15	1.15	1.18
0.525	1.15	1.18	1.13	1.12	1.08	1.12	1.13	1.17	1.13
	1.15	1.18	1.13	1.12	1.12	1.12	1.12	1.12	1.12
0.625	1.10	1.15	1.13	1.12	1.12	1.12	1.14	1.18	1.13
	1.17	1.15	1.13	1.12	1.12	1.12	1.12	1.12	1.12
0.875	1.07	1.12	1.12	1.12	1.12	1.14	1.14	1.15	1.05
	1.17	1.15	1.15	1.15	1.15	1.15	1.15	1.15	1.15

Table G-1 (Cont.)

1.125	1.05	1.10	1.12	1.12	1.10	1.12	1.13	1.15	1.03
	1.15	1.15	1.15	1.15	1.14	1.15	1.15	1.13	1.13
1.375	1.02	1.10	1.10	1.12	1.10	1.12	1.13	1.15	1.02
	1.15	1.15	1.13	1.13	1.13	1.13	1.13	1.13	1.13

* Data of Walton, J.S., Olson, R.L. and Levenspiel, O.

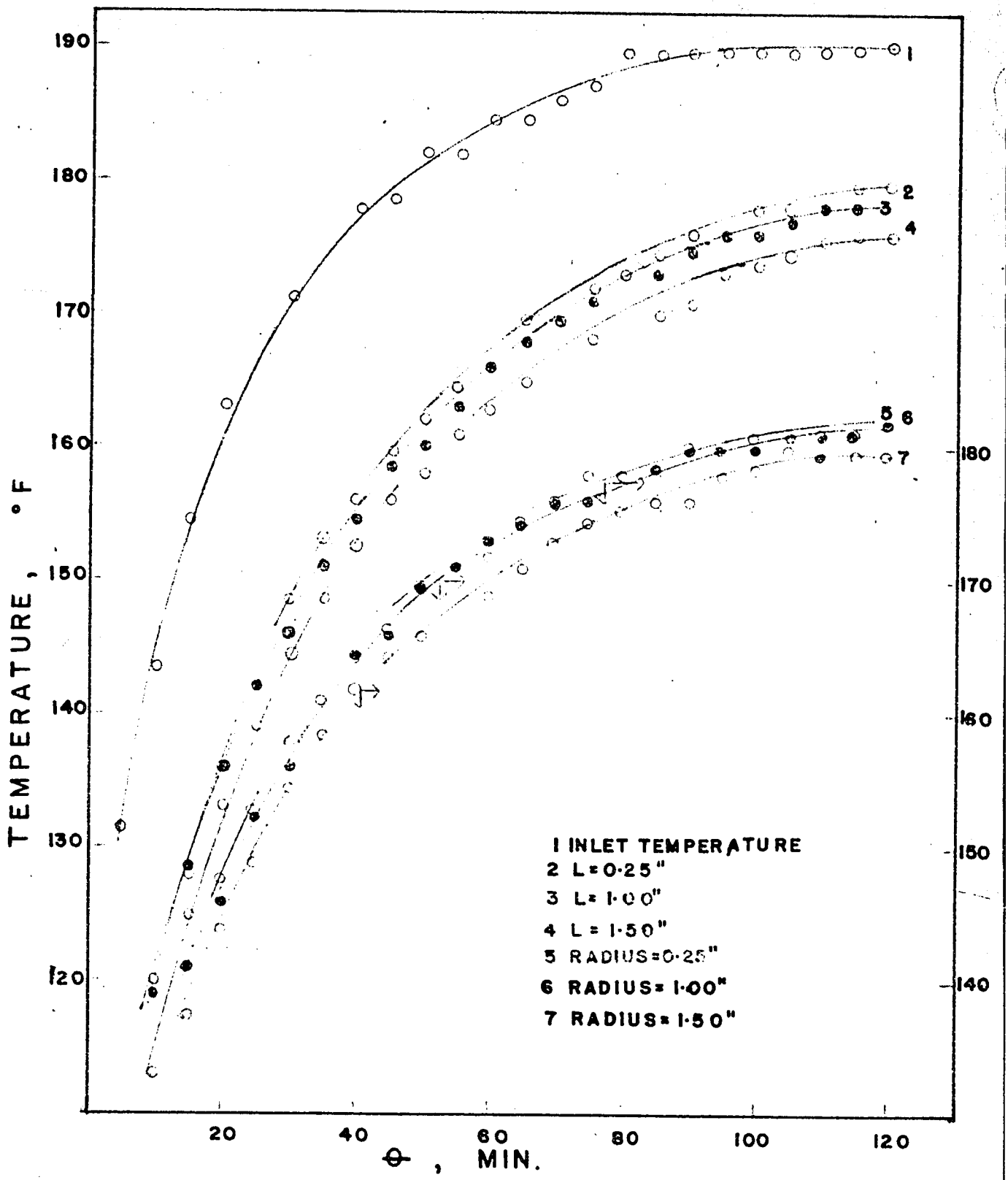

Fig. 6-7. Temperature profile in the fluidized bed